Modelling Perineural Tumour Invasion



Konstantinos Sakellariou

Merton College

University of Oxford

A thesis submitted in partial fulfillment of the requirements for the degree of

MSc by Research

Hillary 2012

Contents

1 Introduction **1**

Overview . . . 1

1.1 Motivation . . . 2

1.2 Mathematical Modelling Approaches . . . 10

1.2.1 Deterministic vs Stochastic Approach . . . 13

1.2.2 Discrete vs Continuum Modelling . . . 16

1.3 Objectives . . . 19

1.4 Thesis Outline . . . 21

2 Biological Background **23**

Overview . . . 23

2.1 PNI Characteristics . . . 24

2.2 Questions and Possible Explanations Regarding PNI . . . 26

2.3 Molecular Basis for PNI . . . 28

2.3.1 Matrix Metalloproteinases (MMPs) . . . 29

2.3.2 NFκB Survival Pathway . . . 30

2.3.3 Neural Cell Adhesion Molecule (NCAM) . . . 31

2.3.4 Nerve Growth Factor (NGF) . . . 31

Summary . . . 34

3 Models of Cell Migration **36**

Overview . . . 36

3.1 Spatial Location of a Single Individual: Occupation Probability Approach . . . 38

3.2 Distribution of Individuals in Space: Master Equation Approach . . . 41

3.3 Position-Jump Processes . . . 43

3.3.1 Simple Random Walk . . . 43

3.3.1.1 Individual Approach . . . 43

3.3.1.2 Boundary Conditions (BCs) . . . 49
3.3.1.3 Population Approach . . . 51
3.3.2 Biased Random Walk . . . 57
3.3.2.1 Individual Approach . . . 57
3.3.2.2 Boundary Conditions . . . 61
3.3.2.3 Population Approach . . . 63
3.4 Velocity-Jump Processes . . . 64
3.4.1 Correlated Random Walk . . . 64
3.4.1.1 Individual Approach . . . 64
3.4.1.2 Boundary Conditions . . . 68
3.4.1.3 Population Approach . . . 70
3.4.2 Biased and Correlated Random Walk . . . 74
3.4.2.1 Individual Approach . . . 74
3.4.2.2 Boundary Conditions . . . 76
Summary . . . 77

4 First-Passage Time Analysis **84**
Overview . . . 84
4.1 Mean First-Passage Time . . . 85
4.2 Direct Methods . . . 87
4.3 Time-Integrated Probability Formulation . . . 91
4.3.1 Simple Random Walk . . . 93
4.3.2 Biased Random Walk . . . 102
4.3.3 Correlated Random Walk . . . 107
4.3.4 Biased and Correlated Random Walk . . . 114
Summary . . . 115

5 Incorporating Cell Proliferation and Death **120**
Overview . . . 120
5.1 Linear Stochastic Model . . . 122
5.2 Nonlinear Stochastic Model . . . 127
5.3 Mean First-Passage Time . . . 132
Summary . . . 135

6 Parameter Regimes For Invasion **137**
Overview . . . 137
6.1 Diffusion-only Scenario . . . 139

6.2 Diffusion-Proliferation Scenario 145
6.3 Diffusion-Proliferation-Reduced Apoptosis Scenario 148
6.4 Advection-Diffusion Scenario 150
Summary 152

7 Discussion **154**
7.1 Conclusion 155
7.2 Future Work 159

A Appendices for Chapter 3. **165**
A.1 Simple Random Walk 165
A.1.1 Occupation Probability in Discrete Space and Time 165
A.1.2 Occupation Probability Approximation as $n \to \infty$ 166
A.1.3 Statistical Measures 168
A.1.4 Gillespie's SSA - Compartment-based Diffusion 169
A.2 Biased Random Walk 171
A.2.1 Derivation of PDE 171
A.2.2 Derivation of the Mean Location and Variance of the BRW . . 172
A.2.3 Derivation of the Zero-flux Boundary Condition given by Equation 3.22 173
A.3 Correlated Random Walk 177
A.3.1 Derivation of the Mean Location and Variance of the CRW . . 178
A.4 Biased and Correlated Random Walk 180
A.4.1 Derivation of the Mean Location and Variance of the BCRW . 181
A.5 Derivation of the Stochastic Mean Equations of a Position-Jump Process from the Master Equation 183

Bibliography **186**

Glossary

The following acronyms are used in this report, with page of first occurrence:

- **BCC** — Basal Cell Carcinoma ..... 4.
- **BCRW** — Biased & Correlated Random Walk ..... 41.
- **BCs** — Boundary Conditions ..... 49.
- **BRW** — Biased Random Walk ..... 40.
- **BDNF** — Brain Derived Neurotrophic Factor ..... 32.
- **CA** — Cellular Automaton ..... 18.
- **CBP** — Contact Birth Process ..... 123.
- **CNS** — Central Nervous System ..... 3.
- **CRW** — Correlated Random Walk ..... 40.
- **DAD1** — Defender Against Cell Death 1 ..... 30.
- **DBP** — Diffusion Birth Process ..... 122.
- **ECM** — Extra-Cellular Matrix ..... 29.
- **NCAM** — Neural Cell Adhesion Molecule ..... 29.
- **NFκB** — Nuclear Factor κB ..... 29.
- **NGF** — Nerve Growth Factor ..... 29.
- **NMSC** — Non-Melanoma Skin Cancer ..... 3 .
- **MFPT** — Mean First-Passage Time ..... 84.
- **MMPs** — Matrix Metalloproteinases ..... 28.
- **MSD** — Mean Squared Displacement ..... 168.
- **ODEs** — Ordinary Differential Equation ..... 10.

- **RDME** — Reaction Diffusion Master Equation ..... 37.
- **PDEs** — Partial Differential Equation ..... 11.
- **PNI** — Perineural tumour Invasion ..... 2.
- **SCC** — Squamous Cell Carcinoma ..... 4.
- **SDEs** — Stochastic Differential Equations ..... 17.
- **SSA** — Stochastic Simulation Algorithm ..... 37.
- **SRW** — Simple Random Walk ..... 38.
- **WHO** — World Health Organisation ..... 1.

Chapter 1

Introduction

Overview

Cancer is a group of multiple distinct diseases, all of which are characterised by two main properties at the cellular level: (a) the ability to reproduce beyond the normal levels of restraint and (b) the ability to invade surrounding tissues and hence conquer territories normally reserved for other cells [Alberts et al., 2008]. Hanahan and Weinberg [2000] enumerated the six distinct alterations (hallmarks of cancer) in the physiology of a healthy cell required for malignant growth. Apart from limitless replicative potential and invasion capabilities, tumour cells exhibit self-sufficiency in growth signals, insensitivity to growth-inhibitory signals, evasion of apoptosis (programmed cell death) and angiogenesis. According to the World Health Organization (WHO), cancer is the second leading cause of death in high- and middle-income countries after coronary heart disease [WHO, 2008].

Cancer arises through genetic changes in the nucleus of healthy cells. These changes lead cells to exhibit selfish behaviour and prosper at the expense of neighbouring cells. The origin of this behaviour is usually a mutation occurring within a single

cell (error during DNA replication or change in the genomic sequence due to external chemical agents, radiation, viruses etc.). However, a single mutation is not sufficient for a tumour to develop. The abnormality is passed on to the progeny of the original cell and only if sufficiently many of these 'occurrences' accumulate in a single cell, does a tumour begin to develop [Alberts et al., 2008]. A few descendants of the single mutant ancestor start multiplying extremely rapidly and form a mass characterised by uncooperative behaviour. The tumour is termed 'benign' if it lacks the invasive properties of cancer and does not lead to fatalities. If, on the other hand, the tumour exhibits either of its two lethal traits, i.e. invasion (movement towards adjacent normal tissue) or metastasis (formation of secondary tumours in distant tissues from the original tumour site), it is termed 'malignant'. It is malignancies that render the tumour extremely difficult to isolate and remove surgically and therefore fatal in most cases.

There are various modes of tumour spread. The most common is the penetration of lymphatic and blood vessels, through which tumour cells travel toward distant tissues (metastasis). Currently, this mode of invasion is called lymphatic or hematogeneous spread. The reason is that the word 'metastasis' is now used in a much broader sense due to the discovery of numerous other kinds of tumour invasion and in order to include other diseases as well[1].

1.1 Motivation

One mode of tumour spread that is associated with very high mortality rates is Perineural Tumour Invasion (PNI). The term describes a type of tumour invasion

[1]The current meaning of the word 'metastasis' is actually closer to its original meaning, namely displacement. Until two centuries ago, however, lymphatic spread of tumour cells was the only mode of invasion of cells to other tissues known to scientists. Recent research has shown that not only are there different ways for tumour cells to invade adjacent and non-adjacent tissues, but also that such a displacement of cells within the organism is present in other diseases as well.

through the nervous system. Certain types of cancer exhibit a propensity to infiltrate neural structures. Since there is no immune response to tumour invasion once the cells have entered a perineural space, the tumour is free to travel towards the Central Nervous System (CNS) through a path of minimal resistance. After a certain time interval (varying greatly from individual to individual), the tumour spreads to the entire body. Even in the rare case where not many tissues are invaded (or if PNI is discovered early enough), the tumour cells still manage to enter the cranial space and degrade the brain. It is most often at this point that symptoms arise as neural or motor functions are lost. In addition, patients start experiencing extreme pain at this point. Furthermore, Leibovitch et al. [2005] have shown that PNI is associated with larger, more aggressive tumours with higher recurrence rates. The vast majority of clinical reports regarding PNI indicate that it correlates with a reduced survival rate and a severe degradation of neural function that leads to a reduced quality of life.

PNI is associated with many different types of cancer (non-melanoma skin cancer, prostate cancer, bile duct cancer, pancreatic cancer, melanoma skin cancer etc.). In this thesis we are primarily interested in Non-Melanoma Skin Cancer (NMSC). NMSC is the type of cancer with the highest incidence in the UK[2] (100,000 estimated cases in 2006, 81,600 of which were registered), the US[3] (1,000,000 estimated cases in 2009) and the world (around 3,000,000 cases in 2008). Fig. 1.1 shows the worldwide incidence and mortality rates of various types of cancer (2008 estimates [WHO, 2008]). It is evident that lung cancer is currently the most common and most lethal type of cancer. Although NMSC has a much higher incidence rate, almost twice that of lung cancer, it is typically excluded from such tables. The reason is twofold: firstly, there are difficulties in collecting and counting tumours of such a high incidence; secondly,

[2]http://info.cancerresearchuk.org/cancerstats/ [2006]
[3]http://www.cancer.gov/cancertopics/types/skin [2009]

due to micrographic surgery, NMSC is gradually becoming less life-threatening, in contrast to the vast majority of other types of cancer. At the present time, it is, in fact, highly treatable. For instance, in 2008 only 491 deaths resulted from 98,800 NMSC registered cases in the UK. However, one cannot neglect the mortality associated with perineural invasion. The two most common forms of NMSC are Basal Cell Carcinoma (BCC) and cutaneous Squamous Cell Carcinoma (SCC). The suggested incidence rate of PNI varies throughout the literature, but has been quoted as being between 2.5% and 14% of the total number of SCC cases and between 0.18% and 10% for BCC [Dunn et al., 2009]. However, more recent studies focusing on perineural invasion [Ratner et al., 2000, Lawrence and Cottel, 1994, Garcia-Serra et al., 2003, Fagan et al., 1998] have shown that the actual incidence rate might be much higher. For instance, Fagan et al. [1998] reported that PNI was present in 52% of 142 NMSC patients.

The reasons why certain tumour cells are potentially attracted to the nerve sheath and the molecular mechanisms behind perineural spread have not yet been identified. There exists a variety of hypotheses worth exploring drawn from the recent literature. Scientists have suggested that there exists a link between specific mechanisms at the molecular level and PNI. The aim of our work is to approach the situation from a mathematical perspective and investigate the underlying mechanisms that may drive PNI during its early stages, before infiltration of the perineural space has occurred.

Despite being known since 1842, perineural tumour invasion has only received attention from the scientific community very recently. The reason is that cancer in general is an emerging non-communicable disease of an ageing population while infectious diseases are in decline. Furthermore, PNI was thought to occur at a low rate (for instance in the case of NMSC, it was estimated as 5% of the total cases [McCord

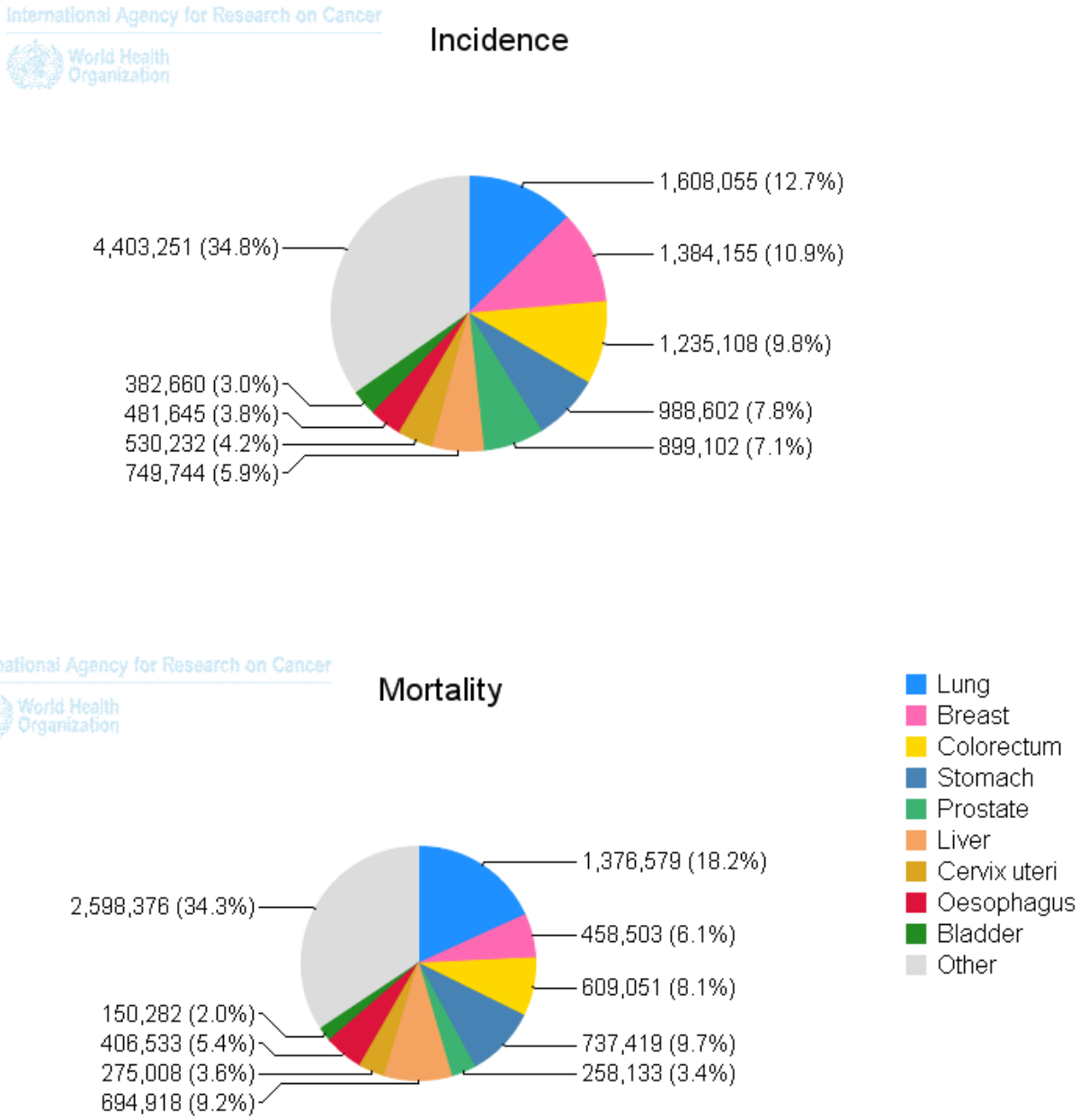


Figure 1.1: The incidence rate (top) and the mortality rate (bottom) of various types of cancer in the world in 2008 are shown. The data were obtained from the GLOBOCAN (global reference for cancer information) project [http://globocan.iarc.fr/, 2008], conducted by the International Agency for Research on Cancer (IARC). The figure is reproduced from the website of IARC's parent organisation, the World Health Organisation (WHO) [WHO, 2008]. Note that although NMSC is the type of cancer with the highest incidence rate in the world, it is typically excluded from such tables as it is generally non-invasive (with the exception of PNI) and hence highly treatable.

et al., 2000]). Over the last 50 years, however, a shift of attention towards PNI has occurred. Clinical reports from 1954 have suggested that PNI may be more frequent than previously thought. Over the last 20 years, scientists have begun to perform experiments on PNI and their results indicate links between PNI and processes at the molecular level. In Chapter 2 we present a detailed report of these interactions. Despite this shift in experimental focus, PNI has so far failed to attract the interest of mathematical modellers.

In the past, scientists studied tumour growth and invasion by observing the phenomenon at the tissue scale. In this context, we treat a *tumour*, or more precisely a *neoplasm*[4], as a single entity. However, a tumour is a collection of several individual tumour cells. Recent advances in biological sciences and experimental techniques, especially during the last few decades, have allowed and also encouraged scientists to focus on the individual components forming an organism and their interaction with other objects of the same scale. This, so called, 'reductionist' approach has proved very successful in molecular biology and genetics and as a result scientists of many disciplines have adopted this mode of thinking. The reasoning behind taking a whole and breaking it down to its components is that, by looking at the lowest level of the chain of cause and effect, one can explain the behaviour of the whole completely. This view has caused a great debate, especially among physiologists, and is in contrast to the philosophy of the 'systems biology' approach, i.e. the study of the networks arising between fundamental objects in biology, such as the cell or the gene. We draw an analogy to how mathematical modelling has been perceived and applied over the years in Section 1.2 and discuss the need to use both approaches in a complementary fashion, if we are to truly understand the behaviour of complex processes.

[4]The word 'tumour', originating from Latin, initially referred to any form of swelling whereas the Greek word 'neoplasm' refers specifically to the formation of a 'new' mass within the body due to the abnormal proliferation of cells. In modern English, however, and only very recently within the scientific community, the word 'tumour' is used more often than and as a synonym of a neoplasm.

Tumours have traditionally been studied within fields such as those of biology, biochemistry or medicine. However, to paraphrase the eminent theoretical ecologist Akira Okubo, if the dynamics of any system under investigation are to be analysed quantitatively, so that predictions can be made, then a mathematical treatment is required [Okubo and Levin, 2001]. Although scientists of every discipline are interested in quantification, as it allows for accurate predictions, mathematical models have only been used in biology relatively recently. This is in stark contrast to physics, for example, where mathematical tools have been utilised continuously since the birth of the science. One of the main reasons is that established principles, analogous to Newton's laws or energy conservation laws in physical systems, have not been observed in the study of interactions between the fundamental units of biology. Biological systems are often far from equilibrium. Processes at the level of the cell are governed by very active dynamics due to functionality, which plays an extremely significant role in the survival of an organism.

However, there are other subtle differences between the physical and life sciences and the phenomena under study are of a completely different nature. In physics there are three important scales (described by quantum mechanics, classical mechanics and the theory of relativity as we move from microscopic to macroscopic), relatively independent from each other. On the other hand, there are several fundamental objects at almost every scale in biology, with constant feedback between scales (from large to small included). Furthermore, millions of years of evolution in biology have made interactions between fundamental objects very complicated, whereas in physics seemingly complex phenomena may arise from simple mechanisms at the scale of the atom. Finally, the relation between the microscopic scale and the macroscopic scale in physics is frequently governed by a special constant, called Avogadro's number. It represents the number of discrete microscopic entities forming a single macroscopic entity. Avogadro's number is of the order of 10^{23}. In other words, every macroscopic

entity that physics studies has numerous constituents. As a result, statistical fluctuations of microscopic processes become negligible and gross characteristics arise. In biology, on the contrary, the mesoscale is perhaps the most important and entities in this scale (such as a portion of tissue) may only consist of a few discrete constituents. These fundamental differences between the two sciences and additional ones are highlighted by Newman [2011]. Mogilner et al. [2006] also motivate the use of mathematical modelling in biology and proceed to discuss its successes so far and potential barriers to its future development.

Lazebnik [2004] presents an interesting view regarding the application of mathematics in the field of biology (or more appropriately the lack thereof) in contrast to sciences such as physics or engineering. The language of biology has traditionally been vague and no clear predictions were required according to the author. He argues that the main reason is a flaw in the approach to biological research rather than the admittedly huge complexity exhibited by biological systems. Experimental research has driven the life sciences since their formation and has proved particularly successful in the fields of genetics and medicine. However, denying the need to accompany experiments with techniques from applied mathematics and engineering, the author argues, is as flawed as 'the idea that arithmetic is enough for problems requiring calculus' [Lazebnik, 2004]. In addition, the eminent physiologist Denis Noble discusses the need for combining the dominant reductionist approach with a systems biology approach in his book the 'The Music of Life' [Noble, 2006]. Different strategies for formulating model architectures are introduced and analysed by Noble [2003]. Along these lines, Ideker et al. [2001] developed a comprehensive and fundamental framework for modelling biological systems according to the underlying interactions. Finally, Tomlin and Axelrod [2007] examine such frameworks for systems biology, but in the context of developmental biology specifically.

It is evident that a 'linear' type of logic and intuition alone are insufficient for understanding far more complex networks than those found in engineering, with a huge amount of feedback present between constituents and scales. Therefore, the need to use mathematics in order to truly understand biological processes is even greater than in engineering or physics. As Lander [2004] argues in his essay, it might be more fruitful to approach scientific questions in the biological sciences with a statement of mechanism in mind, as in the physical sciences, rather than a statement of purpose ('teleology'), which is the traditional view.

Over the last 50 years a shift has occurred and mathematical modelling has come to play a significant role in biology. There are various reasons for this shift. First of all, the recent advances in molecular biology and genetics have brought about an enormous amount of data, which need a quantitative approach in order to be manipulated so as to extract useful information. Secondly, over the years it has become apparent to biologists that intuition alone is either insufficient in explaining the vast amount of mechanistic information available to scientists today or, even worse, that intuitive thinking can lead to false conclusions when applied to complex systems. Thirdly, the very large number of studies conducted on very specific biological topics, such as the role of the p53 protein for instance, have dictated the need for a theoretical framework that will combine all this information, thereby allowing researchers to better cooperate and keep track of the advances in the field. Fourthly, there is a strong belief that this mathematical framework may unveil fundamental laws in biology, just as in the case of physics or chemistry, through data fitting and continuous refinement of the models.

Finally, the most recent argument for the use of mathematical models in biology is that researchers will be able to assemble a comprehensive picture of all possible classes of phenomena arising from a specific situation. Originally mathematical models were

data-driven and were almost exclusively used to test hypotheses generated by experiments. The increasingly rapid progress in computing power has allowed scientists to simulate alternative outcomes of an experiment several times, which is especially useful for systems with inherent randomness. Additionally, each repetition of the simulation, unlike an experiment, comes at little or no extra cost. More recently, the focus has been on the qualitative behaviour of a system. The aim is the investigation of all possible behaviours of a system, an exploration of the parameter space and an elaborate comparison of different outcomes. In this fashion models are used as tools to gain understanding of a phenomenon rather than substitutes for reality [Lander, 2004]. This theoretical approach is rapidly gaining ground with respect to the traditional 'data-fitting' modelling approaches for three reasons: (a) it allows scientists to address very specific questions, (b) one can produce a much more comprehensive assay to gain biological insight about mechanistic properties of systems and (c) this approach does not necessitate the determination of parameter values but rather offers the opportunity to investigate behaviours over large parameter ranges. Furthermore, answers to questions beyond the realm of current experimental techniques may be given or at least suggested by mathematical modelling.

1.2 Mathematical Modelling Approaches

Mathematical modelling in biological sciences has its roots in population ecology. Originally, scientists employed linear and nonlinear Ordinary Differential Equations (ODEs) as their tools in order to formulate models describing the temporal evolution of a population. Some very famous examples of such models are the *logistic equation* studied by Verhulst [Verhulst, 1838, Murray, 2002] and the *predator-prey equations* (also known as the *Lotka-Volterra equations*) which were independently investigated by Lotka [1910] and Volterra [1926]. The main aim of these investigations

was to develop simplistic phenomenological models of population dynamics, whose predictions would be compared to actual data, in a similar fashion to how research in physics has progressed for centuries. The two long-term goals were to formulate theories and laws governing the behaviour of population dynamics and the estimation of parameters through data fitting.

Some very simple models proved extremely successful in describing the dynamics of certain systems, such as the growth of a bacterial population in a culture. This encouraged the scientific community to explore further the advantages offered by mathematical modelling. As a result, ecologists started being interested in modelling the spatial distribution of populations as well, which led to the application of Partial Differential Equations (PDEs) in ecological research.

All the early modelling attempts share two common characteristics. Firstly, they follow a deterministic approach, i.e. for a specified initial condition, the model predicts the same outcome for each realisation of the process under examination. Obviously, this approach is very limited, especially when considering processes where randomness plays an important role in determining the outcome. Secondly, models were formulated phenomenologically, i.e. empirical observations of phenomena are used to make certain assumptions required to formulate a simplified model. Furthermore, early models considered a continuum representation of the population density in continuous space and time, thereby neglecting the discrete nature of the individuals constituting a population. Consequently, although simplistic models are easier to analyse and understand, the assumptions involved may not be valid in reality. Moreover, the more parameters we introduce into a model, in order to make it more realistic, the more complicated it becomes to understand and a lot more possible behaviours arise given combinations of values for the parameters.

Deterministic approaches are particularly successful in the treatment of problems

where very few components are involved. However, even a three-body problem (model of the motion of three particles) is quite a complicated system and analytical solutions in closed form often do not exist. Furthermore, the more the particles involved in a system, the harder it is to estimate all of the forces acting on each individual and the higher the degree of uncertainty regarding each individual's location. Even purely combinatorial analysis cannot provide us with helpful information. Therefore, scientists, and in particular the renowned mathematicians Stanislaw Ulam and John von Neumann working in a research group led by Nicholas Metropolis, developed the *Monte Carlo* method, a technique that allows one to examine a problem by observation rather than by 'abstract thinking' alone [Metropolis and Ulam, 1949].

Furthermore, phenomenological modelling requires assumptions that are either justified by means of an established physical principle (Newton's action-reaction law for instance) or *a posteriori*, i.e. by comparing the results of mathematical analysis and computational simulations to experimental results. This modelling approach has proved quite successful in physics and to a lesser degree in other sciences (due to the lack of similar laws). Therein, however, lies a dangerous notion, especially when justifying assumptions *a posteriori*: we are solving a model by making an assumption which is shown to be true using the solution of the model. Furthermore, in many studies, there is no way of justifying or rejecting phenomenological assumptions, at all, as they consider the scale of the tissue and behaviour at the tissue level is a product of interactions between units at lower scales. Therefore, just as in biology, there is a debate about which scale one should be looking at in order to formulate a model. The equivalent of a reductionist approach here is to consider the cellular scale (most fundamental in biology) and model the ongoing interactions instead. Assumptions at lower scales are more realistic than assumptions regarding the level of the tissue due to advances in the fields of molecular and cellular biology, as compared to advances in physiology. The equivalent of a systems biology approach here

is to use our findings from the examination of the individual processes in order to derive the global behaviour of the tissue. As Denis Noble argues, both approaches are necessary in order to achieve complete understanding of biological phenomena [Noble, 2006]. Despite the stark contrast in strategy between the reductionist (breaking down) and the systems biology (putting back together) approach, both are required in order to understand biological behaviour at all levels completely. Note that in physics, multi-scale modelling evolved similarly, starting from Newtonian mechanics (and the theory of Relativity - examples of phenomenological modelling) to describe the macroscopic scale and moving towards a statistical theory (Quantum Mechanics) to describe the microscopic world. Even with the long history and rapid development of physics, the connection between the macro- and the microscopic scales is still something that evades the scientific community, with theories such as String theory, M theory and Loop Quantum Gravity as potential candidates. In other words, we still do not understand how phenomena occurring at the scale of interest can result from some well-studied microscopic interactions.

In the following subsections we discuss some of these limitations further and present some more recent modelling approaches, based on the Monte Carlo technique, that differ in nature from the traditional deterministic continuum approach. We compare the advantages and disadvantages of each method and explain how they can be used in combination in order to provide us with even more insight about biological systems.

1.2.1 Deterministic vs Stochastic Approach

In order to investigate the motion of populations, one may either track the motion of individual particles through space and time (Lagrangian viewpoint) or observe the flow of individuals past a certain fixed point in space (Eulerian viewpoint). The for-

mer approach certainly seems more attractive and suitable for the study of biological motion as it enables the observer to specify fully the motion of an individual. However, it is often the case that such an approach is either extremely difficult or even impossible because of the inherent randomness involved in the motion of individuals. Eulerian flow, on the other hand, allows one to observe the general properties that may characterise a population, i.e. the behaviour of a collection of individuals *on average*.

A random, or *stochastic*[5], process refers to a type of system whose future evolution cannot be fully determined. There are certain possibilities as to how the process may evolve, some more probable than others perhaps, but one cannot know its future state *a priori*. The motion of cells is one such example and in general most biological processes are stochastic in nature. Given that different realisations of a stochastic process may produce a different outcome, it is sensible to try and describe the process in a probabilistic manner, i.e. estimate the chances of each possible outcome. The Monte Carlo method by Metropolis and Ulam [1949] is the most practical way of estimating these chances because it merely comprises of observing the outcomes of the process over a large number of repeated simulations.

A deterministic process refers to a system whose future evolution may be fully determined according to a set of rules and its current state. An observer can thus characterise a deterministic system with absolute certainty given its initial state. Free fall in a vacuum is such an example. Deterministic problems are described by sets of differential equations, whose solution, either by analytical or by numerical techniques, determines the temporal evolution of the system.

Each of these approaches has its own merits and drawbacks. Stochastic models are more realistic as they contain structural details about the population. In addition,

[5]The Greek adjective στοχαστικός describes an approach where one proceeds by guesswork. It derives from the verb στοχάζομαι, which means 'aim at, guess at, ponder at'.

this approach takes into consideration the randomness characterising the actual underlying process. Another significant advantage is that they are intuitively easy to formulate, in contrast to phenomenological models where conservation laws or other, often less reliable, assumptions have to be made in order to derive the governing equations. This also makes it easier to link stochastic models and their parameters to experimental data. Disadvantages include the fact that they are significantly less tractable analytically compared to deterministic models, they are also slower to simulate and each realisation produces a different result, forcing one to perform multiple simulations.

Deterministic models, on the other hand, can be simulated very quickly, are relatively amenable to mathematical analysis and a single realisation is sufficient to generate a complete picture of the behaviour of the system. However, this approach ignores stochastic effects, parameters are harder to link to realistic concepts (and often even harder to measure experimentally) and only the collective behaviour of a group of individuals can be explored.

Our idea is to treat initially the motion of tumour cells as a stochastic process as this is a more appropriate framework. Our objective will be to determine the probability of finding a cell at a certain location at some time. Afterwards, we shall try to obtain some insight regarding the collective behaviour of a tumour cell population and determine whether or not this behaviour obeys a deterministic description. If such a link is established, it will allow us to treat tumour cell migration, a stochastic process, in the framework of a deterministic system. We shall thus be able to use extensively studied mathematical tools, such as PDEs, to describe the motion of tumour cells.

In conclusion, it is very important to note here that an equivalence between a stochastic process and a deterministic model may not always be possible to obtain. Some-

times a single deterministic model may have links to various stochastic processes and different aspects of a single stochastic process may be described by different deterministic models. It may also be the case that deterministic models are used to describe the 'wrong' stochastic process [Mollison, 1977, Mollison et al., 1986, Mollison and Daniels, 1993], as will be discussed in more detail in Chapter 5. Finally, even when such an equivalence is drawn, one must be very careful when considering the deterministic model alone, as the two approaches are definitely not identical. For instance, Okubo and Levin [2001] consider a simple linear birth and death process of a population with a slightly greater birth rate than death rate. The equivalent deterministic model, which expresses the average state of the stochastic process, always predicts exponential growth since the decay rate is lower than the growth rate. The stochastic model, however, allows for the possibility of decay, especially if the population is small. Therefore, the size of the population is critical in establishing a link between a deterministic and a stochastic model. Stochastic fluctuations, which are a result of the randomness characterising interactions at the individual level, tend to become unimportant and to give rise to deterministic behaviour on the average as the number of individuals increases.

1.2.2 Discrete vs Continuum Modelling

Another major distinction between mathematical models is drawn according to whether one needs to treat the underlying variables in a continuum or discrete manner. The former refers to types of models where the underlying variables may assume all possible values within an interval, whereas the latter refers to models where the underlying variables only take certain discrete values from an interval. Although not always the case, most often, discrete models follow a stochastic approach, whereas continuum models are of a deterministic nature. Notable exceptions are *Stochastic Differential*

Equations (SDEs) , for instance the *Smoluchowski equations* [Smoluchowski, 1906, 1916], which fall into the category of stochastic continuum models, and discrete deterministic models such as the *logistic map* [May, 1976].

The choice between a discrete and a continuum model lies in the physical context of the process we are modelling. For instance, a discrete approach is usually more sensible when considering a small population of 10-20 constituents, whereas a continuum approach normally suffices if the population consists of 10000 individuals. The discrete nature of individuals might be lost by the approximation of the population density as a continuum, but other gross characteristics of collective behaviour, which may be more important in describing the process, become evident. There exists a variety of both discrete and continuum models of tumour growth in the literature. Models of invasion, however, are increasingly following a discrete approach, in contrast to traditional approaches where reaction-diffusion equations were much more common, as they retain the cellular identity and usually involve fewer cells.

Cell-based approaches, which are of a discrete nature, aim at modelling the interactions between individual cells. These interactions give rise to local changes, which determine events at the tissue scale. Brodland [2004] has performed a very comprehensive review of computational models of cell-cell interactions and here we provide a brief summary of all the broad categories into which cell-based models fall.

All of the different types of cell-based models share a common framework. They assign a property to the cell-cell or cell-medium interface. This property may result from adhesion, surface tension, it may represent an energetic configuration or the state of a lattice, e.g. the spatial distribution of a population inhabiting the lattice. In every model, the central idea is to find a way of representing the interactions between individual cells.

The two main categories of cell-based models are lattice-based and off-lattice-based

models. Lattice models can be subdivided into *Cellular Automaton* (CA) models and *sub-cellular lattice* (or *Potts*) models. Off-lattice models may be subdivided into *cell-centre* models and *vertex-based* models.

Cellular automata, the simplest and earliest of cell-based models, are essentially simulations that are discrete in time, space and state and often involve lattice sites arranged in a regular grid. The number of possible states for each site may be as low as two, namely an on/off (or empty/occupied by a cell in this case) scheme. As a result, they are very simplistic models that do not usually reflect a realistic situation. They do not take compression or adhesion effects into account (in general) and may be inappropriate for situations where cell movement at long distances is involved as the lattice is fixed. However, this approach has three main advantages. First of all, it enables one to model cellular processes, such as cell proliferation and cellular metabolism, at the individual cell level. Secondly, CA models are simple. Thus, both the implementation and the analysis of CA models is less involved in comparison to other cell-based models. Finally, one can eliminate a certain mechanism from consideration as impossible or at least very unlikely through CA models. Moreira and Deutsch [2002] provide a detailed review of early and recent CA models and show how they can be used in various situations and in very different ways.

In Potts models, cells occupy a number of lattice sites, as opposed to CA models where they occupy a single lattice site. The cellular interactions are usually modelled through an 'energy per unit of interface' function (usually derived from thermodynamic laws) and the resulting state corresponds to a minimum energy equilibrium configuration. Just as in the case of CA models, Potts models are not very involved to implement and can be used to simulate a wide variety of biological phenomena. One of the main disadvantages is that cell boundaries are forced to follow lattice boundaries and so realistic angles are neglected [Brodland, 2004]. Glazier and Graner

[1993] have performed a seminal study of adhesion-driven re-arrangement of cells using cellular Potts models. The authors explained a variety of biological phenomena through the simulation of their Potts models.

Off-lattice models, whether cell-centre or vertex-based models, are mainly used in order to incorporate mechanistic details into the model and make use of the fact that a Voronoi tesselation (decomposition of a metric space determined by distances between a discrete set of points - the centre of the cells in this case) of the plane provides a good approximation of the cell boundaries in two dimensions. On the one hand, cell-centre models represent cellular actions and interactions through a single point, the cell's centre, and geometric changes result from the displacement of this point. In vertex-based models, on the other hand, configurations are produced from the coordinated movement of pairs of nodes. The main advantage of off-lattice models is the meaningful treatment of geometric properties of a cell, such as the cell shape, cell volume, cell surfaces and angles. This property allows cell edge lengths to change smoothly during cellular interactions. The main disadvantages are the fact that the cytoplasm is not considered in the case of vertex-based models and the fact that they are only suitable for modelling cells of isotropic shape in the case of cell-centre models. Pathmanathan et al. [2009] provide a very extensive treatise of mechanical tissue models, highlighting the main differences, advantages and disadvantages of each off-lattice approach.

1.3 Objectives

The long-term goal of modelling PNI is to identify the mechanistic details underlying this special type of tumour spread. Clinical observations and biochemical experiments do not offer a clear picture as to why tumour cells show such a propensity towards

invading the nerve sheath. As a result, there exist various hypotheses, ranging from the up-regulation of the proliferation and migration rates of tumour cells due to the over-expression of nuclear factors, to the existence of a chemical gradient attracting the cells to the nerves due to the over-expression of certain neurotrophins and their receptors. One particular characteristic of PNI, which we intend to exploit, is that it progresses very rapidly towards deeper tissue of up to 4mm, with typical time scales of up to six weeks [Gilmore et al., 2009].

To incorporate all of the experimental observations into a model of tumour invasion is a formidable task, to say the least. Furthermore, deciding on the simplifying assumptions that are necessary is quite difficult. In addition, as we mentioned earlier, there is no great gain from building a realistic but necessarily complicated model which we cannot understand and interpret. We believe that model building can prove much more useful if it is performed incrementally, i.e. start from a very simple model and then extend it by including a new feature each time. In this fashion, one can see the effect of each additional parameter on the overall process.

Our intention is to initially explore several basic mechanisms of cell migration through a comparison of discrete stochastic models with equivalent (in some limit) deterministic continuum models. We begin by investigating the interactions of the individual components of a tumour and then try to see the behaviour that arises at the tissue level, following the notions of systems biology and multi-scale modelling discussed in the previous section. We consider the lower scale first so as to be able to justify the assumptions we make *a priori*.

We work in one dimension since the fastest route for a tumour cell to reach a nerve is a straight line. We shall then try to determine a characteristic time scale for each process under investigation with respect to the rate of migration of tumour cells. Afterwards, we shall introduce additional cellular processes such as proliferation and

death due to the immune response of the organism. Creating this mathematical setting and comparing the models with each other using typical invasion time scales will allow us to make an estimate of the parameter values required to produce an invasion of the epidermal layer of the skin within 6 weeks from the development of the initial tumour site. These parameters, which are model-dependent, will include the rates of cell migration and proliferation, the strength of a potential chemical gradient and the degree of the immune response. This analysis will then be assessed in the light of experimentally generated values for the parameters in order to determine which of the following hypotheses regarding the underlying mechanism behind PNI is more probable:

- Random motion alone is sufficient to produce the clinically observed invasion rate.
- Up-regulation of the tumour cell proliferation rate is necessary and sufficient, while random motion alone cannot produce such rapid invasion.
- A combination of an up-regulated proliferation rate and a reduced apoptotic rate is required to produce the observed invasion rate.
- A strong bias towards the nerve sheath, possibly due to the existence of some chemical attractant, is required in order to produce the observed invasion rate.

1.4 Thesis Outline

In Chapter 2 we present a literature review of PNI. We discuss its clinically observed characteristics and some of the existing evidence regarding its molecular basis. Following that, in Chapter 3, we introduce two modelling approaches, one from the perspective of an individual and the other from the perspective of a population, for each of the four basic models of cell migration considered.

The mathematical tool we use in order to compare the time scales of different migration mechanisms is the theory of *first-passage processes*, studied thoroughly by Redner [2001]. There exist various techniques for estimating the time it takes for a process to reach a certain boundary, each with its unique advantages depending on the specific model under examination. In Chapter 4, we present two such techniques.

In Chapter 5, we incorporate cell proliferation and death into the models of migration. We consider two different models of proliferation, a simple linear birth rate and a logistic-type birth rate that takes limited space and resources into account. We see how these additional processes affect the average time scale of a migration-only process.

Finally, in Chapter 6 we present the results of the comparison between our analysis and numerical experiments with the experimental findings, and the conclusions drawn will be discussed in Chapter 7. An outline of future work is also provided.

Chapter 2

Biological Background

Overview

Perineural invasion was first reported by Cruveilher [1835]. Since then, it has been reported in association with various types of cancer [Hassan and Maksem, 1980, Seefeld and Bargen, 1943, Taylor and Norris, 1967, Ballantyne et al., 1963, Mohs and Lathrop, 1952], but never received sufficient focus as its incidence was thought to be rare, despite suspicions of the opposite [Ballantyne et al., 1963, Ackerman and del Regato, 1954]. Only recently have scientists begun considering the subcellular mechanisms that may drive PNI. In Section 2.1 we summarise some central characteristics of PNI as observed and reported by surgeons, dermatologists, pathologists, oncologists and radiologists. In Section 2.3 we present some of the more recent findings on perineural invasion. These findings are from biochemical studies which have shed light on the possible cellular and subcellular mechanisms behind PNI.

2.1 PNI Characteristics

Reports on perineural invasion vary, particularly with regards to its incidence rate, but in general one can extract several common characteristics from the literature. First of all, every single study we considered shows that PNI correlates with increased aggressiveness compared to tumours that do not present any evidence of PNI [Ballantyne et al., 1963, Mark, 1977, Gormley and Hirsch, 1978, Bourne, 1980, Jacobs et al., 1982, Seki et al., 1993, Lawrence and Cottel, 1994, Fagan et al., 1998, McCord et al., 2000, Brown and Perry, 2000, Ratner et al., 2000, Endrizzi and Seay, 2000, Feasel et al., 2001, Mendelhall et al., 2002, Garcia-Serra et al., 2003, Ayala et al., 2004, Walling et al., 2004, Leibovitch et al., 2005, Geist et al., 2008, Dunn et al., 2009]. Furthermore, all papers show evidence of a correlation with recurrence and reduced survival rate compared to non-PNI tumours. Secondly, the majority of the studies state that the most common locations of the initial tumour site include: the forehead; the cheeks; the maxilla; the eyelids; and the auricular area. The cranial nerves that are invaded more frequently are the facial nerve, and the maxillary and mandibular divisions of the trigeminal nerve. The former's main function is to control the muscles of facial expression, while that of the latter is to process sensory information from the face.

Most clinical papers report that the incidence of PNI in NMSC cases is around 5-6%. However, there are papers that report a higher incidence: Ratner et al. [2000] report an incidence of 6.7%, and 10% of BCC in particular, Lawrence and Cottel [1994] report 14% (having considered SCC only), Garcia-Serra et al. [2003] report 23% of 597 patients and Fagan et al. [1998] report 52% of 142 patients. On the other hand, Brown and Perry [2000] report a 3% incidence, while Dunn et al. [2009] report a 2.5% incidence for SCC and 1% of BCC. However, in their literature review they have noticed that reports vary between 2.5-14% for SCC and 0.18-10% for BCC. Here,

it is worth noting that the majority of clinical papers performed studies with 20-60 patients and therefore the statistics may not be that reliable. Ayala et al. [2004] and Endrizzi and Seay [2000] published a focused study on the molecular basis of PNI in prostate cancer and they reported an incidence of 85% and 48%, respectively. It is evident that there is no agreement on the incidence of perineural invasion between researchers and a discussion on this matter is presented in the next section.

Another characteristic of PNI is that it correlates with greater tumour size compared to non-PNI tumours [Ballantyne et al., 1963, Geist et al., 2008, McCord et al., 2000, Garcia-Serra et al., 2003, Leibovitch et al., 2005], it is more frequent in males (70% on average) and older patients (mean age of 65 years), it is characterised by unpredictable behaviour, a variety of uncommon shapes (described below) and poor cellular cohesion [Gormley and Hirsch, 1978], it invades deeper tissue [Jacobs et al., 1982, Lawrence and Cottel, 1994, Brown and Perry, 2000] than non-PNI tumours and finally, the host's ability to produce immunologic response decreases considerably compared to non-PNI tumours [Ratner et al., 2000].

Observations about shapes, patterns and modes of spread vary, which leads us to believe that perineural invasion employs a variety of spreading mechanisms and is thus unpredictable. Mark [1977] observed tumour nests or 'tongues' extending from the epidermis into the papillary and reticular dermis, surrounded by myxoid connective tissue. He also reports extensive endoneurial growth (however this is uncommon) and that tumour cells lay opposed to but external to the perineurium. Gormley and Hirsch [1978] report that BCC of the scalp presents a diffusely infiltrating pattern, creating tumour nests in the epidermis and forms duct-like structures. Most of the tumour cells are pleomorphic and there exists a propensity for invasion through collagen, fat, fascia, muscle and bone. Jacobs et al. [1982] observed PNI tumour cells in small groups with a spiky or irregular outline and an irregular infiltrating edge as

opposed to non-PNI tumour cells which were organised in large groups with smooth round borders. Moreover, PNI tumour cells demonstrated nuclear pleomorphism and a higher tendency for spindle-shaped nuclei and finally more intercellular bridges (prickles) surrounded by a hyaline stroma. Fagan et al. [1998] report that the most frequent pattern of perineural invasion is the encirclement of the nerve. However, they gathered evidence of less frequent patterns such as 'sandwiching', 'onion-skin' lamination, tangential contact of tumour ribbons and neural permeation. They noticed solid (and rarely non-solid) sheet-like structures, tumour islands and strands (cords or finger-like) and many diffusely arranged individual cells. Furthermore, they observed that non-solid patterns were more invasive and tended to track along a nerve while solid patterns flowed around the nerve.

It seems that PNI may be extremely complicated due to the huge variety of patterns and modes of spread exhibited by PNI tumours. Section 2.2 raises certain questions about the characteristics of PNI we collected from the literature and discusses the possible explanations for these observations.

2.2 Questions and Possible Explanations Regarding PNI

Following the clinical reports on perineural invasion, there are many questions raised. The first and most intriguing one regards the rate of incidence of PNI on the various types of cancer where it occurs. A number of reasons for the disagreement on this matter exist: Firstly, as Fagan et al. [1998] state, most studies and clinical reports do not focus specifically on PNI. Since PNI is hard to identify (especially in the earlier studies where we see that smaller incidence rates were reported), a study which does not focus on PNI may miss a lot of cases. Secondly, most clinical papers

admit that PNI is extremely hard to confirm, especially in the early stages when it is very frequently asymptomatic since no cranial nerves are involved yet. Thirdly, only recently have scientists begun to agree on a more standardised definition of PNI, such as the one proposed by Dunn et al. [2009]. Fourthly, studies, especially older ones and clinical ones, considered a small number of patients, a fact which makes the statistics somewhat unreliable. Note that perineural invasion is a relatively slow process and it may take years before starting to show aggressive behaviour and present symptoms. Finally, as Dr Mohs, the inventor of Mohs Micrographic Surgery, which is currently the most efficient technique against NMSC and PNI, once stated:"of two neoplasms with identical histologic type and equal access to the same nerves, one might show a strong tendency to follow the nerves and the other no such tendency" [Mohs and Lathrop, 1952]. Cancer cells do show a strange affinity for nerve sheaths, but their behaviour may be stochastic rather than deterministic [Ratner et al., 2000, Dunn et al., 2009].

Another interesting aspect of PNI is its higher frequency with SCC and affinity for specific nerves. Ayala et al. [2004] hypothesise that proximity to the nerve may provide greater growth and survival advantages. However, BCC is the carcinoma originating closer to the nerve and not SCC. As far as affinity for certain nerves is concerned, it may relate to the location of the initial tumour site since the most common locations described previously are connected to the facial and trigeminal nerves through a denser innervation.

The correlation of PNI with tumour size and recurrence is also crucial. A possible explanation for the former may be related to the increased aggressiveness exhibited by PNI tumours compared to non-PNI ones. Perhaps their proliferation is uncontrolled at a greater degree which implies a larger tumour size and a propensity to invade deeper tissues. The level of recurrence, however, is very striking. Ballantyne et al.

[1963] and Fagan et al. [1998] suggest that this may be due to a centrifugal/centripetal propagation of SCC along the perineural space. Ayala et al. [2004] believe that this may have to do with increased cell diameter. Other papers suggest that since PNI is very difficult to identify exactly and remove surgically, certain tumour cells that lay undetected during the initial therapy may start proliferating beyond normal restraints again after some time.

Finally, another interesting question regarding PNI is its increased frequency in older males. This may be a natural consequence of the fact that cancer is a disease affecting people more than 65 years old at a considerably higher degree compared to younger people. No hypotheses have been offered as to why PNI is more common in males than females and it might relate to specific hormones or other molecules found only in males. This relates to the next section on the molecular basis of PNI, which is a much more recent attempt to explain the possible causes. However, PNI does not affect men only, which means it might be related to substances that are more abundant in males but not absent in females.

2.3 Molecular Basis for PNI

During the last two decades researchers have begun exploring the molecular basis of PNI. Despite the fact that few studies have focused specifically on the ongoing interactions occurring at the subcellular level during PNI, scientists have found evidence linking the latter with degradative enzymes, neurotrophins, adhesion molecules and survival pathways. Matrix Metalloproteinases (MMPs) have been known to play a key role in tumour invasion by degrading the extracellular matrix and stimulating tumour cell migration via haptotaxis. Their role in PNI is described in Section 2.3.1. Section 2.3.2 describes the findings of the studies that suggest that tumour cells in a

perineural location enjoy survival advantages compared to normal tissue due to the nuclear factor κB (NFκB) pathway. Studies that have demonstrated a correlation between PNI and the levels of Neural Cell Adhesion Molecule (NCAM) are shown in Section 2.3.3. Finally, the links between the Nerve Growth Factor (NGF) and its receptors with PNI are described in Section 2.3.4.

2.3.1 Matrix Metalloproteinases (MMPs)

Kerkela and Saarialho-Kere [2003] examined the relationship between the progression of BCC and SCC and the over-expression of matrix metalloproteinases in their review article. MMPs are degradative enzymes that play an important role in many processes conducted by normal tissue. For instance, reproduction or wound healing are dependent on the controlled degradation of the Extracellular Matrix (ECM). In general, they are highly regulated with regard to secretion and activity at multiple levels, whether that is transcription or secretion or compartmentalisation etc. However, evidence from various recent studies shows that MMPs play a key role in tumourigenesis, neoangiogenesis and metastasis [Friedl and Wolf, 2003, Wolf and Friedl, 2005].

Liotta et al. [1980] found a correlation between MMP levels and the ability of tumour cells to invade surrounding tissue. McCawley and Matrisian [2000] then showed that MMPs have a key role in growth, cell migration and angiogenesis. Furthermore, later studies showed that they can cleave receptors involved in cell adhesion, activate growth factors and enable epithelial cells to invade through basement membranes and form new blood vessels. MMPs can be expressed by tumour, stromal and inflammatory cells and lead to efficient breakdown of the ECM, which leads to invasiveness. As a result, MMPs may play a significant role in the progression of PNI by influencing a favourable environment for rapid cell migration.

2.3.2 NFκB Survival Pathway

Ayala et al. [2004] performed a study on prostate cancer PNI using both an *in vitro* model and human tissue cells. They observed that cancer cells in a perineural position exhibit a reduced apoptotic rate and an increased proliferation rate. Furthermore, they observed an over-expression of certain genes related to proliferation and apoptosis in the same cells, thereby establishing a relation between the two and so deducing that PNI tumour cells may be offered a growth and survival pathway in the perineural space.

In particular, the nuclear factor NFκB along with its downstream targets PIM-2 and Defender Against cell Death (DAD-1) were up-regulated in cancer cells associated with nerves. These cells exhibited a reduced rate of apoptosis, which could be reversed by genistein and BAY 11-7085, an inhibitor of IκB phosphorylation, by lowering the levels of the effectors of the NFκB pathway. They also showed that strong nuclear over-expression and translocation of NFκB (which was present only in 30% of tumour cells within the nerves as opposed to cytoplasmic over-expression which was present in all of them) correlates with reduced survival and recurrence.

Following their observations, Ayala et al. [2004] hypothesize that cancer cells may have different biological capabilities according to the environment that surrounds them. This could explain why PNI cells exhibit increased aggressiveness and higher tumour volume if the perineural environment does indeed offer them a growth and survival advantage through the NFκB pathway or higher levels of neural cell adhesion molecule, or even a minimal resistance pathway. Dai et al. [2005] and Ayala et al. [2006] present further evidence regarding the up-regulation of components of the NFκB in cells located at a perineural environment and the resulting survival advantages gained by tumour cells (reduced apoptotic index).

2.3.3 Neural Cell Adhesion Molecule (NCAM)

Studies have shown that there exists a positive correlation between PNI and levels of NCAM. Li et al. [2003] conducted a study on 50 prostate cancer patients, 42 of whom exhibited PNI. They found that 73% of these cases had NCAM up-regulation compared to non-PNI nerves. Hutcheson et al. [2000] observed a similar relationship in adenoid cystic carcinoma of the head neck, while Seki et al. [1993] reported such a relation in a study of bile duct cancer patients.

NCAM supports neurite outgrowth and stimulates regeneration and is consequently expressed after neural injury. It is also known to mediate cell-to-cell and cell-to-substrate adhesion. Li et al. [2003] suggest that the tumour cells may use a paracrine loop in order to signal the nerves to increase NCAM production. This facilitates cancer cells to migrate toward the nerves and promote adhesion and perineural spread. Migration may be either due to chemotaxis or contact mediation. Furthermore, they deduced that NCAM may trigger specific cascades that induce NFκB (discussed in the next section), i.e. a survival pathway for the tumour cells. The reason is that NCAM binding to a neuron's surface leads to the degradation of the NFκB inhibitor protein, which allows greater quantities to bind to the DNA and increase transcription levels.

2.3.4 Nerve Growth Factor (NGF)

Nerve growth factor is a neurotrophic protein that affects the development and survival of a variety of neural cells. Zhu et al. [1999] found a correlation between NGF expression in human pancreatic cancer cells and PNI, which is present in 85-100% of the total pancreatic cancer cases reported. In particular, NGF and TrkA (a high affinity receptor of NGF) mRNA levels were 2.7 and 5.6 times greater in pancreatic

tumour cells, respectively, compared to normal pancreas tissue. NGF was strongly present in the cytoplasm of the tumour cells, while TrkA was present in the perineurium of pancreatic nerves. Furthermore, they observed that PNI was more frequent with tumours that expressed high NGF and TrkA levels. The authors assumed that since TrkA binds to NGF in the perineurium in order to induce nerve growth and axonal regeneration in normal tissue, it may act as a positive chemotaxin (rather than NGF itself) that facilitates contact with target tissues and thus mediates tumour invasion.

The next example comes from a study on neurotrophin expression and the corresponding receptors in stromal and epithelial cells of the prostate. Dalal and Djakiew [1997] found that muscle stromal cells expressed NGF, Brain Derived Neurotrophic Factor (BDNF) and TrkC while epithelial cells expressed TrkA, TrkB and TrkC in two prostate cell lines. The results suggest that firstly NGF and BDNF interact with TrkA and TrkB via paracrine mechanisms and secondly that the malignant transformation of epithelial tumour cells in the prostate may lead to an autocrine expression of neurotrophins and a paracrine independence on stromal cell derived neurotrophins. Therefore, the invasion capabilities of the tumour cells may be extended through the up-regulation of this autocrine expression of neurotrophins.

Di Marco et al. [1993] assert that NGF binds to normal human keratinocytes through high (tropomyosin receptor kinases) and low affinity ($p75^{NGFr}$) receptors which mediate its activity. In addition, they show that it plays a key role in epithelial cell proliferation through an autocrine loop and that its receptors' activity decreases once differentiated and fully stratified epithelium is obtained. Iwamoto et al. [1996] reinforce the conclusions drawn for the role of the p75 receptor in their study on perineural spread of desmoplastic melanoma. They found a strong correlation between the expression of the p75 receptor and desmoplastic melanoma, which is a variant with a

known propensity for neurotropism. This supports the hypothesis that PNI involves p75, an NGF receptor, and its ligands.

A more recent study attempted to provide some further insight on the effect of neurotrophins on perineural spread. Chen-Tsai et al. [2004] conducted a study involving 4 PNI BCCs, 5 PNI SCCs, 4 non-PNI BCCs and 3 non-PNI SCCs in order to check for expression of NGF, TrkA, TrkB, TrkC, $p75^{NGFr}$ and NCAM. Their objective was to try and link all of the above factors to PNI and produce a clearer picture on their effects since previous studies established links to perineural spread but no concrete theory of how the mechanism works. Their results are described briefly below. Increased NCAM expression was exhibited in 75% of all BCCs and 25% of SCCs (regardless of perineural invasion). All BCCs expressed high levels of NGF while 7 of 8 SCCs expressed NGF at lower levels. 87% of BCCs expressed TrkA, TrkB and TrkC, of which all PNI-positive expressed very low amounts. On the other hand, 75% of non-PNI BCCs expressed high levels. These receptors were also expressed by 75% of SCCs, with PNI-positive ones exhibiting greater amounts. $p75^{NGFr}$ was expressed at a high or moderate level by 75% of BCCs, but different spatial patterns were observed according to the presence of PNI. The positive ones exhibited an equal staining perineurally as well as elsewhere in the tumour while the negative ones exhibited staining only at the edges. In the case of SCC, 7 of 8 expressed $p75^{NGFr}$, with PNI-positive ones exhibiting higher intensity. The authors conclude that NCAM cannot be regarded as a PNI indicator, but may play a role in the adhesive and motile behaviour of malignant cells and in their growth regulation. Trk expression may be a predictor of perineural invasion in SCCs but not in BCCs. NGF was present in almost every tumour specimen so they speculate that in an NGF-rich microenvironment SCCs may up-regulate the expression of $p75^{NGFr}$, or down-regulate its degradation, and $p75^{NGFr}$ may in turn prevent a tumour necrosis factor-mediated immune response against malignant keratinocytes.

Evidently, neurotrophins play a key role in various aspects of perineural invasion, such as invasiveness and metastatic potential, regulation of proliferation, survival and infiltration patterns. The exact mechanism is not yet understood and may be quite complicated. However, recent studies at the molecular level have offered us several suggestions and a number of hypotheses that scientists are currently attempting to test.

Summary

In this chapter, we described the clinical characteristics of PNI and reviewed some of the existing evidence on possible sub-cellular mechanisms behind PNI. As we saw, PNI exhibits certain particular features that distinguish it from other types of tumour invasion. The variety of shapes of invasion (with a tendency towards 'disconnected island' or 'finger-like' patterns[1]) and the short time scale of invasion, in particular, are two of the most useful characteristics of PNI, since they can be used for a qualitative comparison between possible mathematical models and the actual process.

Apart from these central properties, PNI exhibits other important characteristics such as a correlation with recurrence and a reduced survival rate, a correlation with a greater tumour size compared to non-PNI tumours, a correlation with older male patients and finally poor cellular cohesion. All of these observations give rise to several questions regarding perineural spread. However, they may also be used as a foundation for mathematical modelling treatises on the subject. We shall use the average time scale of PNI as the basis of our study.

In Section 2.3, we saw that there are at least four potential sub-cellular mechanisms

[1]Such patterns cannot be reproduced by a one-dimensional model so one would have to consider higher-dimensional geometries to investigate PNI from this perspective (see Chapter 7 for a discussion).

involved in perineural spread. All the mechanisms we described may be connected to cellular- or tissue-level characteristics of tumour invasion and so they offer potential hypotheses for the mechanism behind PNI. In particular, the NFκB pathway may be involved in the up-regulation of the proliferation rate and the reduction of the apoptotic rate of tumour cells. NGF, NCAM and MMPs may be involved in the creation of a chemical gradient that induces active migration towards the nerve sheath. Consequently, one can assess, at least qualitatively, the role of these sub-cellular mechanisms on PNI and distinguish between NFκB and the other three if more is known about the tissue-level mechanism behind PNI.

Mathematical modelling enables a quantitative comparison between the different possible tissue-level mechanisms of invasion. Initially this comparison will be entirely within a theoretical frame, which will allow us to define and explore the effect of important parameters on each process under study. At a later point, this framework will prove useful upon relating it to the biological problem, the early stages of PNI, and comparing the simulations with experimental observations and data regarding realistic parameter ranges. In the following chapter we introduce some basic models of cell migration and discuss their merits and limitations.

Chapter 3

Models of Cell Migration

Overview

Biological dispersal, i.e. the spread of a population of individuals, is a very frequent phenomenon in the lifetime of many organisms. It might often be favourable for the survival of both animals and micro-organisms to abandon their site of inhabitation and migrate to a new environment where the competition for resources will be less limited. Although organisms actively seek to put themselves in an advantageous position, the movement of two individuals of the same population in the same environment is not identical. Consequently, it is necessary to treat the motion of organisms as a random process.

The movement of tumour cells (or any other population of particles) may be examined from two different perspectives: either by tracking the spatial location of a single individual or by observing the density of individuals over the spatial domain of interest. In the former approach, the *random variable* under consideration is the location of the individual at each point in time. Its probability distribution is sufficient for describing the motion completely. This approach led to the formulation of the so-

called *random walk* models, which are defined and discussed in Section 3.1, where we introduce the reader to the some of the most significant studies in the existing literature on the topic. For a comprehensive review of all types of random walk models and their applications in biology the reader is directed to the work of Codling et al. [2008]. Random walk models, an example of discrete stochastic models, can generally be classified into two basic categories, in both continuous and discrete form, which will be defined in Section 3.1.

The second approach, on the other hand, considers the spatial distribution of a population of particles and as such the number of particles over the entire domain is treated as a random variable. This formulation is more appropriate for systems where particle division or loss is observed. An example of such a system is that of a chemical reaction, a process consisting of molecules colliding with each other to form different molecules (and hence molecules of a certain type are created, while molecules of a different species are annihilated). In fact, quite a few of the techniques based on this approach were developed within the field of chemical kinetics. The stochastic models that are formulated within the context of population redistribution may be treated analytically by the so-called *Reaction-Diffusion Master Equation* (RDME) formulation, i.e. the derivation of a governing equation that describes the temporal evolution of a system which can be in a countable number of states at a given time. Furthermore, in this context the models can be simulated more efficiently through *Gillespie's Stochastic Simulation Algorithm* (SSA) [Gillespie, 1977] than through a simple Monte Carlo algorithm. We shall introduce this approach and review the origins of the techniques we employ in Section 3.2.

3.1 Spatial Location of a Single Individual: Occupation Probability Approach

One of the most widely used and extensively studied category of mathematical models of animal dispersal is that of random walk models. The term 'random walk' refers to the mathematical formalisation of a process which forms a trajectory consisting of successive random jumps from one point to another. The underlying random variable is usually a spatial variable defining the location of the individual under examination. This is the case, for instance, when studying the migration of tumour cells or the motion of a molecule as a random walk. However, this need not always be the case as random walks are perfectly suited for describing any process involving random successive jumps from one state of the random variable to another. The financial status of a gambler is such an example.

The earliest and most intuitive model, the *Simple Random Walk* (SRW) model, was used to describe the irregular motion of pollen particles in plants, first observed by Brown [1828] and thus termed *Brownian motion*. The model was first posed as a problem by Pearson [1905] in the journal *Nature* and a response was subsequently published by Rayleigh [1905]. Physicists were quickly attracted to the subject due its wide applications and as a result emerging theories and fields were developed. Some of the original mathematical contributions are due to Albert Einstein [Einstein, 1905, 1906] and the pioneer of statistical physics Marian Smoluchowski [Smoluchowski, 1906, 1916]. Physicists Adriaan Focker and Max Planck then derived a differential equation that describes the temporal evolution of the probability density function of the velocity of a particle, the *Fokker-Planck* equation. It can be generalised to any other observable as well and is a valuable tool in connecting a stochastic process with an equivalent deterministic model. Chandrasekhar [1943] published an elaborate

treatise of random walk models and their application to physical systems, while Berg [1983] provides a very interesting but non-technical introduction to random walk models as used in biology. A more technical and more general introduction to the topic of stochastic processes is that by Gardiner [1985]. Montroll and collaborators also examined various properties of lattice-based models analytically and have presented their results in a series of papers [Montroll, 1956, Montroll and Weiss, 1965, Montroll, 1969]. One other noteworthy and extensive study of models of animal motion and cell migration is that by Okubo [1986], with a focus on the approximation of discrete stochastic processes by continuum deterministic models in certain limits.

The SRW model is the basis of most theories regarding random walk models and diffusive processes. There is no overall bias towards one direction, i.e. the walker is equally likely to move in every possible direction, nor is there any correlation between steps, i.e. the walker ignores its previous direction upon deciding where to move next. Hence successive jumps are completely independent and the process is Markovian[1] with regards to the spatial location. Jumps occur at a constant rate. The probability of finding a particle at a specific location at some fixed time can be shown to satisfy the simple diffusion equation as the number of steps becomes very large [Edelstein-Keshet, 2005, Murray, 2002, Okubo and Levin, 2001, Skellam, 1973].

The SRW model is quite simplistic as far as actual biological dispersal is concerned. Its mathematical formulation is clearly too restrictive for systems where some form of *taxis* (response due to a directional stimulus) due to the environment exists, systems where persistence in the direction of motion is observed, systems where random time intervals between successive jumps elapse etc. As such, there are several extensions to the SRW model.

The simplest extensions to the SRW model include the introduction of a global di-

[1] A *Markov* process refers to a stochastic process where the future state of the system depends only on its present state and is independent of all its past states.

rectional bias and a waiting time between jumps. In this model, which is termed a *Biased Random Walk* (BRW), we consider a walker who has a greater probability of moving in a certain direction. Othmer [1988] generalised the framework within which such jump processes should be considered in the context of population redistribution. Uncorrelated random walks, such as the SRW and BRW models, are classified as *position-jump processes*, since it is the position of the walker that involves random changes. Othmer and Hillen [2002] derived a correspondence between the stochastic process and a deterministic model of chemotaxis derived phenomenologically.

Another important extension includes the consideration of a correlation between successive step orientations. Physically, this notion often represents the *persistence* of animals to their previous direction of motion. Correlation between successive jumps produces a local directional bias as the walker is more likely to move in its previous direction although there is no preferred direction overall. This model is termed a *Correlated Random Walk* (CRW) and was originally formulated and studied independently by Goldstein [1951] and Kac [1947], which is why it is sometimes referred to as the *Goldstein-Kac* model. Obviously, this process is not Markovian with regards to the location. However, the walker will change direction with a certain probability and all such turning events are independent of each other. Hence, the process is Markovian with regards to the velocity. Othmer [1988] showed that CRWs should be considered within a different framework from uncorrelated random walks. In particular, if correlation is present, then the velocity of the walker changes randomly at every step, therefore such processes are categorised as *velocity-jump processes*. Position-jump processes can be shown to be asymptotic approximations of corresponding models that belong to the latter class and are generally valid only for large time scales. Hillen and Othmer [2000] derived a deterministic model that describes the limiting behaviour of such a process (see Renshaw and Henderson [1981] and Weiss [2002] for an extensive analysis of the CRW model). Finally, we should mention that if a global

bias exists in a correlated model, then the process is termed a *Biased and Correlated Random Walk* (BCRW) .

In the following section we introduce a different perspective for considering the same jump processes. We track the behaviour of a population of particles rather than the motion of an individual particle.

3.2 Distribution of Individuals in Space: Master Equation Approach

So far, we have discussed random walks in the context of a single individual. We considered the probability that an individual lies at a specified location in space at some specified time. However, it is often more practical to consider several individuals performing the same process independently at the same time and examine their spatial distribution. This approach will enable us to simulate a stochastic process exactly, as would be the case with a Monte Carlo method, but faster and more efficiently, especially in the case of models of processes such as cell proliferation and death. The population approach is equivalent to the individual approach as long as we are dealing with non-interacting particles. As such, we expect the individual and population models to produce the same output when we consider migration only. Once proliferation is incorporated into the model, the particles start interacting with each other and hence differences between the two approaches will arise. In Chapter 5 we discuss why the individual approach is more appropriate for our purposes in such a case.

Gillespie [1976] introduced a numerical method for simulating the temporal evolution of stochastic processes, the so-called *Stochastic Simulation Algorithm* formally defined by Gillespie [1977] (for a practical guide see Erban et al. [2007]), which was also

developed independently and in a different form by Kurtz [1972]. Initially, the algorithm addressed the simulation of systems of chemical reactions specifically. Gillespie showed that the SSA is equivalent to treating the same process analytically using the RDME formulation and later performed a rigorous derivation of the master equation, starting from the underlying physical principles governing a chemical reaction [Gillespie, 1992, 2007]. Furthermore, Gillespie also established that the RDME formulation may be approximated by Langevin-type equations, i.e. SDEs, and examined the reliability of deterministic models in approximating the 'stochastically correct' master equation [Gillespie, 2000]. Bimolecular reactions (two interacting species are involved in the reaction) were considered by Gillespie [2009] and Erban and Chapman [2009], while appropriate boundary conditions were studied by Erban and Chapman [2007]. The SSA and many techniques from chemical kinetics may also be used in the context of a jump process and will form the basis for treating models involving particle division or loss.

In Section 3.3, we shall formally define the two simplest position-jump processes, i.e. the SRW (Section 3.3.1) and BRW (Section 3.3.2) models. When viewed from a macroscopic continuum perspective, these two discrete stochastic processes can be shown to produce the same behaviour as a diffusion and an advection-diffusion process, respectively. In Section 3.4 we introduce the two stochastic models corresponding to velocity-jump processes, the CRW (Section 3.4.1) and BCRW (Section 3.4.2) models. These two models can be shown to produce the same behaviour as an unbiased and a biased telegraph process, respectively.

These four models of migration will form the foundation for the ensuing analysis in the rest of the thesis. Each model will first be formulated from the perspective of a single individual and examined in what will be termed an *Individual Approach* in what follows. Afterwards, we shall formulate each model and treat it from the

perspective of the entire population, in what will be termed a *Population Approach*. We shall thus formulate two stochastic models for each of the four different stochastic processes (with the exception of the BCRW model for reasons discussed in Section 3.4.1.3).

3.3 Position-Jump Processes

3.3.1 Simple Random Walk

3.3.1.1 Individual Approach

Model Formulation

Consider an individual particle (also referred to as 'walker' or 'jumper' hereinafter), which may represent a biological cell, placed at some point on an infinite one-dimensional uniform lattice. The lattice is separated into discrete points, each a distance Δx apart. The particle can move a fixed distance Δx either to the right or to the left in a fixed time Δt. The motion of any type of particle considered in this thesis is characterised by inherent randomness. Consequently, there is a certain chance associated with jumping to a neighbouring lattice site during a time interval Δt. This chance will be represented mathematically using the notion of a probability measure.

Our first assumption is that the motion of the particle is completely random without any directional bias. As such, the probability of moving either to the right or to the left is equal to $\frac{1}{2}$. Therefore, a particle placed at position x at time t will be found either at $x + \Delta x$ or $x - \Delta x$ at time $t + \Delta t$. One could also allow for the possibility that the particle does not move during the time interval Δt, i.e. introduce a waiting time between jumps. In that case, the probability of moving in either direction would

be, say, α, with $0 < \alpha < \frac{1}{2}$ and the probability of waiting would be equal to $1 - 2\alpha$. We formally incorporate a waiting time into the following model, the BRW, as the SRW model is only a special case of the BRW with a zero bias and the technique introduced to analyse the BRW is more practical and easier to manipulate in order to examine the effect of the waiting time.

Our second assumption is that successive steps are completely independent of each other, i.e. the motion of the particle does not depend on any of its previous actions (Markovian process).

Suppose we place a particle at the origin $x = 0$ at $t = 0$. At $t = \Delta t$, there is an even chance that the particle will be found at $x = \Delta x$ or $x = -\Delta x$. At $t = 2\Delta t$, the particle may be found either at $x = 2\Delta x$ or $x = -2\Delta x$ with a probability equal to $\frac{1}{4}$ or it will have returned to the origin with a probability equal to $\frac{1}{2}$ (as it can move to the origin both from $x = \Delta x$ and $x = -\Delta x$). Note that after an odd number of steps, the particle will be at an odd distance away from the origin, while after an even number of steps, it will be at an even distance from the origin.

Occupation Probability

In order to investigate a stochastic model formulated from the perspective of the individual, we need to study the individual's occupation probability. This is defined as the probability that a particle will be found at a position $x = m\Delta x$ ($m > 0$) after n time steps ($m \leq n$). It will be denoted by $p(m, n)$ in the discrete model and, using combinatorial theory (for a derivation see Section A.1.1 of Appendix A), it can be shown to satisfy the following expression

$$p(m,n) = \left(\frac{1}{2}\right)^n \cdot \binom{n}{\frac{n+m}{2}} = \frac{n!}{2^n(\frac{n-m}{2})!(\frac{n+m}{2})!}, \tag{3.1}$$

with $n \pm m$ even (odd[2]) since n, m are even (odd). The function $p(m, n)$ is the probability mass function of the binomial distribution with $p(m, n) = 0$ for m odd (even) and as expected

$$\sum_{m=-n}^{m=n} p(m, n) = \left(\frac{1}{2} + \frac{1}{2}\right)^n = 1.$$

Being interested in the long term behaviour of the particle, i.e. as $n \to \infty$, and seeking to understand if there is an underlying pattern or structure in the motion of the particle, we may use Stirling's approximation of factorials to obtain a simplified expression for (3.1). For $n \to \infty$, $m \ll n$, $m \gg 1$, equation (3.1) may be approximated by

$$p(m, n) = \sqrt{\frac{2}{\pi n}} \exp\left(-\frac{m^2}{2n}\right). \tag{3.2}$$

Section A.1.2 of Appendix A provides the details of the approximation. Fig. 3.1 shows that the approximation is quite accurate even for relatively small values of n and m. Note that the probability $p(m, n)$ is zero for m odd since all values of n are even. This is not the case, however, if we consider a waiting time between jumps, i.e. include a non-zero probability that the walker will attempt no transition during one time step into the model (see generalisation in Section 3.3.2). The SRW model we have presented is a discrete stochastic model since we have considered a random process over a discretised spatial domain in discrete time steps. All the information regarding the location of the individual after n ($n \in \mathbb{N}$) time steps is given by the probability mass function (3.1). However, we may be interested in a continuum description for space and time if it is more suitable for the process under study.

In such a case, in order to exploit the information provided by the discrete model, we must let $\Delta x \to 0$, $\Delta t \to 0$ and $n \to \infty$, $m \to \infty$ in such a way that $x = m\Delta x$

[2]We can examine the case n, m odd in the exact same fashion.

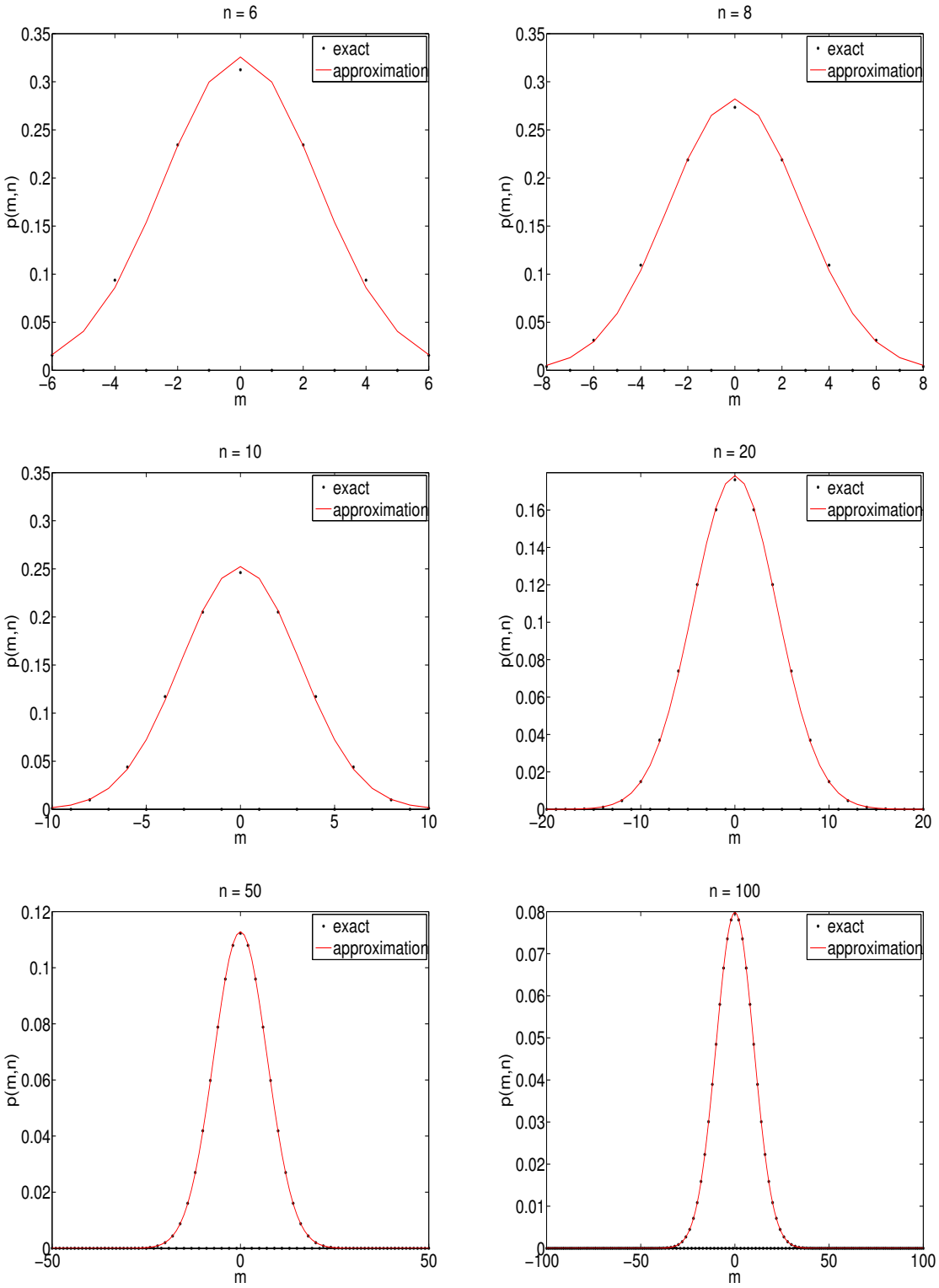


Figure 3.1: Plot of the probability mass function $p(m, n)$ given by (3.1) and its approximation given by (3.2) for (a) $n = 6$, (b) $n = 8$, (c) $n = 10$, (d) $n = 20$, (e) $n = 50$ and (f) $n = 100$. Note that for m odd, $p(m, n) = 0$.

and $t = n\Delta t$ are finite. We can then define the occupation probability, $p(x, t; x_0)$, as the probability that a particle, released at $x = x_0$ at $t = 0$, is located in the interval $(x, x + \Delta x)$ after time t. This is related to $p(m, n)$ by the formula

$$\lim_{m,n\to\infty} p(m, n) = \lim_{\Delta x\to 0} 2\Delta x \cdot p(x, t),$$

where we omit $x_0 = 0$ for ease of notation. This relation results from the fact that the probability of finding our walker at a certain interval in the discrete model is equivalent to the probability of finding our walker at any location within the same interval in the continuum model. The factor '2' reflects the fact that n, m are either both even or both odd in the discrete model, whereas the continuum model shares no such restriction. After some algebra and by defining the constant, D, as

$$D = \lim_{\Delta x,\Delta t\to 0} \frac{\Delta x^2}{2\Delta t},$$

where we require this limit to be positive and finite, we obtain

$$p(x, t) = \sqrt{\frac{1}{4\pi Dt}} \cdot e^{-\frac{x^2}{4Dt}}, \tag{3.3}$$

which is the fundamental solution of the *diffusion equation*,

$$\frac{\partial p}{\partial t} = D\frac{\partial^2 p}{\partial x^2}, \tag{3.4}$$

where D is the *diffusion coefficient*, with a point source as an initial condition, $p(x, 0) = \delta(x - x_0)$, and boundary conditions of the form

$$\lim_{|x|\to\infty} p(x, t) = 0.$$

This result shows that the occupation probability of the stochastic model obeys a

deterministic model only in a certain spatiotemporal limit specified by the definition of the constant D. The approximation fails if the process is taking place far from this limit. Note also that if we define the *instantaneous velocity* of the jumper by

$$v = \lim_{\Delta x, \Delta t \to 0} \frac{\Delta x}{\Delta t} = \lim_{\Delta x, \Delta t \to 0} \frac{2D}{\Delta x} \to \infty,$$

we see that it becomes infinite in the limit $\Delta x \to 0$, which is a severe limitation of the SRW model and position-jump processes in general.

While a random walk model may be fully described by the distribution of the occupation probability, it is often more practical to consider only the first two moments of the walker's spatial location, the random variable denoted by X_t. Physically, the first moment, the *mean location*, denoted by $E(X_t)$, represents the 'average location of the walker in time', whereas the second moment, the *mean squared displacement*, denoted by $E(X_t^2)$, represents the 'average amount of fluctuations' from the origin. It is often more useful to consider the variance, denoted by σ_t^2, which represents the amount of fluctuations from the mean location. These are formally defined in Section A.1.3 of Appendix A.

The expected location of a particle, which is released at the origin and is performing a simple random walk, can be derived through the substitution of equation (3.3) into the expression for the first moment. It is equal to

$$E(X_t) = 0, \tag{3.5}$$

i.e. the origin. This result indicates that, on the average, no overall movement occurs. The interpretation is that the particle has no preferred direction. The MSD

and variance, both equal in this case, are given by

$$E(X_t^2) = \sigma_t^2 = 2Dt. \tag{3.6}$$

Evidently the MSD increases linearly with time, a standard property of a diffusive process. Fig. 3.2 shows a plot of the mean location predicted by the stochastic model over (a) 100 and (b) 10000 realisations. The red solid line represents the analytical expression of the deterministic equivalent, given by equation (3.5). Fig. 3.3 compares the variance of the individual's motion predicted by the stochastic and deterministic models, respectively. Both figures show that the deterministic model can only make accurate predictions and approach the stochastic model if the number of simulations is large enough. The *Law of Large Numbers* [Grimmet and Stirzaker, 2001] provides a theoretical foundation supporting this observation. In fact, the *Central Limit Theorem* [Grimmet and Stirzaker, 2001] implies that the error between the mean location of a stochastic model and its theoretical value decreases with the square root of the number of simulations.

3.3.1.2 Boundary Conditions (BCs)

So far, our analysis is entirely theoretical. Once we apply it to the biological problem under examination, we shall have to consider the actual geometry of the tissue in question. Throughout this thesis, we assume as simple a geometry as possible, in one dimension for reasons mentioned earlier and which will be discussed more extensively in Chapter 7. However, a minimum requirement upon consideration of the biological properties of this geometry, is to introduce boundaries into the model which will represent the edge of the skin and the nerves lying in deeper subcutaneous tissue. Therefore, we consider a reflective boundary at the left end of the domain, $x = 0$, to represent the edge of the skin, and the epidermis in particular. At this boundary,

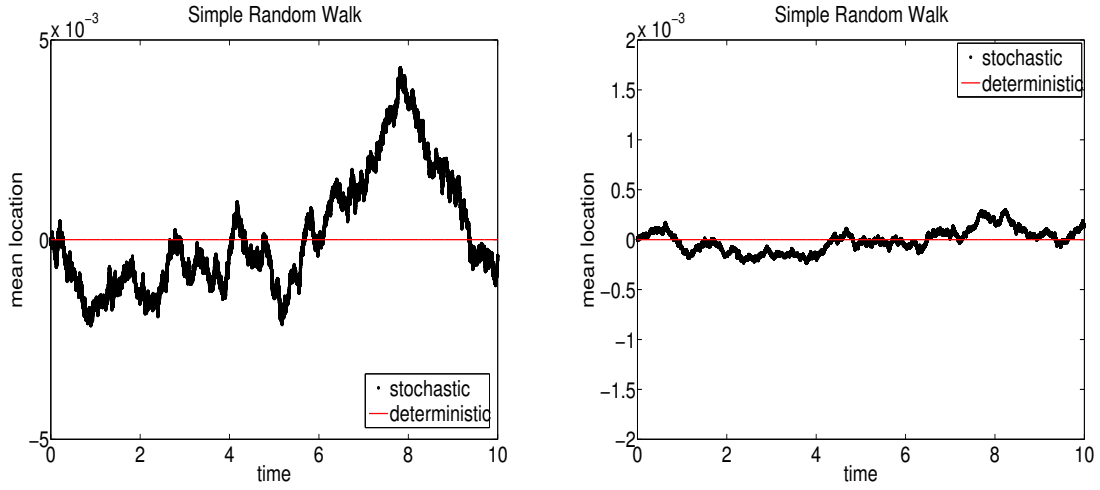


Figure 3.2: Plot of the evolution of the mean location, $E(X_t)$, over time in the SRW model (in black dots) versus the analytical expression obtained from the deterministic model given by equation (3.5) (red solid line). The left and right panels show the results over 100 and 10000 simulations, respectively. We have used $\Delta x = 10^{-4}$ and $\Delta t = 5 \cdot 10^{-5}$ ($D = 10^{-4}$).

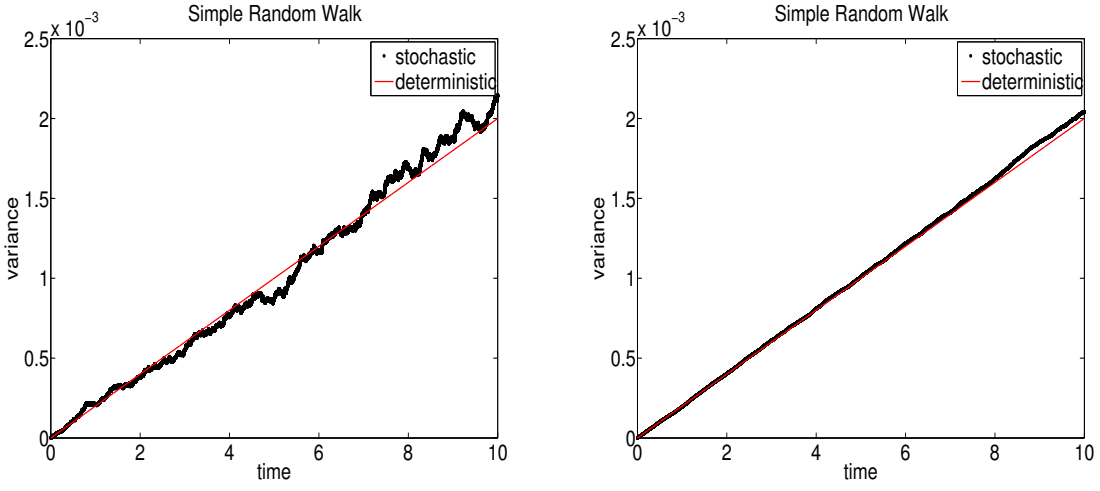


Figure 3.3: Plot of the evolution of the variance, σ_t^2, over time in the SRW model (in black dots) versus the analytical expression obtained from the deterministic model given by equation (3.6) (red solid line). The left and right panels show the results over 100 and 10000 simulations, respectively. We have used $\Delta x = 10^{-4}$ and $\Delta t = 5 \cdot 10^{-5}$ ($D = 10^{-4}$).

we require that no cell can escape the domain. At the right end of the domain, $x = L$, we consider an absorbing boundary to model a permeable surface, a nerve in particular. For more complicated BCs as well as a more extensive discussion and a derivation of the corresponding BCs in the deterministic model, we refer the reader to Section 3.3.2. The random walk model introduced in Section 3.3.2 can be regarded as a generalisation of the SRW model and the techniques presented in that section are more suitable for a derivation of the BCs.

3.3.1.3 Population Approach

Model Formulation

As we mentioned in the introductory sections of this chapter, we shall examine each stochastic process we consider from the viewpoint of a population. The notation and schematics we introduce in this section are going to be used in every section termed 'Master Equation Approach' for each of the stochastic processes.

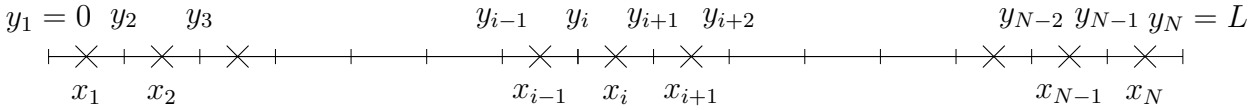
Consider a population of individuals moving on the one-dimensional domain $x \in [0, L]$. We separate our domain into N equal intervals of size Δx and denote each discrete point by

$$y_i = i\Delta x, \quad i = 0, ..., N,$$

where $\Delta x = \frac{L}{N}$. Each compartment or interval is centred at

$$x_i = \left(i - \frac{1}{2}\right)\Delta x, \quad i = 1, ..., N.$$

Each individual is restricted to move on the grid defined by x_i, as the following schematic shows.



We are now interested in the number of individuals in the i-th compartment of the domain, the random variable u_i, and wish to observe the evolution of the density of individuals over the entire spatial domain, $\mathbf{u}(t) = [u_1(t), u_2(t), ..., u_i(t), ..., u_N(t)]$, in time. We also use the term u_{N+1} to denote the number of individuals in the immediate interval to the right of the domain.

Initially n_0 particles are released at some point in the domain. We consider a reflective boundary at point $y_1 = 0$ and an absorbing (or partially absorbing) boundary at $x = L$ in every stochastic process we study. A particle has an even chance of moving right or left so all possible transitions during one time step may be represented schematically by the following diagram

$$u_1 \underset{d}{\overset{d}{\rightleftharpoons}} u_2 \underset{d}{\overset{d}{\rightleftharpoons}} ... \underset{d}{\overset{d}{\rightleftharpoons}} u_{i-1} \underset{d}{\overset{d}{\rightleftharpoons}} u_i \underset{d}{\overset{d}{\rightleftharpoons}} u_{i+1} \underset{d}{\overset{d}{\rightleftharpoons}} ... \underset{d}{\overset{d}{\rightleftharpoons}} u_{N-1} \underset{d}{\overset{d}{\rightleftharpoons}} u_N \xrightarrow{d} u_{N+1}, \tag{3.7}$$

where u_i denotes the total population in the i-th compartment and d denotes the transition rate. We do not specify its value yet; we rather derive an appropriate rate so that an equivalence with a deterministic model is drawn.

The boundary conditions are evident in the sketch by considering the possible transitions from the first and last compartments. In the latter case, we have added the compartment x_{N+1}, which is outside the domain, for ease of comprehension. We are not interested, unless otherwise stated in later chapters, in the population density of the $(N+1)$-th compartment. Note that if a particle is located in the left-hand end of the domain at some time and attempts to move to the left, it will be reflected back in the same interval. Thus, a transition to the left of x_1 is impossible. If the particle is located at the right-hand end, and attempts to move to the right, it will be absorbed without any chance of returning, hence the transition from interval $N+1$ to interval N is also impossible.

To complete the formulation of this stochastic model, we define the rules regarding

possible transitions. In particular, the probability that a transition from interval i to interval j, $i, j = 1, ..., N$, occurs in the time interval $(t, t + \Delta t)$ is taken to be proportional to the density of individuals in the compartment and is thus equal to

$$T(j|i) = d \cdot u_i(t)\Delta t, \;\; j = i \pm 1, \quad T(j|i) = 0, \;\; \forall j \neq i \pm 1. \tag{3.8}$$

The transition rules at the boundaries are given by

$$T(1|0) = 0, \;\; T(0|1) = 0, \;\; T(N|N+1) = 0, \;\; T(N+1|N) = d \cdot u_N(t). \tag{3.9}$$

One can define $\alpha_i = d \cdot u_i(t)$, which is similar to the notion of a *propensity function* in the study of chemical reactions. For ease, we also use the term hereinafter and each stochastic model that follows shall be formulated with regards to its propensity functions $\alpha_i(t)$, which will mean that $\alpha_i(t)\Delta t$ is the probability of a possible transition from interval i.

If we simulate the stochastic model in the usual fashion, as was the case with the algorithms used to simulate the stochastic processes in Section 3.1, a random number will be drawn for every compartment at each time step in order to determine the occurrence or non-occurrence of a transition. Note that it is too costly, computationally, to have to generate N random numbers so as to simulate a stochastic process during a single time step. For instance, if an event occurs with a probability equal to $\frac{1}{1000}$ every time step, one has to simulate 1000 time steps for the event to occur once, using 1000 random numbers, which seems inefficient. Instead, Gillespie's SSA requires only two random numbers to simulate exactly one occurrence of an event [Gillespie, 1976, 1977, Erban et al., 2007]. The first random number is used to determine when the next transition occurs while the second one is used to determine which transition, from a set of all possible transitions, occurs next. We present the details

of the algorithm used to simulate this model in Section A.1.4 of Appendix A.

Population Density

In order to relate this stochastic model to a deterministic one, we must consider all the possible states of the spatial distribution of the population and this can be done by using the RDME formulation. To begin, we define $P(\mathbf{n}, t; \mathbf{n}_0)$ as the probability that the density of individuals, $\mathbf{u}$, is equal to $\mathbf{n}$ at time t, given that it was at state $\mathbf{n}_0$ at $t = 0$. For ease of notation, we shall often use $P(\mathbf{n}, t)$ or $P(\mathbf{n})$, instead to denote the same probability. Define further the operators $R_i : \mathbb{R}^N \to \mathbb{R}^N$, for $i = 1, 2, ..., N$ and $L_i : \mathbb{R}^N \to \mathbb{R}^N$, for $i = 2, 3, ..., N$ by

$$R_i : \mathbf{n} \to [n_1, ..., n_{i-1}, n_i + 1, n_{i+1} - 1, ..., n_N],$$
$$L_i : \mathbf{n} \to [n_1, ..., n_{i-1} - 1, n_i + 1, n_{i+1}, ..., n_N].$$

Essentially, the operator R_i moves an individual to interval i from the right, while L_i moves an individual to interval i from the left. The probability that the density of individuals $\mathbf{u}$ is at state $\mathbf{n}$ at time $t + \Delta t$ is equal to the sum of the probabilities of all possible transitions to the right and left in the interval $(t, t + \Delta t)$ plus the probability that no transitions occur (either to the right or to the left) in this time interval. In mathematical terms, considering a forward step in time, we have

$$\begin{aligned} P(\mathbf{n}, t + \Delta t) = &\sum_{i=1}^{N} d(n_i + 1) P(R_i \mathbf{n}, t) \Delta t \\ &+ \sum_{i=2}^{N} d(n_i + 1) P(L_i \mathbf{n}, t) \\ &+ \left(1 - \sum_{i=1}^{N} dn_i \Delta t - \sum_{i=2}^{N} dn_i \Delta t \right) P(\mathbf{n}, t), \end{aligned} \tag{3.10}$$

i.e. the probability that the particle density is at state $\mathbf{n}$ at time $t + \Delta t$ is equal to the sum of all possible transitions to the right plus the sum of all possible transitions

to the left plus the probability that no transition occurs during the time interval $(t, t + \Delta t)$ (last term of equation).

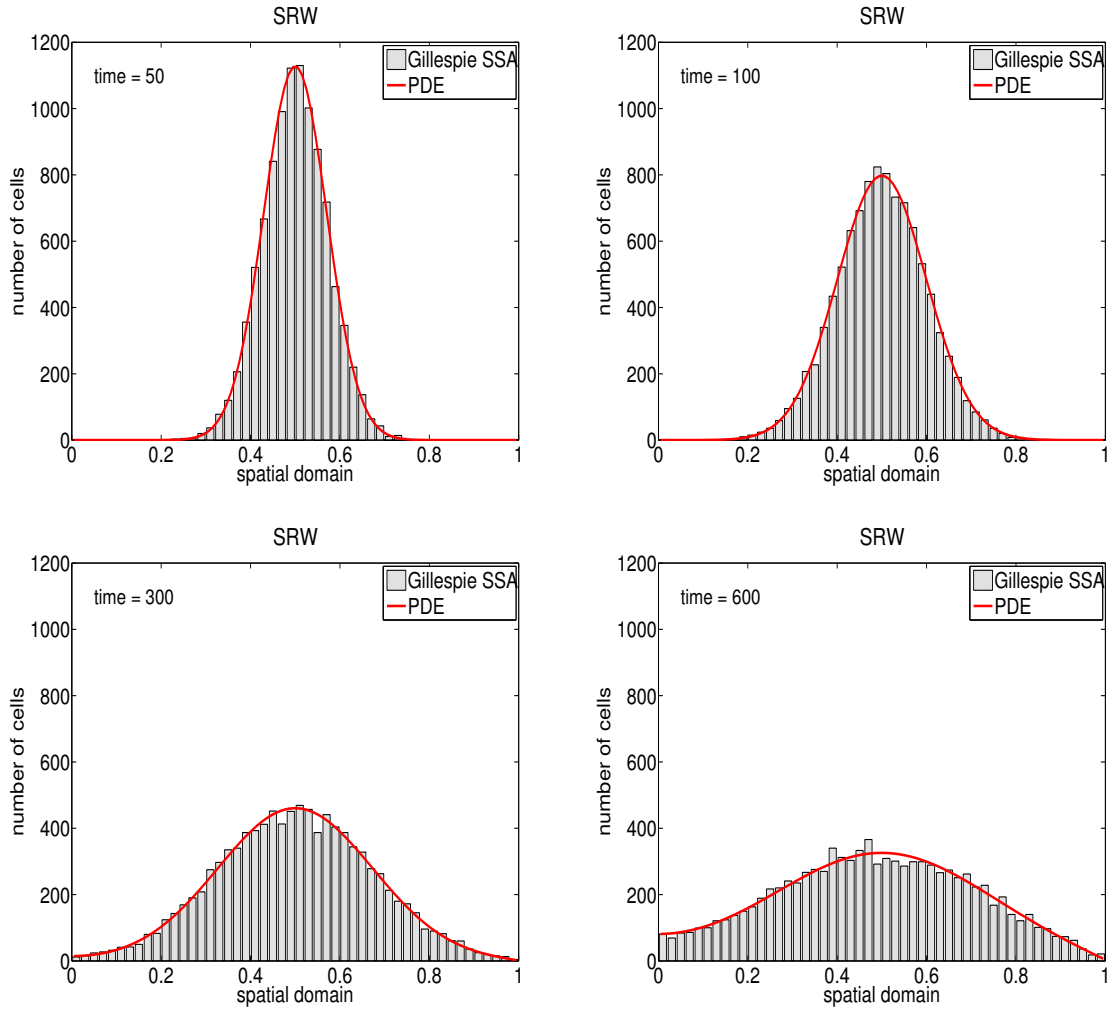


Figure 3.4: Plot of the evolution of the stochastic mean, $\mathbf{M}(t)$, over time in the SRW model (in black dots) versus the numerical solution of the diffusion equation (3.4) (red solid line). One realisation is shown for times $t = 50, 100, 300, 600$. The domain $[0, 1]$ is discretised into 50 compartments and 10000 particles are released at $t = 0$ at the point $x = 0.5$ with diffusion coefficient $D = 5 \cdot 10^{-5}$.

Then the master equation for this model can easily be shown to take the form

$$\frac{\partial P}{\partial t}(\mathbf{n}, t) = \sum_{i=1}^{N} d[(n_i + 1)P(R_i\mathbf{n}, t) - n_i P(\mathbf{n}, t)] + \sum_{i=2}^{N} d[(n_i + 1)P(L_i\mathbf{n}, t) - n_i P(\mathbf{n}, t)]. \tag{3.11}$$

If we define the stochastic mean particle density as $\mathbf{M}(t) = [M_1(t), M_2(t), ..., M_N(t)]$,

where

$$M_j(t) = \sum_{\mathbf{n}=0}^{\infty} n_j P(\mathbf{n}, t) = \sum_{n_1=0}^{\infty} \sum_{n_2=0}^{\infty} ... \sum_{n_N=0}^{\infty} n_j P(\mathbf{n}, t) \tag{3.12}$$

represents the mean number of particles in the j-th compartment, then we can use the master equation to derive the equations this mean obeys and compare them to the corresponding deterministic model, if it does indeed exist. Section A.5 of Appendix A shows the details of the derivation which results in the following system of equations:

$$\begin{aligned} \frac{dM_1}{dt} &= d(M_2 - M_1), \\ \frac{dM_i}{dt} &= d(M_{i+1} - 2M_i + M_{i-1}), \quad i = 2, ..., N-1, \\ \frac{dM_N}{dt} &= d(M_{N-1} - 2M_N). \end{aligned} \tag{3.13}$$

Provided that $d = \frac{D}{\Delta x^2}$, this system of equations forms a discretised version of the diffusion equation with a zero-flux Neumann boundary condition at $x = 0$, evident in the first equation, and a zero Dirichlet boundary condition at $x = L$, evident in the last equation (corresponding to a reflecting and an absorbing boundary as shown in the previous section). Fig. 3.4 shows a histogram of the number of particles in each compartment (for $N = 50$) versus the numerical solution of the diffusion equation for subsequent times. As expected, the particle density evolves as a Gaussian centred at the point $x = 0.5$, the initial location. In the long-term, the density of individuals will gradually decrease to zero since particles are leaving the domain at $x = L$, which is consistent with the approximations we have made.

Some straightforward extensions of the SRW model towards a more general framework are the introduction of a waiting time between jumps and the consideration of unequal probabilities of stepping to the right and to the left (which will result in a bias towards one direction). Section 3.3.2 presents a more general type of random walk and a new technique to derive its link to a PDE.

3.3.2 Biased Random Walk

3.3.2.1 Individual Approach

Model Formulation

The mathematical formulation of the BRW model is similar to that of the SRW model, only in this case the probabilities of moving to the right or to the left are unequal, i.e. there is a directional bias. Therefore, the SRW model may be regarded as a special case of the BRW model. In order to derive the governing PDE of the occupation probability for the BRW model, we shall employ a different method to the one used for the SRW model. This technique consists of deriving a recurrence relation for the occupation probability and then looking at its limit as the spatial step and the time step tend to zero. It will allow us to derive the governing equations for more complex random walk models in an easier fashion.

Consider a walker that moves on a one-dimensional lattice as before. At each time step Δt, the walker moves a distance Δx either to the right with probability α or to the left with probability β ($\alpha + \beta \leq 1$), or stays in the same location with probability $1 - \alpha - \beta$ (i.e. 'waits'). Note that the SRW model corresponds to the case $\alpha = \beta = \frac{1}{2}$. As in the case of the SRW model, successive steps are completely independent of each other.

Occupation Probability

Suppose that the walker is at location x at time $t + \Delta t$. At time t, the walker was either at location $x + \Delta x$ and moved to the left, or at location $x - \Delta x$ and moved to the right or at location x and stayed there. Thus, the occupation probability $p(x, t)$ satisfies

$$p(x, t + \Delta t) = \alpha p(x - \Delta x, t) + \beta p(x + \Delta x, t) + (1 - \alpha - \beta)p(x, t). \tag{3.14}$$

If we let Δx and Δt tend to zero, we can expand the terms in equation (3.14) in Taylor series about the point (x, t).

By writing $\epsilon = \alpha - \beta$, $k = \alpha + \beta$ and letting $\Delta x, \Delta t \to 0$ such that the limits

$$u = \lim_{\epsilon, \Delta x, \Delta t \to 0} \frac{\epsilon \Delta x}{\Delta t}, \quad \text{and} \quad D = \lim_{\Delta x, \Delta t \to 0} k \frac{\Delta x^2}{2\Delta t}, \tag{3.15}$$

where Δx^2 denotes the square of the spatial step $(\Delta x)^2$, are positive and finite, we obtain the governing PDE for the BRW model

$$\frac{\partial p}{\partial t} = -u \frac{\partial p}{\partial x} + D \frac{\partial^2 p}{\partial x^2}, \tag{3.16}$$

the *advection-diffusion equation* (see Section A.2 of Appendix A for a derivation). Here, u represents the advection term. Notice that the diffusion coefficient differs by a factor of $k = \alpha + \beta < 1$ from the diffusion coefficient of the SRW model. This is the effect of allowing the walker to stay (wait) at its current location. In the absence of a waiting time, this factor k becomes equal to unity and we obtain the standard limit for the diffusion coefficient. Note also that the requirement that $\frac{\Delta x^2}{2\Delta t}$ remains finite as $\Delta x, \Delta t \to 0$ implies that $\epsilon \sim O(\Delta t^{\frac{1}{2}})$ and $\epsilon \to 0$ in the same limit for the advection coefficient to be finite. Therefore, α and β are not fixed, but rather vary with Δx and Δt such that the limits given by (3.15) exist, in order for the continuum approximation of the stochastic model to be valid.

For the same initial and boundary conditions, the solution of the advection-diffusion equation is given by

$$p(x, t) = \sqrt{\frac{1}{4\pi D t}} \cdot e^{-\frac{(x-ut)^2}{4Dt}}, \tag{3.17}$$

which is the solution of the diffusion equation translated by ut. Hence, the occupation probability of the BRW model also has a Gaussian distribution, with its centre shifting linearly with time when the advection term is constant. This is reflected by the fact

that the expected location of the BRW model is equal to

$$E(X_t) = ut. \tag{3.18}$$

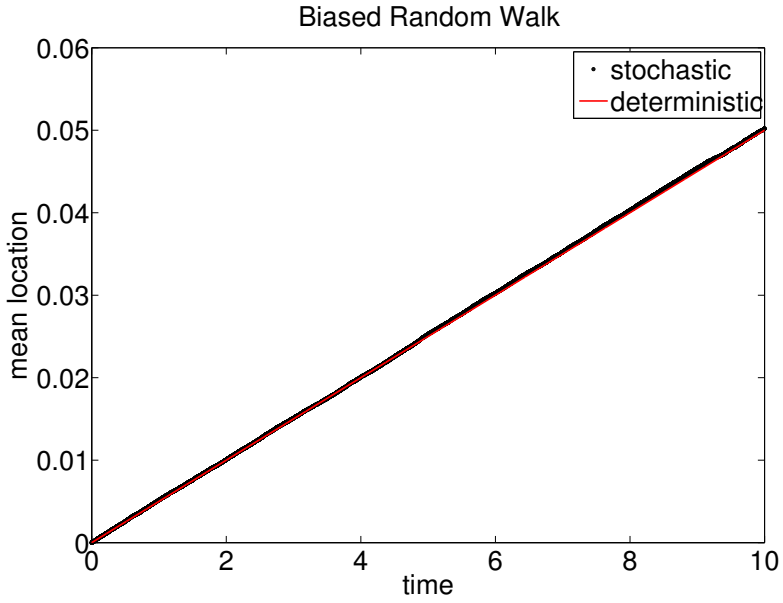


Figure 3.5: Plot of the evolution of the mean location, $E(X_t)$, over time in the BRW model (in black dots) versus the analytical expression obtained from the deterministic model given by equation (3.18) (red solid line). We performed 10000 simulations and we have taken $\Delta x = 10^{-4}$, $\Delta t = 5 \cdot 10^{-5}$ ($D = 10^{-4}$) and $u = 5 \cdot 10^{-3}$.

Fig. 3.5 shows how this theoretical estimate compares with the results from the simulation of the stochastic model. In the BRW, the mean location increases linearly with time due to the bias towards the right. The constant of proportionality is the advection term, so the stronger the bias, the faster a particle moves to the right. The derivation of this analytical expression, and of any moments, in general, of the spatial location in any random walk model that follows, is performed through manipulating the governing PDE rather than the actual solution of the occupation probability, which was how we treated the SRW model. This technique, presented in Section A.2 of Appendix A, is more helpful when dealing with more complicated models where only the governing PDE might be known. The MSD of the BRW model is given

by

$$E(X_t^2) = u^2t^2 + 2Dt, \tag{3.19}$$

which shows that the long-term behaviour of the BRW is similar to that of a propagating wave as $E(X_t^2) \sim t^2$. However, the variance is equal to

$$\sigma_t^2 = 2Dt. \tag{3.20}$$

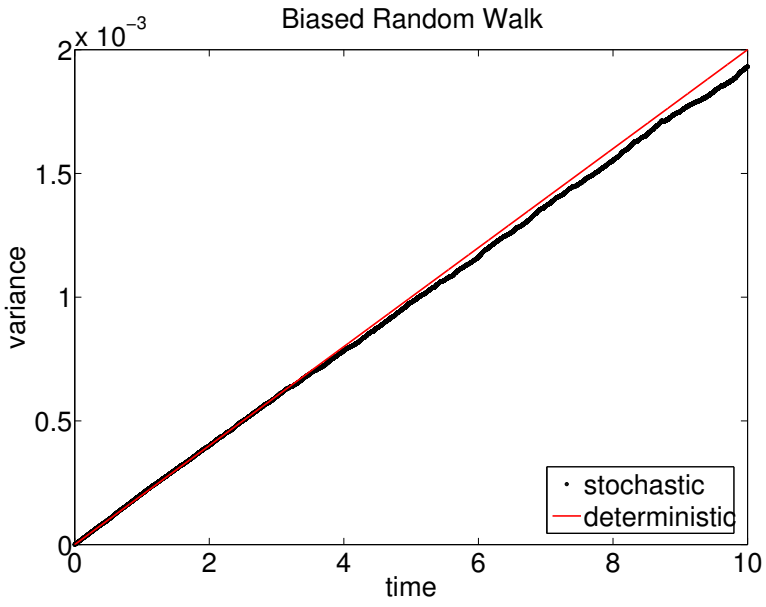


Figure 3.6: Plot of the evolution of the variance, σ_t^2, over time in the BRW model (in black dots) versus the analytical expression obtained from the deterministic model given by equation (3.20) (red solid line). We performed 10000 simulations and we have taken $\Delta x = 10^{-4}$, $\Delta t = 5 \cdot 10^{-5}$ ($D = 10^{-4}$) and $u = 5 \cdot 10^{-3}$.

Thus, the dispersal about the mean location is linear in time, a characteristic of a diffusive process. Fig. 3.6 shows a plot of the variance of the stochastic model compared to equation (3.20) (red solid line). As is evident from the figure, there is a discrepancy between the theoretically predicted variance and the results from the stochastic simulation of the BRW model. This difference between the simulation data and the theoretical estimate grows larger as time increases. This discrepancy, which is also present in the SRW model (Fig. 3.3) and the correlated models (following sections),

results from the approximations involved in estimating the theoretically predicted variance. In the analysis of the difference (master) equations that are satisfied by the occupation probability we neglect higher order terms that represent derivatives of the occupation probability with respect to space and time (in the case of the BRW model, for instance, see Section A.2 of Appendix A). We perform an approximation where the spatial and temporal steps tend to zero in order to derive the deterministic models that describe the average behaviour of the system over several realisations. However, when we simulate the stochastic model, the errors associated with these approximations become obvious since the spatial and time steps (using a Monte Carlo algorithm) are small but not infinitesimal as assumed in the approximation. As the number of simulations of the stochastic model increases, the discrepancy becomes smaller as the approximation improves; the deterministic model describes the observed behaviour more accurately. The error, however, does not vanish.

Before introducing the models representing velocity-jump processes, we should first consider barriers for the SRW and BRW in order to model migration in a confined space, such as a specific portion of a tissue for example. We present a method for deriving the correct boundary conditions to be applied on the deterministic model as a correspondence to the boundaries of the stochastic model is not trivial.

3.3.2.2 Boundary Conditions

At the left end of the domain, $x = 0$, we consider a reflective barrier, i.e. a particle attempting to move to the left of interval will be reflected back. This may represent the edge of an epidermal tissue, where we require that no cell can escape the domain from this end. At the right end of the domain, $x = L$, we consider an absorbing boundary initially and a more general partially absorbing boundary later; these model a fully or partially permeable tissue, respectively. If an individual attempts to move

to the right (outside the domain), it will be trapped and will not be able to return inside the domain. As we shall see, these boundary conditions are easy to implement in the stochastic model but more care is needed when drawing an equivalence to the deterministic model, especially in the reactive-boundary case [Erban and Chapman, 2007].

At $x = 0$, the occupation probability obeys the relation

$$p(0,t+\Delta t) = \beta p(0,t)+\beta p(\Delta x,t)+(1-\alpha-\beta)p(0,t) = \beta p(\Delta x,t)+(1-\alpha)p(0,t), \quad (3.21)$$

since if a particle is located at $x = 0$ at $t + \Delta t$, then there are two possibilities for its location at time t: either it was located at $x = 0$ (through attempting a move to the left and being reflected back or through attempting no jump at all) or it was located at $x = \Delta x$ and moved to the left. After expanding as a Taylor series, we obtain

$$p(0,t)+\Delta t\frac{\partial p}{\partial t}(0,t)+\frac{\Delta t^2}{2}\frac{\partial^2 p}{\partial t^2}(0,t)+O(\Delta t^3) = (1-\alpha+\beta)p(0,t)+\beta\Delta x\frac{\partial p}{\partial x}(0,t)+\beta\frac{\Delta x^2}{2}\frac{\partial^2 p}{\partial x^2}+O(\Delta x^3).$$

In the limit as $\Delta x, \Delta \to 0$ and $\epsilon = \alpha - \beta \to 0$ and after some algebra (Section A.2.3 of Appendix A shows the derivation), (3.21) may be approximated by the zero-flux Neumann condition,

$$D\frac{\partial p}{\partial x}(0,t) - up(0,t) = 0, \quad (3.22)$$

in the PDE model. It reduces to the zero-flux condition,

$$\frac{\partial p}{\partial x}(0,t) = 0, \quad (3.23)$$

in the case of the SRW model.

At $x = L$, on the other hand, we consider a probability of absorption $0 < \theta\Delta x < 1$, i.e. the particle will be absorbed fully as $\theta \to \infty$ such that $\theta\Delta x = 1$ and reflected

fully if $\theta = 0$. The relevant difference equation is given by

$$p(L, t + \Delta t) = \alpha p(L - \Delta x, t) + \alpha(1 - \theta\Delta x)p(L, t) + (1 - \alpha - \beta)p(L, t), \quad (3.24)$$

which corresponds to the equation

$$D\frac{\partial p}{\partial x}(L, t) - up(L, t) = -\theta Dp(L, t), \quad (3.25)$$

in the deterministic model, which reduces to

$$D\frac{\partial p}{\partial x}(L, t) = -\theta Dp(L, t),$$

in the case of the SRW model. In the special case of a fully absorbing barrier, i.e. when $\theta\Delta x = 1$, the condition (3.25) becomes

$$p(L, t) = 0, \quad (3.26)$$

for both models.

3.3.2.3 Population Approach

Model Formulation

The formulation of the stochastic model corresponding to a BRW, as viewed from the perspective of a population, is the same as that of the SRW, except for the fact that we consider different transition rates between a jump to the right and a jump to the left. Suppose these transition rates are denoted by d^+ and d^-, respectively. Then, this process may be represented by the following schematic

$$u_1 \underset{d^-}{\overset{d^+}{\rightleftharpoons}} u_2 \underset{d^-}{\overset{d^+}{\rightleftharpoons}} \ldots \underset{d^-}{\overset{d^+}{\rightleftharpoons}} u_{i-1} \underset{d^-}{\overset{d^+}{\rightleftharpoons}} u_i \underset{d^-}{\overset{d^+}{\rightleftharpoons}} u_{i+1} \underset{d^-}{\overset{d^+}{\rightleftharpoons}} \ldots \underset{d^-}{\overset{d^+}{\rightleftharpoons}} u_{N-1} \underset{d^-}{\overset{d^+}{\rightleftharpoons}} u_N \xrightarrow{d^+} u_{N+1}. \quad (3.27)$$

The propensity functions is this case take the form

$$\begin{aligned} \alpha_i^+(t) &= d^+ u_i(t), \quad i = 1, ..., N, \\ \alpha_i^-(t) &= d^- u_i(t), \quad i = 2, ..., N \end{aligned} \tag{3.28}$$

for transitions to the right and left, respectively.

Population Density

The derivation of a master equation corresponding to this scheme is very similar to that of the previous section, except we replace d by $d^{\pm}$ to obtain

$$\frac{\partial P}{\partial t}(\mathbf{n}, t) = \sum_{i=1}^{N} [d^+(n_i+1)P(R_i\mathbf{n}, t) - d^+ n_i P(\mathbf{n}, t)] + \sum_{i=2}^{N} [d^-(n_i+1)P(L_i\mathbf{n}, t) - d^- n_i P(\mathbf{n}, t)], \tag{3.29}$$

by a consideration of the particle density in a forward step in time as before.

The differential equations satisfied by the mean density of individuals are given by

$$\begin{aligned} \frac{dM_1}{dt} &= d^- M_2 - d^+ M_1, \\ \frac{dM_i}{dt} &= d^- M_{i+1} - (d^+ + d^-)M_i + d^+ M_{i-1}, \quad i = 2, ..., N-1, \\ \frac{dM_N}{dt} &= d^+ M_{N-1} - (d^+ + d^-)M_N. \end{aligned} \tag{3.30}$$

If $d^{\pm} = \frac{D}{\Delta x^2} \pm \frac{u}{2\Delta x}$, then the above system is a discretised version of the advection-diffusion equation (3.16) with a zero-flux condition at $x = 0$ (of the form specified in Section 3.3.2), and a zero Dirichlet condition at $x = L$. Fig. 3.7 shows how the particle density in the BRW model evolves over time. In this case, the Gaussian is moving towards the right due to the effect of advection.

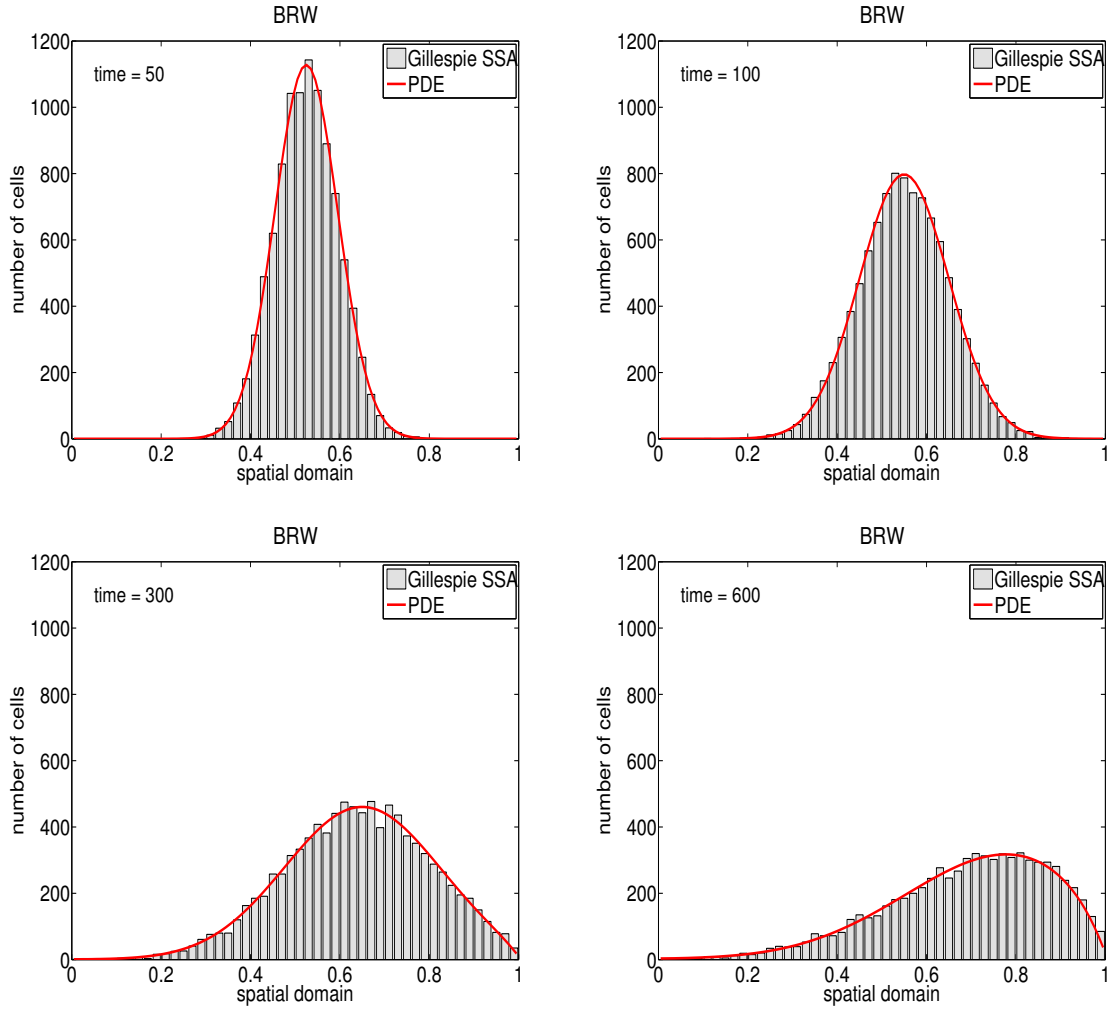


Figure 3.7: Plot of the evolution of the stochastic mean number of particles, $\mathbf{M}(t)$, over time in the BRW model (in black dots) versus the numerical solution of the advection-diffusion equation (3.16) (red solid line). One realisation is shown for times $t = 50, 100, 300, 600$. The domain $[0, 1]$ is discretised into 50 compartments and 10000 particles are released at $t = 0$ at the point $x = 0.5$ with diffusion coefficient $D = 5 \cdot 10^{-5}$ and advection coefficient $u = 5 \cdot 10^{-4}$.

3.4 Velocity-Jump Processes

3.4.1 Correlated Random Walk

3.4.1.1 Individual Approach

Model Formulation

In this section, we introduce the notion of persistence, i.e. the tendency to move in the previous direction, into the random walk. In this case, the walker has a certain probability of continuing its movement in the same direction and a probability of changing direction rather than a fixed probability of moving rightward or leftward. It is obvious that the location of the walker no longer forms a Markov process, as was the case with the SRW and BRW models. In the CRW, the variable that follows a Markov process is the velocity of the walker, whose magnitude is finite in stark contrast to the SRW and BRW models.

Consider a walker moving on a one-dimensional infinite lattice. We denote the probability of being at location x at time t by $\alpha(x,t)$ if the walker has arrived from location $x-\Delta x$ and by $\beta(x,t)$ if the walker has arrived from $x+\Delta x$. The unconditional occupation probability is equal to the sum of the probability that the walker is right-moving and the probability that it is left-moving, $p(x,t)=\alpha(x,t)+\beta(x,t)$. At each time step, the walker either changes direction with a probability $\lambda\Delta t$ or moves in the same direction as previously with a probability $1-\lambda\Delta t$, i.e. turning events occur as a Poisson process with intensity rate λ. The process is Markovian with respect to the velocity of the walker because successive turning events are independent.

Occupation Probability

The recurrence relations satisfied by the probabilities $\alpha(x,t)$ and $\beta(x,t)$ are given

by

$$\begin{aligned}\alpha(x,t+\Delta t) &= (1-\lambda\Delta t)\alpha(x-\Delta x,t)+\lambda\Delta t\beta(x-\Delta x,t),\\ \beta(x,t+\Delta t) &= \lambda\Delta t\alpha(x+\Delta x,t)+(1-\lambda\Delta t)\beta(x+\Delta x,t).\end{aligned} \tag{3.31}$$

In the limit $\Delta x, \Delta t \to 0$ such that

$$v = \lim_{\Delta x,\Delta t\to 0}\frac{\Delta x}{\Delta t}, \tag{3.32}$$

is positive and finite, and expanding the terms in the system of equations (3.31) in Taylor series about (x,t) (Section A.3 of Appendix A), we obtain

$$\begin{aligned}\frac{\partial\alpha}{\partial t} &= -v\frac{\partial\alpha}{\partial x}+\lambda(\beta-\alpha),\\ \frac{\partial\beta}{\partial t} &= v\frac{\partial\beta}{\partial x}-\lambda(\beta-\alpha).\end{aligned} \tag{3.33}$$

The unconditional occupation probability can be shown (Section A.3 of Appendix A) to satisfy

$$\frac{\partial^2 p}{\partial t^2}+2\lambda\frac{\partial p}{\partial t} = v^2\frac{\partial^2 p}{\partial x^2}, \tag{3.34}$$

which is the *telegrapher's equation*. To complete the formulation of the CRW model, we need to specify the initial condition and the rules for the first time step. Suppose that initially the walker is released at x_0, i.e a point source in the deterministic model,

$$p(x,0) = \delta(x-x_0),$$

as previously. Without loss of generality, we can pick the origin as x_0 in what follows. Since the walker does not have a previous direction, the question is how does it proceed during the first time step. There are two possible answers: the walker can either have an equal probability ($=\frac{1}{2}$) of moving in either direction or it will have a tendency to move in one direction. Suppose this tendency is represented by a probability of

moving to the right, say ϕ, and a probability of moving to the left equal to $1-\phi$. Then, we have

$$\alpha(x,0;x_0) = \phi \cdot \delta(x-x_0), \quad \beta(x,0;x_0) = (1-\phi)\cdot\delta(x-x_0).$$

In the deterministic model, this is reflected by the second initial condition, $\frac{\partial p}{\partial t}(x,0) = -(2\phi-1)v\delta'(x-x_0)$ [Weiss, 2002].

The expected location of the CRW model can be shown (Section A.3 of Appendix A) to be given by

$$E(X_t) = 0, \tag{3.35}$$

and the MSD and variance, which are equal in this case, can be obtained (Section A.3 of Appendix A) by solving the equation

$$\frac{d^2}{dt^2}[E(X_t^2)] + 2\lambda\frac{d}{dt}[E(X_t^2)] - 2v^2 = 0, \tag{3.36}$$

subject to the following initial conditions

$$E(X_0^2) = 0, \quad \frac{d}{dt}[E(X_0^2)] = 0.$$

The solution is

$$E(X_t^2) = \sigma_t^2 = \frac{v^2}{\lambda}\left(t - \frac{1}{2\lambda}(1-e^{-2\lambda t})\right). \tag{3.37}$$

Fig. 3.8 and Fig. 3.9 show a comparison between the stochastic and deterministic models through a plot of the first two moments of the spatial location. Firstly, note that there is no overall bias towards any direction just as in the case of the SRW model. The mean dispersal about the origin exhibits a quadratic relation to time for small t, in fact if the quantity λt is small, $E(X_t^2) \sim O(v^2t^2)$, which is characteristic of a wave process. However, when the quantity λt is large, either because we are

observing the process on a long time scale or because λ is very large, which means essentially that there is no correlation since $1 - \lambda t \to 0$, $E(X_t^2) \sim O(v^2 t/\lambda)$, which is characteristic of a diffusive process. In fact, Othmer [1988] showed that the telegraph process and a diffusion process with diffusion coefficient equal to $\frac{v^2}{2\lambda}$ tend to the same limit as $t \to \infty$.

Note also that turning events occur as a Poisson process and so the mean time between turning events is $\Delta t = \frac{1}{\lambda}$. The mean distance moved is $\Delta x = \frac{v}{\lambda}$, so an effective diffusion coefficient for the telegraph process, in the limit as $\lambda, v \to \infty$ so that $\Delta t, \Delta x \to 0$,, is given by

$$D = \frac{\Delta x^2}{2\Delta t} = \frac{v^2}{2\lambda}. \tag{3.38}$$

The telegraph process behaves as a diffusion process at large time scales because short-term correlation effects become less evident as particle will have spread to a greater degree on average.

3.4.1.2 Boundary Conditions

The relation of the boundary conditions between the stochastic model and its deterministic equivalent are more complex in models describing velocity-jump processes. The reason is that we need to consider the previous direction of a particle reaching the boundary and determine the conditions in terms of the two components of the occupation probability, $\alpha(x,t)$ and $\beta(x,t)$. We start by considering the reflective boundary at $x = 0$. In the stochastic model, a particle that reaches this boundary will come from the right, since it will be released at $x_0 > 0$. If it persists in its previous direction and attempts to move to the left, it will be reflected back, and will become right-moving in the next step. Hence, the probability that the particle is

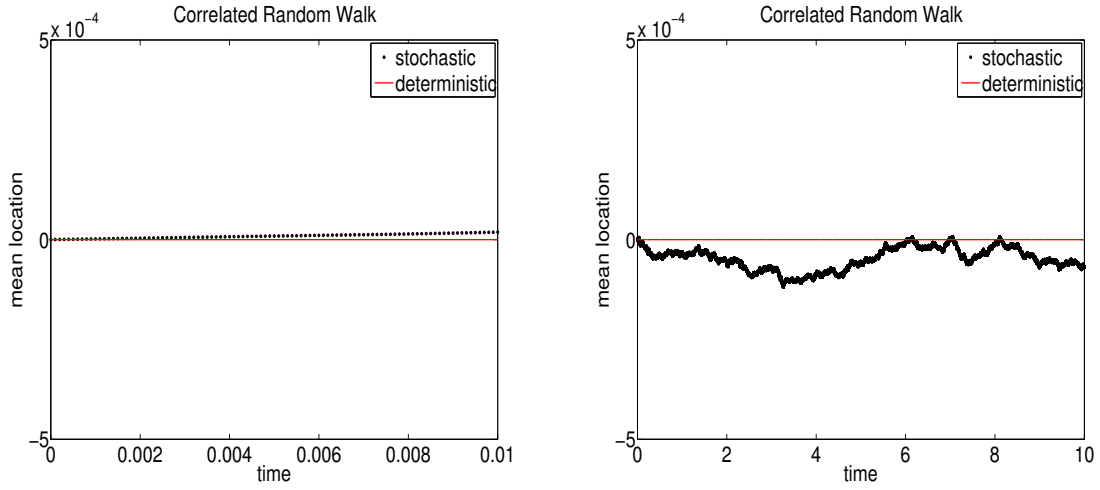


Figure 3.8: Plot of the evolution of the mean location, $E(X_t)$, over time in the CRW model (in black dots) versus the analytical expression obtained from the deterministic model given by equation (3.35) (red solid line). The left and right panels show the results for We performed 10000 simulations and have taken $\Delta x = 10^{-4}$, $\Delta t = 10^{-3}$ ($v = 10^{-1}$) and $\lambda = 100$.

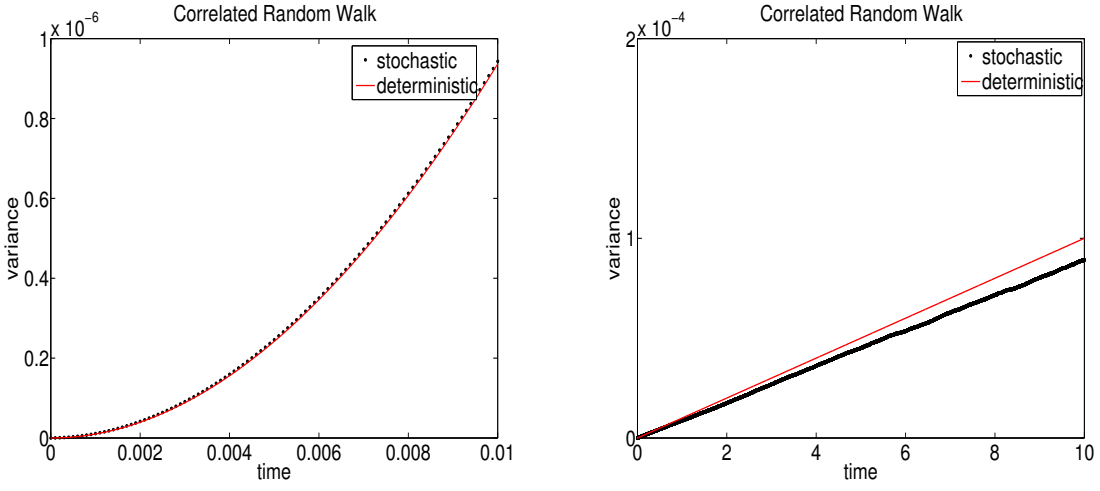


Figure 3.9: Plot of the evolution of the variance, σ_t^2, over time in the CRW model (in black dots) versus the analytical expression obtained from the deterministic model given by equation (3.37) (red solid line). We performed 10000 simulations and we have taken $\Delta x = 10^{-4}$, $\Delta t = 10^{-3}$ ($v = 10^{-1}$) and $\lambda = 100$.

right-moving at time $t + \Delta t$ is equal to

$$\alpha(0, t + \Delta t) = (1 - \lambda \Delta t)\beta(0, t).$$

Expanding in Taylor series about point $(0, t)$ in the limit as $\Delta t \to 0$, we obtain the appropriate boundary condition at $x = 0$ in the continuum model [Weiss, 2002]

$$\alpha(0, t) = \beta(0, t). \tag{3.39}$$

In order to relate this to the unconditional probability, we need to add and subtract the equations of system (3.33) and substitute for $p(x, t)$ to obtain

$$\begin{aligned} \frac{\partial p}{\partial t} &= v\frac{\partial(\beta - \alpha)}{\partial x}, \\ \frac{\partial(\beta - \alpha)}{\partial t} &= v\frac{\partial p}{\partial x} - 2\lambda(\beta - \alpha). \end{aligned} \tag{3.40}$$

From the second of these equations we see that the condition we are looking for is

$$\frac{\partial p}{\partial x}(0, t) = 0. \tag{3.41}$$

At $x = L$, we consider an absorbing (or partially absorbing in the general case) boundary as in the models of position-jump processes. In this case, a particle at $x = L$ at time $t + \Delta t$ can only have come from the left. If it persists in its direction and moves to the right, it will be absorbed with a probability equal to $0 < \theta < 1$. Otherwise, it will be reflected back and become left-moving. Hence,

$$\beta(L, t + \Delta t) = (1 - \lambda \Delta t)(1 - \theta)\alpha(L, t).$$

In the limit as $\Delta t \to 0$, the condition becomes [Weiss, 2002]

$$\beta(L,t) = (1-\theta)\alpha(L,t). \tag{3.42}$$

In the special case where the boundary is fully absorbing, $\theta = 1$ and $\beta(L,t) = 0$. In terms of the unconditional occupation probability, if we substitute the previous equation into the second equation of the system (3.40), it will reduce to

$$\theta\frac{\partial p}{\partial t}(L,t) + (2-\theta)v\frac{\partial p}{\partial x}(L,t) + 2\lambda\theta p(L,t) = 0, \tag{3.43}$$

or in the special case of a fully absorbing boundary,

$$\frac{\partial p}{\partial t}(L,t) + v\frac{\partial p}{\partial x}(L,t) + 2\lambda p(L,t) = 0. \tag{3.44}$$

3.4.1.3 Population Approach

Model Formulation

The corresponding stochastic model for a CRW varies slightly from the models describing position-jump processes, as we need to consider two distinct populations in each compartment. The first one, whose density is denoted by **A**, describes the right-moving individuals while the second one, with a density denoted by **B**, describes the left-moving individuals. We require that a right-moving individual in the i-th compartment can move either to the right with rate d^+ (to be derived), so it will remain a right-moving individual, or to the left with rate d^- (to be derived), in which case it will become a left-moving individual. For a left-moving individual inhabiting x_i, possible transitions include movement to the left with rate d^+ or movement to the right with rate d^- and a transformation to a right-moving individual. Essentially, d^+ and d^- represent rates of persisting in the previous direction or of turning direction,

respectively. Schematically, all possible transitions can be represented by

$$\begin{aligned}
&A_1 \xrightarrow{d^+} A_2 \xrightarrow{d^+} ... \xrightarrow{d^+} A_{i-1} \xrightarrow{d^+} A_i \xrightarrow{d^+} A_{i+1} \xrightarrow{d^+} ... \xrightarrow{d^+} A_{N-1} \xrightarrow{d^+} A_N \xrightarrow{d^+} A_{N+1},\\
&B_1 \xleftarrow{d^+} B_2 \xleftarrow{d^+} ... \xleftarrow{d^+} B_{i-1} \xleftarrow{d^+} B_i \xleftarrow{d^+} B_{i+1} \xleftarrow{d^+} ... \xleftarrow{d^+} B_{N-1},\\
&\qquad\qquad A_1 \xleftarrow{d^+} B_1,\\
&\qquad\qquad A_i \underset{d^-}{\overset{d^-}{\rightleftharpoons}} B_{i-1}, \quad i = 2, ..., N
\end{aligned} \tag{3.45}$$

where A_i and B_i denote the number of individuals in the i-th compartment, respectively. The propensity functions in this model are defined by

$$\begin{aligned}
&\alpha_i^+(t) = d^+ A_i(t), \quad i = 1, .., N,\\
&\beta_i^+(t) = d^+ B_i(t), \quad i = 2, ..., N-1,\\
&\alpha_i^-(t) = d^- A_i(t), \quad i = 2, .., N,\\
&\beta_i^-(t) = d^- B_i(t), \quad i = 1, ..., N-1,\\
&\beta_1^+(t) = d^+ B_1(t),
\end{aligned} \tag{3.46}$$

the last equation being a result of the reflecting boundary at $x = 0$.

Population Density

In order to use the RDME approach in this model, we first need to define the joint probability that the density of right-moving individuals $\mathbf{A}$ equals $\mathbf{n}$ and the density of left-moving individuals $\mathbf{B}$ equals $\mathbf{m}$ at time t, denoted by $P(\mathbf{n}, \mathbf{m}, t)$. Define also the operators $J_i^- : \mathbb{R}^N \to \mathbb{R}^N$ and $J_i^+ : \mathbb{R}^N \to \mathbb{R}^N$, for $i = 1, 2, ..., N$, by

$$\begin{aligned}
&J_i^- : \mathbf{n} \to [n_1, ..., n_{i-1}, n_i - 1, n_{i+1}, ..., n_N],\\
&J_i^+ : \mathbf{n} \to [n_1, ..., n_{i-1}, n_i + 1, n_{i+1}, ..., n_N].
\end{aligned}$$

Then, considering a forward step in time, we obtain

$$
\begin{aligned}
P(\mathbf{n},\mathbf{m},t+\Delta t) = & \sum_{i=1}^{N} d^{+}(n_i+1)P(R_i\mathbf{n},\mathbf{m},t)\Delta t \\
& + \sum_{i=2}^{N-1} d^{+}(m_i+1)P(\mathbf{n},L_i\mathbf{m},t)\Delta t \\
& + \sum_{i=2}^{N} d^{-}(n_i+1)P(J_i^{+}\mathbf{n},J_{i-1}^{-}\mathbf{m},t)\Delta t \\
& + \sum_{i=1}^{N-1} d^{-}(m_i+1)P(J_{i+1}^{-}\mathbf{n},J_i^{+}\mathbf{m},t)\Delta t \\
& + d^{+}(m_1+1)P(J_1^{-}\mathbf{n},J_1^{+}\mathbf{m},t)\Delta t \\
& + \left[1 - d^{+}\Delta t\left(m_1+\sum_{i=1}^{N} n_i + \sum_{i=2}^{N-1} m_i\right) + d^{-}\Delta t\left(\sum_{i=2}^{N} n_i + \sum_{i=1}^{N-1} m_i\right)\right] P(\mathbf{n},\mathbf{m},t),
\end{aligned}
\tag{3.47}
$$

i.e. the state probability at time $t+\Delta t$ is equal to the sum of all possible transitions for species A to the right and all possible transitions for species B to the left (correlation effects) plus all the possible transitions for species A to the left and for species B to the right (turning effects) minus the probability that no transition occurs within the time interval in question. Consequently, the master equation takes the form

$$
\begin{aligned}
\frac{\partial P}{\partial t}(\mathbf{n},\mathbf{m},t) = & \sum_{i=1}^{N} d^{+}[(n_i+1)P(R_i\mathbf{n},\mathbf{m},t) - n_iP(\mathbf{n},\mathbf{m},t)] \\
& + \sum_{i=2}^{N-1} d^{+}[(m_i+1)P(\mathbf{n},L_i\mathbf{m},t) - m_iP(\mathbf{n},\mathbf{m},t)] \\
& + \sum_{i=2}^{N} d^{-}[(n_i+1)P(J_i^{+}\mathbf{n},J_{i-1}^{-}\mathbf{m},t) - n_iP(\mathbf{n},\mathbf{m},t)] \\
& + \sum_{i=1}^{N-1} d^{-}[(m_i+1)P(J_{i+1}^{-}\mathbf{n},J_i^{+}\mathbf{m},t) - m_iP(\mathbf{n},\mathbf{m},t)] \\
& + d^{+}[(m_1+1)P(J_1^{-}\mathbf{n},J_1^{+}\mathbf{m},t) - m_1P(\mathbf{n},\mathbf{m},t)].
\end{aligned}
\tag{3.48}
$$

If we further define the mean number of individuals in the j-th compartment, for

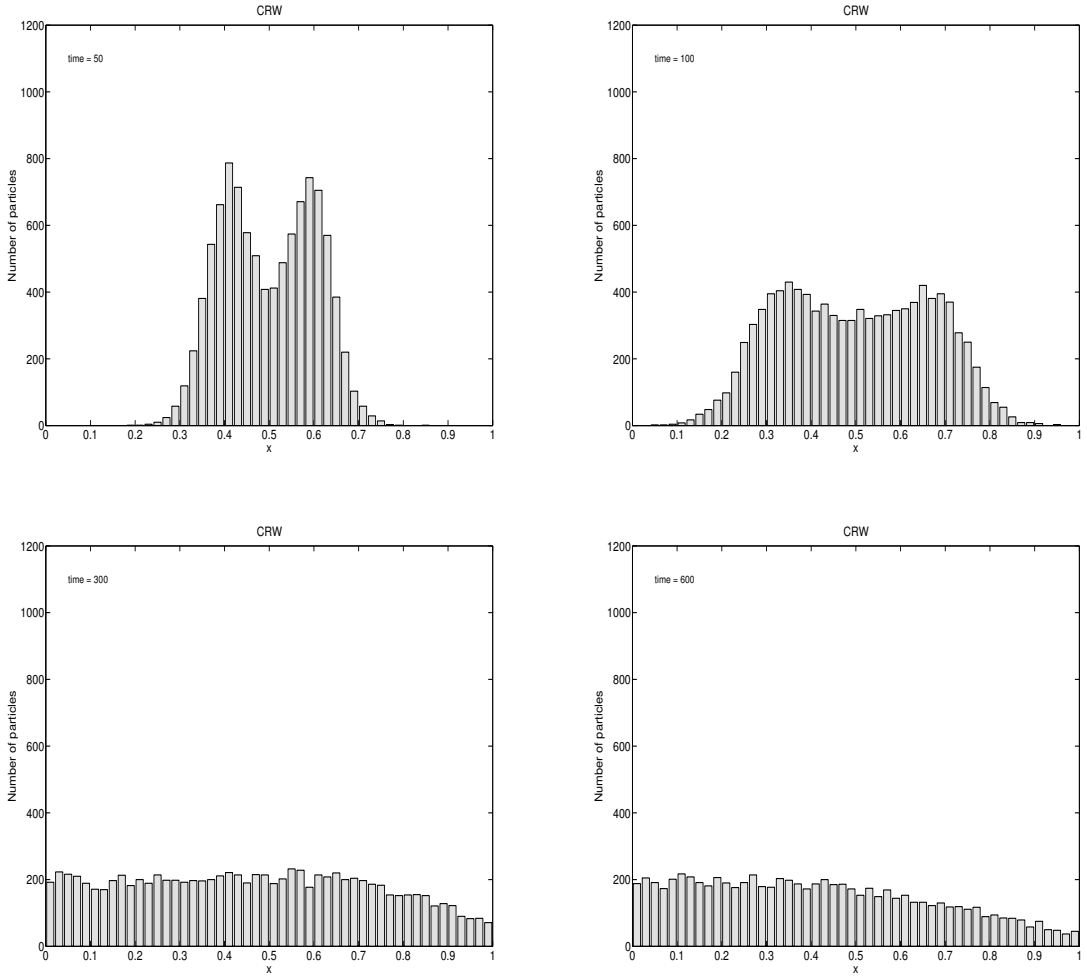


Figure 3.10: Plot of the evolution of the stochastic mean of the total populations $\mathbf{M}(t) = \mathbf{M}^A(t) + \mathbf{M}^B(t)$ over time in the CRW model. One stochastic realisation is shown for times $t = 50, 100, 300, 600$. The domain $[0, 1]$ is discretised into 50 compartments and 10000 particles are released at $t = 0$ at the point $x = 0.5$, half of species A and half of species B.

populations A and B by, respectively,

$$\begin{aligned} M_j^A(t) &= \sum_{\mathbf{n}=0}^{\infty} n_j P(\mathbf{n}, \mathbf{m}, t) = \sum_{n_1=0}^{\infty} \sum_{n_2=0}^{\infty} ... \sum_{n_N=0}^{\infty} n_j P(\mathbf{n}, \mathbf{m}, t), \\ M_j^B(t) &= \sum_{\mathbf{m}=0}^{\infty} m_j P(\mathbf{n}, \mathbf{m}, t) = \sum_{m_1=0}^{\infty} \sum_{m_2=0}^{\infty} ... \sum_{m_N=0}^{\infty} m_j P(\mathbf{n}, \mathbf{m}, t), \end{aligned} \tag{3.49}$$

we can obtain, using the master equation, a system of differential equations that the

stochastic means obey. This system is given by

$$\begin{aligned}
\frac{dM_1^A}{dt} &= d^+ M_1^A + d^-[M_1^B - M_1^A], \\
\frac{dM_i^A}{dt} &= -(d^+ + d^-)[M_i^A - M_{i-1}^A] + d^-[M_{i-1}^B - M_{i-1}^A], \quad i = 2, ..., N-1, \\
\frac{dM_N^A}{dt} &= -(d^+ + d^-)[M_N^A - M_{N-1}^A] - d^- M_{N-1}^A, \\
\frac{dM_1^B}{dt} &= d^+ M_1^B - d^-[M_1^B - M_1^A], \\
\frac{dM_i^B}{dt} &= (d^+ + d^-)[M_i^B - M_{i-1}^B] - d^-[M_{i-1}^B - M_{i-1}^A], \quad i = 2, ..., N-1, \\
\frac{dM_N^B}{dt} &= -(d^+ + d^-)[M_N^B - M_{N-1}^B] + d^- M_{N-1}^A.
\end{aligned} \tag{3.50}$$

For $d^+ = \frac{v}{\Delta x} - \lambda$ and $d^- = \lambda$, this is a discretised version (backward Euler instead of central difference) of the system of equations (3.33) with the appropriate boundary conditions for a reflecting boundary at $x = 0$ and an absorbing boundary at $x = L$, which is consistent with the results of the single-individual approach.

Fig. 3.10 shows the spatial distribution of individuals as time progresses. Initially, the motion is wave-like and for small t, the right- and left-moving populations move fast towards the right and left, respectively. This is expected as the two populations have an initial tendency to move right/left, respectively, and the strength of persistence in the previous direction of motion is very important at this stage. In the long run, however, the particle distribution behaves as a decaying Gaussian. In this limit, the telegraph process exhibits characteristics of a diffusive process as the effects of persistence become negligible. The same effect may be achieved earlier in time if the correlation coefficient is very large.

3.4.2 Biased and Correlated Random Walk

3.4.2.1 Individual Approach

Model Formulation

In this model we consider a correlated random walk but with different turning rates depending on the direction of motion. If the walker is right-moving, then it will have a probability $\lambda_1 \Delta t$ of changing direction, while a left-moving walker will change direction with a probability of $\lambda_2 \Delta t$. Every other aspect of this stochastic model is the same as in the case of the CRW model and the derivation of a PDE satisfied by the occupation probability is very similar to the unbiased case. We use the same initial condition as in the CRW model, namely a point source at $x = x_0$, which we take to be zero without loss of generality.

Occupation Probability

As before, we start with a recurrence relation regarding the conditional occupation probabilities at time $t + \Delta t$. These are

$$\begin{aligned} \alpha(x, t + \Delta t) &= (1 - \lambda_1 \Delta t)\alpha(x - \Delta x, t) + \lambda_2 \Delta t \beta(x - \Delta x, t), \\ \beta(x, t + \Delta t) &= \lambda_1 \Delta t \alpha(x + \Delta x, t) + (1 - \lambda_2 \Delta t)\beta(x + \Delta x, t). \end{aligned} \tag{3.51}$$

Expanding as usual in Taylor series about the point (x, t) and by defining a finite velocity in the limit as $\Delta t \to 0$ and $\Delta x \to 0$ such that

$$v = \lim_{\Delta t \to 0, \Delta x \to 0} \frac{\Delta x}{\Delta t} \neq 0,$$

we find the governing PDEs for the conditional probabilities. In the case of a right-

moving individual, this reads

$$\frac{\partial \alpha}{\partial t} = -\lambda_1 \alpha + \lambda_2 \beta - v \frac{\partial \alpha}{\partial x}. \tag{3.52}$$

In a similar fashion, we obtain the PDE for $\beta(x,t)$,

$$\frac{\partial \beta}{\partial t} = \lambda_1 \alpha - \lambda_2 \beta + v \frac{\partial \beta}{\partial x}. \tag{3.53}$$

These equations reduce to the system of equations (3.33) in the special case $\lambda_1 = \lambda_2$. The equation satisfied by the unconditional occupation probability is given by

$$\frac{\partial^2 p}{\partial t^2} + (\lambda_1 + \lambda_2)\frac{\partial p}{\partial t} + v(\lambda_2 - \lambda_1)\frac{\partial p}{\partial x} = v^2 \frac{\partial^2 p}{\partial x^2}, \tag{3.54}$$

which is the biased telegrapher's equation (see Section A.4 of Appendix A for a derivation). The expected location of a particle moving according to the BCRW model is given by

$$E(X_t) = \frac{v(\lambda_2 - \lambda_1)}{\lambda_1 + \lambda_2}\left(t - \frac{1}{\lambda_1 + \lambda_2}(1 - e^{-(\lambda_1 + \lambda_2)t})\right). \tag{3.55}$$

Fig. 3.11 shows how this expression compares to the results of the simulation. Clearly there is a strong bias towards the right. This is a consequence of the fact that we have chosen $\lambda_1 < \lambda_2$ in the simulation, i.e. the particle has a stronger tendency to turn direction if it is left-moving. This tendency is stronger in the short-term as $E(X_t) \sim t^2$. As t becomes large, the mean is moving linearly with time as in the case of the BRW model.

The MSD satisfies the following equation

$$\frac{d^2}{dt^2}[E(X_t^2)]+(\lambda_1+\lambda_2)\frac{d}{dt}[E(X_t^2)]-2v^2-\frac{2v^2(\lambda_2-\lambda_1)}{\lambda_1+\lambda_2}\left(t-\frac{1}{\lambda_1+\lambda_2}(1-e^{-(\lambda_1+\lambda_2)t})\right)=0, \tag{3.56}$$

with initial conditions

$$E(X_0^2)=0, \quad \frac{d}{dt}[E(X_0^2)]=0.$$

By solving the ODE and substituting the solution into (A.11), we can derive an analytical expression for the variance in closed form,

$$\begin{aligned}\sigma_t^2 = &\frac{2v^2}{\lambda_1+\lambda_2}\left(1-\frac{(\lambda_2-\lambda_1)^2}{(\lambda_1+\lambda_2)^2}\right)t \\ &+\frac{(\lambda_2-\lambda_1)^2v^2}{(\lambda_1+\lambda_2)^4}(2e^{-(\lambda_1+\lambda_2)t}-e^{-2(\lambda_1+\lambda_2)t}) \\ &+\frac{5(\lambda_2-\lambda_1)^2v^2}{(\lambda_1+\lambda_2)^4}-\frac{2v^2}{(\lambda_1+\lambda_2)^2}.\end{aligned} \tag{3.57}$$

Fig. 3.12 shows a plot of this expression (red solid line) versus the data produced by the simulation of the stochastic model. We see that there is good agreement between the analytical results and the results from the Monte Carlo simulation. The discrepancy grows with time but if we perform more simulations or make Δx and Δt even smaller, this discrepancy will become smaller.

3.4.2.2 Boundary Conditions

We consider a reflecting boundary at $x = 0$ and an absorbing (or partially absorbing) boundary at $x = L$ as usual. The respective boundary conditions in the deterministic

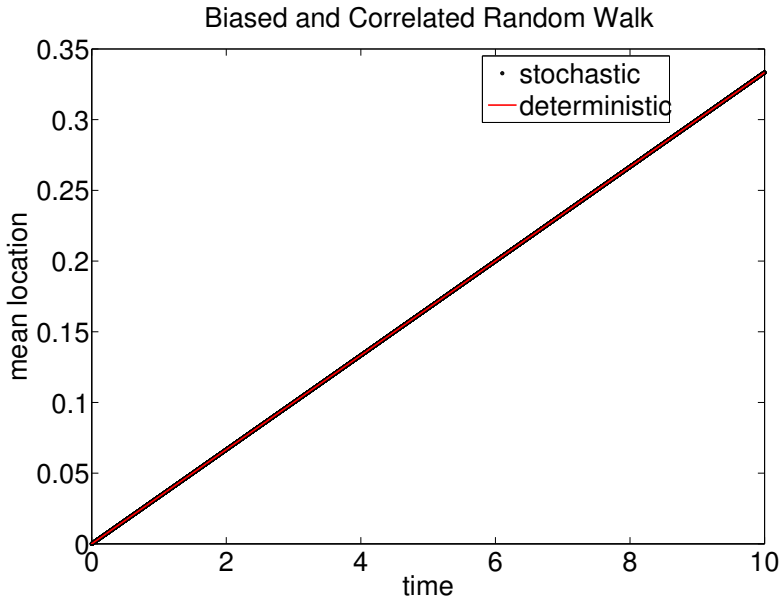


Figure 3.11: Plot of the evolution of the mean location, $E(X_t)$, over time in the BCRW model (in black dots) versus the analytical expression obtained from the deterministic model given by equation (3.55) (red solid line). We performed 10000 simulations and we have taken $\Delta x = 10^{-4}$, $\Delta t = 10^{-3}$ ($v = 10^{-1}$), $\lambda_1 = 10$ and $\lambda_2 = 100$.

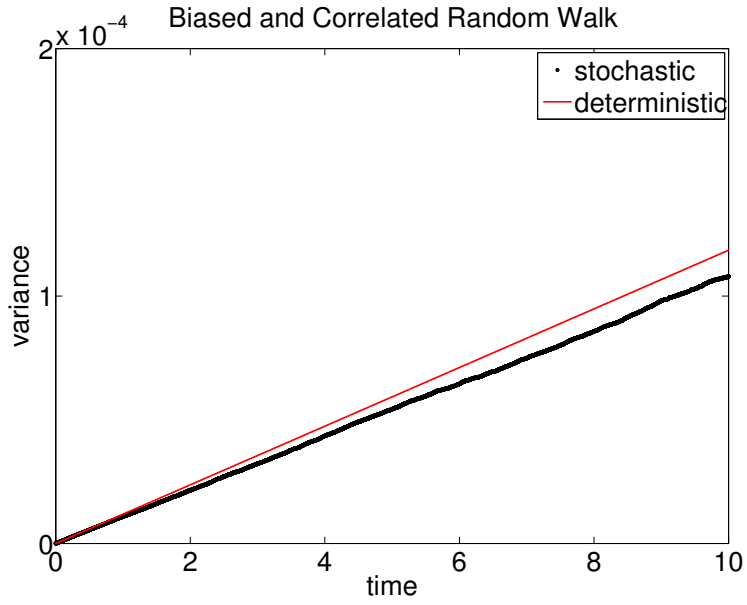


Figure 3.12: Plot of the evolution of the variance, σ_t^2, over time in the BCRW model (in black dots) versus the analytical expression obtained from the deterministic model given by equation (3.57) (red solid line). We performed 10000 simulations and we have taken $\Delta x = 10^{-4}$, $\Delta t = 10^{-3}$ ($v = 10^{-1}$), $\lambda_1 = 10$ and $\lambda_2 = 100$.

model take the form

$$\begin{aligned} \alpha(0,t) &= \beta(0,t), \\ \beta(L,t) &= 0, \quad \text{or}, \\ \beta(L,t) &= (1-\theta)\alpha(L,t), \end{aligned} \tag{3.58}$$

as was the case in the CRW model. A similar derivation (Section A.4 of Appendix A) through the set of equations (3.52) and (3.53) leads to the appropriate boundary conditions in terms of the unconditional probability, $p(x,t)$,

$$\begin{aligned} &v\frac{\partial p}{\partial x}(0,t) + (\lambda_1 - \lambda_2)p(0,t) = 0, \\ &\frac{\partial p}{\partial t}(L,t) + v\frac{\partial p}{\partial x}(L,t) + 2\lambda_1 p(L,t) = 0, \quad \text{or}, \\ &\theta\frac{\partial p}{\partial t}(L,t) + (2-\theta)v\frac{\partial p}{\partial x}(L,t) + (2\lambda_1 - 2\lambda_2 + 2\lambda_2\theta)p(L,t) = 0. \end{aligned} \tag{3.59}$$

Summary

In this chapter, we introduced four different stochastic processes, two position- and two velocity-jump processes, both from the perspective of an individual particle and from the perspective of a population of particles. We will use these stochastic processes as simplified models of cell migration in order to describe the time scale of invasion quantitatively. Initially, we considered migration from a microscopic view, i.e. the interactions at the cellular level, which are stochastic in nature, using stochastic models. Then, we established a connection to deterministic models that describe the macroscopic behaviour of cell migration, i.e. the tissue-level effects.

As we showed, the global behaviour of a stochastic process may be approximated by a deterministic model in certain limits. Various approaches may be used in order to establish such an equivalence. For each process, we first considered an individual approach, where the spatial location of a single particle is the random variable and

we seek the occupation probability distribution. Following that, we considered a population approach, where the observable is the spatial distribution of a population of particles. We also mentioned a third approach which is very powerful due to its generality [Othmer, 1988]. The authors defined a general framework for position- and velocity-jump processes, which considers a general waiting time distribution and a general redistribution kernel. As such, it may be used to model any jump process. The results of their analysis provide a way of deriving the deterministic model that describes the macroscopic behaviour of a jump-process, if it exists.

We also considered two different algorithms for simulating the stochastic processes computationally. The Monte Carlo method, which is intuitively easier to formulate, was used to simulate the models of the individual approach. The models formulated from a population perspective are simulated much more efficiently by Gillespie's SSA, but the validity of the algorithm as a model of a given stochastic approach needs to be derived through a master equation approach [Gillespie, 1977].

This chapter lays the foundation for the ensuing analysis of the first-passage properties of models of cell migration. The mathematical and computational techniques introduced here will also be used in order to consider other cellular processes, such as proliferation and death, that are involved in tumour migration. The comparison between the results of stochastic simulations and the analytical results derived from deterministic models make us confident that we can rely on them for an accurate description of the macroscopic behaviour of the processes we study. However, we need to consider carefully the assumptions and approximations of all the models and assess their validity when we apply them to test biological hypotheses in Chapter 6.

Chapter 4

First-Passage Time Analysis

Overview

How long does a process, such as diffusion, take? It takes an infinite amount of time to come to equilibrium so the question is not that simple and we would like a quantitative measure in order to define a mean time scale.

A wide range of stochastic processes may be explored through their first-passage properties. A *first-passage process* in the context of cell migration is defined as an event that occurs for the *first time* during the process. For instance, in all the models we consider in this thesis, we are interested in the time it takes for tumour cells to hit an absorbing boundary, representing a nerve, for the first time. The time it takes for such an event to occur is called the *first-passage time* (FPT), and its first moment, the *mean first-passage time* (MFPT), is often a very important aspect of the process from a biological point of view as it is a measure of its time scale. The theory of first-passage processes will allow us to compare the models presented in Chapter 3 through the estimation of the average time scale characterising each process under investigation.

The estimation of a mean first-passage time in the stochastic model is fairly straightforward as we only need to measure the time it takes an individual to hit the absorbing boundary over multiple simulations and calculate the mean. As far as corresponding deterministic models are concerned, various techniques have been developed but the majority are model-dependent.

4.1 Mean First-Passage Time

We present two of the most powerful techniques from our application perspective that start by considering the stochastic process and briefly mention one that treats deterministic models directly. Redner [2001] provides one of the most complete and formal treatises of first-passage processes. In Section 4.2, we present a method that consists of directly deriving an ODE for the MFPT, while in Section 4.3 we present a more flexible method, which provides an estimate for the MFPT indirectly. The former was originally introduced by Berg [1983] and independently, in a different form, by Gardiner [1985] and further developed by McKenzie et al. [2009], and the second by Redner [2001]. The former is very powerful due to its generality, especially when applied to one of the two broad categories of cell migration models, position-jump processes, but quite limited when applied to the other, velocity-jump processes, while the latter is much more model-dependent but it is suitable for any type of process. Techniques for finding the MFPT of velocity-jump processes have mainly been studied by Weiss and collaborators [Weiss, 1981, 1984, 2002, Masoliver et al., 1989]. Their method is useful for models of velocity-jump processes but it does not generalise easily and certain assumptions, especially with regards to the boundary conditions in the continuum deterministic description, are not straightforward deductions from the microscopic description. For a treatise of the MFPT of processes that occur in more complex or confined media, the reader is referred to the work of Condamin and

collaborators [Condamin et al., 2005, 2007].

The technique that begins with the macroscopic deterministic description of the process is that of the *Mean Action Time* (MAT), a quantity that represents the 'average' time taken for a disturbance introduced at one point of a domain to reach a boundary [Landman and McGuiness, 2000]. It is a useful quantitative measure for diffusive processes where the notion of an average time scale is hard to define. McNabb originally developed this approach [McNabb, 1975a, McNabb and Wake, 1991, McNabb, 1993] and applied it to the Stefan problem [McNabb, 1975b]. Landman and McGuiness [2000] re-derive some of the basic principles presented in the McNabb series of papers. The authors analyse some of the properties of MAT, such as the governing ODE it satisfies, using more rigorous definitions and formal presentation than McNabb. They also review several applications of this measure in physical problems such as the kinetics of water transport in human eye lenses [Moffat et al., 1999].

We merely mention the MAT formulation in this thesis and opt for the two MFPT approaches, discussed above, in the ensuing analysis, for two reasons. Firstly, the MAT approach is far more complicated and counter-intuitive an approach compared to the MFPT approaches. Simplifying assumptions in the approximations we need to make are less obvious and the method is only appropriate for relatively simple position-jump processes. Secondly, this theory considers the macroscopic continuum deterministic description of a stochastic process exclusively, whereas the MFPT approaches initially consider the stochastic model and so boundary conditions are derived rather than modelled phenomenologically using simplifying assumptions.

4.2 Direct Methods

One of the first treatments of the MFPT in an ecological context was performed by Berg [1983], who derived the governing equation that the MFPT obeys in simplistic models of cell migration. The author initially considered the stochastic process described by an SRW model by defining the 'mean time to capture' (to use the author's terminology; the meaning is the same to that of the term 'MFPT'), say $T(x)$, as the average time it takes for a walker located at $x \in (0, L)$ to reach an absorbing boundary for the first time. The walker can move to either $x - \Delta x$ or $x + \Delta x$ with equal probability during the next time step. Thus, the mean time to capture from point x is equal to the mean time to capture from points $x-\Delta x$ and $x+\Delta x$ times the probability of moving left or right, respectively, plus one time step. In mathematical terms,

$$T(x) = \Delta t + \frac{1}{2}T(x - \Delta x) + \frac{1}{2}T(x + \Delta x). \tag{4.1}$$

If we expand the last two terms of the RHS of equation (4.1) as a Taylor series about the point x, we obtain

$$\frac{1}{2}\Delta x^2 \frac{d^2T}{dx^2} + \Delta t = 0. \tag{4.2}$$

If the limit $D = \lim_{\Delta x \to 0} \frac{\Delta x^2}{2\Delta t} > 0$ exists, then the ODE satisfied by the mean time to capture is

$$\frac{d^2T}{dx^2} = -\frac{1}{D}. \tag{4.3}$$

To complete the problem we need to find the appropriate boundary conditions satisfied by T. If a particle is located at the absorbing boundary, it will be absorbed immediately and so we have

$$T(L) = 0.$$

If, on the other hand, the particle is located at the reflecting boundary at the origin, then we consider the difference equation it satisfies,

$$T(0) = \Delta t + \frac{1}{2}T(\Delta x) + \frac{1}{2}T(0),$$

since the particle can either arrive at $x = 0$ from position $x = \Delta x$ or from position $x = 0$, if it attempted to move to the left in the previous step but was reflected back to the same interval. This simplifies to

$$\frac{dT}{dx}(0) = 0.$$

The solution is given by

$$T(x) = \frac{1}{2D}\left(L^2 - x^2\right). \tag{4.4}$$

If, on the other hand, we tried to solve the difference equation (4.1) directly, the problem could be written in the form

$$-\frac{1}{2}T_{i+2} + T_{i+1} - \frac{1}{2}T_i = \Delta t, i = 0, 1, ..., N, \tag{4.5}$$

where i denotes each compartment and $N = \frac{L}{\Delta x}$. The required conditions are given by

$$\frac{1}{2}(T_0 + T_1) = \Delta t, \tag{4.6}$$

and

$$T_N = 0. \tag{4.7}$$

The solution is given by

$$T_i = \frac{[(2N-1)i^2 + (3-2N^2)i + N^2 - 3N]\Delta t}{1-2N}. \tag{4.8}$$

In the more general case of a biased random walk, the appropriate boundary conditions for T are the same but the corresponding equation to (4.1) is

$$T(x) = \Delta t + \alpha T(x + \Delta x) + \beta T(x - \Delta x). \tag{4.9}$$

This can be expanded to give

$$-(\beta - \alpha)\Delta x \frac{dT}{dx} + \frac{1}{2}\Delta x^2 \frac{d^2T}{dx^2} + \Delta t = 0, \tag{4.10}$$

through a series expansion at first order. The resulting ODE in this case is given by

$$D\frac{d^2T}{dx^2} + u\frac{dT}{dx} + 1 = 0. \tag{4.11}$$

The solution for the particular BCs is given by

$$T(x) = \frac{(L - x)}{u} + \frac{D}{u^2}(e^{-\frac{u}{D}L} - e^{-\frac{u}{D}x}). \tag{4.12}$$

In calculating the mean first-passage time, we assumed zero-flux boundary conditions at the surface of the skin, i.e. tumour cells cannot cross this boundary. However, in healthy tissue, cell loss is observed at the edge of the skin. Cells in the epidermis gradually migrate towards the surface where cell shedding occurs, i.e. dead squamous cells at the surface of the skin are constantly shed and replaced by basal cells being pushed toward the outer layers by the underlying mitotic activity (the entire journey of a cell from the basal layer to the surface takes about 60 days [Gawkrodger, 2003]. Hence, a study of the problem with an absorbing or partially absorbing barrier at $x = 0$ (Dirichlet or Robin boundary condition in the corresponding deterministic model) would provide a more realistic picture of the problem. If, in addition, the presence of healthy cells travelling in the opposite direction to that of tumour cells

(towards the surface of the skin) is investigated, the problem becomes even more realistic but also significantly more complicated.

In this thesis we will additionally examine the effect of an absorbing boundary at the surface of the skin and see how it compares with the results for the case of a reflecting boundary. We only show the results for the simple position-jump model, the SRW, as they suffice to explain the influence of such a boundary on the first-passage time. This investigation will also be a good example of showing that the direct method has more limitations than the second method we will present in the following section. Although the direct method is seemingly simpler as we only have to solve the ODE satisfied by the MFPT, the boundary conditions are not at all intuitive in the deterministic model, i.e. if we use a zero Dirichlet boundary condition for the MFPT at the absorbing boundary $x = 0$, the solution we obtain is

$$T(x) = \frac{1}{2D}\left(Lx - x^2\right), \tag{4.13}$$

which is similar to the result given by equation (4.4). As we shall see in the following section, this result happens to be correct but the Dirichlet boundary condition for the MFPT at $x = 0$ is not justified since we cannot say that a particle released at the absorbing boundary $x = 0$ will take no time to be absorbed at the absorbing boundary $x = L$. The second method does not necessitate the prescription of boundary conditions for the MFPT. Instead it requires boundary conditions for the occupation probability, which are easier to derive directly from the stochastic model (as we have already shown in the previous chapter).

McKenzie et al. [2009] formalised this technique and extended it to include processes taking place in spatially heterogeneous landscapes. The authors established a connection to the backward Fokker-Planck equation and then compared their results to existing theories of first-passage processes [Redner, 2001, Condamin et al., 2007, Gar-

diner, 1985]. However, it is evident that a treatment of a velocity-jump process with this method is much more involved since one would have to consider two components for the mean time until capture, one for each sub-population. The following section presents a more promising approach.

4.3 Time-Integrated Probability Formulation

We now present the *time-integrated probability* formulation by Redner [2001]. The main idea of this method is to consider the probability distribution of the first-passage time to a fixed boundary, rather than deriving a differential equation for the MFPT. The power of this method will become evident when we consider velocity-jump processes.

Suppose a particle is performing either a position- or a velocity-jump process. At the beginning of the process, the particle is released at $x = x_0 > 0$. We are interested in the average time it takes the particle to hit a fixed boundary, say $x = L > x_0$, which may be absorbing or partially absorbing/partially reflecting (also called 'reactive'). We start with the former type and we shall introduce the more general latter type of boundary later. At $x = 0$, there is a reflective boundary so that the particle cannot escape the domain from the left.

To begin, we define the *first-passage probability* $F(t; x_0)$ as the probability that a particle released from x_0 at $t = 0$ hits the boundary at $x = L$ in the interval $0 < t < t + dt$. The mean first-passage time may then be defined as

$$E[t(x_0)] =< t(x_0) >= \int_0^\infty t \cdot F(t; x_0) dt. \tag{4.14}$$

The complementary cumulative distribution of the first-passage probability, defined

as

$$S(t;x_0) = \int_t^\infty F(s;x_0)ds = 1 - \int_0^t F(s;x_0)ds, \tag{4.15}$$

is identical to the *survival probability*, the probability that the particle will not escape the domain (i.e. reach $x = L$) by time t. By differentiating with respect to t, we obtain

$$F(t;x_0) + \frac{\partial S}{\partial t}(t,x_0) = 0. \tag{4.16}$$

This is a very useful relation because we can use it to integrate the expression (4.14) by parts. This leads to

$$< t(x_0) >= \int_0^\infty S(t;x_0)dt - [tS(t,x_0)]_0^\infty, \tag{4.17}$$

where the second term vanishes since the probability that the particle survives as $t \to \infty$ tends to zero, or $\lim_{t\to\infty} S(t,x_0) \to 0$. Finally, recall the occupation probability, $p(x,t;x_0)$, i.e. the probability that a walker released at $x = x_0$ at $t = 0$ is located at x at time t, and define the *time-integrated occupation probability*,

$$P_0(x) = \int_0^\infty p(x,t;x_0)dt, \tag{4.18}$$

as the probability that a particle, released at x_0, is at position x at any time. Note also that the survival probability is equal to

$$S(t,x_0) = \int_0^L p(t,x;x_0)dx. \tag{4.19}$$

We can now apply Fubini's theorem to equation (4.17) to obtain

$$< t(x_0) >= \int_0^\infty \int_0^L p(x,t;x_0)dxdt = \int_0^L \int_0^\infty p(x,t;x_0)dtdx, \tag{4.20}$$

provided that

$$\int_0^L \int_0^\infty |p(x,t;x_0)| dt dx < \infty.$$

As a result, we have derived a relation between the time-integrated occupation probability and the MFPT,

$$< t(x_0) >= \int_0^L P_0(x) dx. \tag{4.21}$$

4.3.1 Simple Random Walk

We start by integrating the governing equation satisfied by the occupation probability with respect to time in order to obtain an ODE satisfied by the time-integrated probability, $P_0(x)$. In the SRW model, this corresponds to integrating the diffusion equation from $t = 0$ to $t = \infty$ to obtain

$$D\frac{d^2 P_0}{dx^2} = -\delta(x - x_0), \tag{4.22}$$

since $p(x, 0) = \delta(x - x_0)$ and $\lim_{t\to\infty} p(x, t; x_0) = 0$. Equation (4.22) is a linear second-order ODE but the solution is not straightforward due to a discontinuity in the derivative at $x = x_0$. We therefore have to split it into parts, $P_0^-(x)$ for $x < x_0$ and $P_0^+(x)$ for $x > x_0$, and substitute into equation (4.22) to obtain

$$\begin{aligned} D\frac{d^2 P_0^-}{dx^2} &= 0, \quad x < x_0, \\ D\frac{d^2 P_0^+}{dx^2} &= 0, \quad x > x_0, \end{aligned} \tag{4.23}$$

and solve it along with the boundary conditions at $x = 0, L$ and two extra conditions we need to derive at the point x_0. Recall that for a reflective boundary at $x = 0$, the appropriate condition for the occupation probability is $\frac{\partial p}{\partial x}(0, t) = 0$. This implies

$$\frac{dP_0^-}{dx}(0) = 0. \tag{4.24}$$

At $x = L$, the appropriate condition for an absorbing boundary is $p(L,t) = 0$, hence, in terms of the time-integrated occupation probability, we have

$$P_0^+(L) = 0, \tag{4.25}$$

or in the case of a partially absorbing boundary, where the boundary condition reads $\frac{\partial p}{\partial x}(L,t) = -\theta p(L,t)$, the condition we need is given by

$$\frac{dP_0^+}{dx}(L) = -\theta P_0^+(L). \tag{4.26}$$

We require that the solution is continuous at $x = x_0$, i.e. $\lim_{x_0^- \nearrow x_0} P_0(x_0^-) = \lim_{x_0^+ \swarrow x_0} P_0(x_0^+)$ and hence our third condition is

$$P_0^-(x_0) = P_0^+(x_0). \tag{4.27}$$

In order to obtain an expression for the fourth and final boundary condition, we need to estimate the size of the discontinuity at point x_0. This may be achieved by integrating equation (4.22) with respect to x from x_0^- to x_0^+ which results in the condition

$$\frac{dP_0^+}{dx}(x_0) - \frac{dP_0^-}{dx}(x_0) = -\frac{1}{D}. \tag{4.28}$$

Solving the system (4.23) with boundary conditions given by (4.24), (4.25), (4.27) and (4.28) in the case of an absorbing boundary at $x = L$, we obtain

$$P_0(x) = \frac{1}{D}(L - x^*), \tag{4.29}$$

where $x^* = \max(x, x_0)$. Replacing condition (4.25) by (4.26) to model a partially absorbing boundary at $x = L$, we obtain

$$P_0(x) = \frac{1}{D}\left(L - x^* + \frac{1}{\theta}\right). \tag{4.30}$$

Equation (4.21) allows us to derive an expression for the MFPT as a function of the initial point of release, which, in the case of a simple random walk, reads

$$< t(x_0) >= \frac{1}{2D}(L^2 - x_0^2), \tag{4.31}$$

or

$$< t(x_0) >= \frac{1}{2D}(L^2 - x_0^2) + \frac{L}{\theta D}, \tag{4.32}$$

respectively. Equation (4.31) is the same as equation (4.4), i.e. the solution of the PDE satisfied by the MFPT, obtained using the direct method.

Fig. 4.1 shows a comparison between the analytical expression for the MFPT in the SRW model and the results from the stochastic simulation for an absorbing and a partially absorbing boundary (left and right panel, respectively). As expected, the MFPT decreases as the diffusion coefficient increases since the particle is more motile. The MFPT also reduces quadratically with the initial location, therefore if we release a particle twice as far from the origin, the mean time it takes to reach the boundary will decrease by a factor of four. Furthermore, the larger the parameter θ, the less the time required until absorption at the boundary $x = L$ since the particle has a higher chance of being absorbed when at the boundary. As $\theta \to 0$, the boundary at $x = L$ becomes fully reflective and hence the MFPT tends to infinity, as expected since the particle will not be absorbed at all if this is the case.

We now consider an absorbing boundary at the surface of the skin using the time-integrated probability formulation. We need to solve the system of equations (4.23)

with the same boundary conditions except for the condition at $x = 0$ which now becomes $P_0^-(0) = 0$. The solution for the time-integrated occupation probability, in this case, is given by

$$\begin{aligned} P_0^- &= \left(\frac{1 - \frac{x_0}{L}}{D}\right) x, \quad x < x_0, \\ P_0^+ &= \left(\frac{1 - \frac{x}{L}}{D}\right) x_0, \quad x > x_0. \end{aligned} \tag{4.33}$$

The expression for the MFPT is given by

$$< t(x_0) >= \frac{1}{2D}\left(Lx - x^2\right), \tag{4.34}$$

which is identical to the expression obtained by the direct method. This result indicates that, in the presence of an absorbing boundary at the surface of the skin, the MFPT is smaller than in the case of a reflecting boundary. This result, which is further reinforced by the results of the simulation of the stochastic model (not shown here), is of course counter-intuitive. In order to understand and explain this, we have to consider the way in which we have defined and consequently record the MFPT in the stochastic model. Once a particle is released at x_0, it will either be absorbed at $x = L$, in which case we will record the time it takes to reach $x = L$, or it will move towards the left and will be absorbed at the boundary $x = 0$. If this is the case, we will not be able to record the *time it takes to reach* $x = L$, i.e. the required first-passage time, at all. In our simulation, it is recorded as zero or completely ignored, in which case the MFPT (recall the *average* first-passage time) will be less than the corresponding MFPT for the case of a reflecting boundary at $x = 0$. In that case, particles moving towards the left of the domain are reflected and take more time to reach the boundary $x = L$ and be absorbed there. Therefore, the effect of an absorbing boundary at the surface of the skin is to reduce the MFPT of those particles that actually reach the boundary $x = L$. On the other hand, if we are to

prescribe a certain level of particles, say 1000, that we require to reach the boundary $x = L$, out of say 10000 particles initially released, in order to be able to record their FPT at $x = L$, then there would be no difference in the MFPT between the case of an absorbing and that of a reflecting boundary at $x = 0$ as we would record the fastest particles in each case, i.e. those that are moving towards the right of the domain. Therefore, we see that the type of boundary at the surface does not really have any impact on the MFPT, i.e. the average timescale of the process, but rather on the number of particles actually reaching the right-hand boundary. Depending on the way we record the first-passage and the number of particles we take into consideration, the MFPT will be different: either it will be the same for each type of boundary or smaller in the case of the absorbing boundary, in which case however, it will be less representative and useful a quantity as we will have ignored a number of particles absorbed at the surface of the skin. The comparison between the two cases will be misleading.

Sometimes the mean first-passage time may not be that useful a measure as a criterion for whether invasion occurs or not. For example, the average timescale of invasion may be less indicative of the dynamics if there is a large variance. For instance, a few isolated tumour cells may be able to reach the nerve endings of the dermis in time, even if the mean suggests that this is not possible. Consequently, one should also look at the variance of the first-passage time so as to evaluate the conclusions reached from estimating the average timescale.

In order to calculate the variance of the first-passage time, we must resort to first principles as we did for the MFPT in the first part of this section. First of all, we need to consider the second moment of the first-passage probability, $F(t; x_0)$, with respect to time and then use the well-known formula that relates the first two moments of a probability distribution to its variance. The second moment of $F(t; x_0)$ is defined

as

$$< t(x_0)^2 >= \int_0^\infty t^2 F(t; x_0) dt. \tag{4.35}$$

This is equal to

$$[-t^2 S(t; x_0)]_0^\infty + 2 \int_0^\infty t S(t; x_0) dt,$$

if we integrate by parts and substitute the survival probability into the integral using the relation given by equation (4.16). Assuming that the survival probability decays to zero faster than any power of the first-passage time as the latter tends to infinity, i.e.

$$\lim_{t \to \infty} \frac{S(t; x_0)}{t^n} \to 0 \ \ \forall n,$$

we obtain

$$< t(x_0)^2 >= 2 \int_0^\infty t \left[\int_0^L p(x, t) dx \right] dt, \tag{4.36}$$

by using the definition of the survival probability. Assuming the absolute value of the above integral is finite, we can use Fubini's theorem to interchange the integration operations and obtain

$$< t(x_0)^2 >= 2 \int_0^L P_1(x) dx, \tag{4.37}$$

where $P_1(x) = \int_0^\infty t p(x, t) dt$ denotes the first moment of the occupation probability with respect to time (as opposed to the zeroth moment, the time-integrated probability, P_0). Therefore, the variance of the first-passage time is given by

$$Var[t(x_0)] =< t(x_0)^2 > - < t(x_0) >^2 = 2 \int_0^L P_1(x) dx - < t(x_0) >^2 . \tag{4.38}$$

Consequently, in order to calculate the variance of the first-passage time for each model, we need to first find an analytical expression for $P_1(x)$. We do this by multiplying the governing PDE for the occupation probability by t and integrating with respect to time, similarly to how we obtained the ODEs obeyed by $P_0(x)$.

In the SRW model, this ODE is given by

$$D\frac{d^2P_1}{dx^2} = -P_0, \tag{4.39}$$

which is a linear second-order ODE but the solution is not straightforward due to the discontinuity in the derivative at $x = x_0$. We therefore have to split it into two parts, $P_1^-(x)$ for $x < x_0$ and $P_1^+(x)$ for $x > x_0$, as previously, and substitute into equation (4.39) to obtain

$$\begin{aligned} D\frac{d^2P_1^-}{dx^2} &= \frac{x_0 - L}{D} + \left(\frac{1}{\theta D}\right), \quad x < x_0, \\ D\frac{d^2P_1^+}{dx^2} &= \frac{x - L}{D} + \left(\frac{1}{\theta D}\right), \quad x > x_0. \end{aligned} \tag{4.40}$$

The term in the brackets corresponds to the system concerning a partially absorbing boundary at $x = L$. The boundary and matching conditions are given by

$$\begin{aligned} \frac{dP_1^-}{dx}(0) &= 0, \\ P_1^+(L) &= 0, \\ P_1^-(x_0) &= P_1^+(x_0), \\ \frac{dP_1^-}{dx}(x_0) &= \frac{dP_1^+}{dx}(x_0). \end{aligned} \tag{4.41}$$

The second of these four conditions is replaced by

$$\frac{dP_1^+}{dx}(L) = -\theta P_1^+(L), \tag{4.42}$$

in the case of a partially absorbing boundary at $x = L$. Solving the above ODE boundary-value problem, we obtain

$$P_1(x) = \frac{1}{D^2}\left(\frac{L^3}{3} - \frac{L(x^2 + x_0^2)}{2} + \frac{x_+^3}{6} + \frac{x_0 x_- x}{2}\right), \tag{4.43}$$

where $x_- = \min(x, x_0)$ and $x_+ = \max(x, x_0)$. In the case of a partially absorbing boundary at $x = L$ we have

$$P_1(x) = \frac{1}{D^2}\left(\frac{L^3}{3} - \frac{L(x^2 + x_0^2)}{2} + \frac{x_+^3}{6} + \frac{x_0 x_- x}{2} + \frac{x^2 - x_0^2}{2\theta} - \frac{L}{\theta^2}\right). \tag{4.44}$$

The corresponding expressions for the variance of the first-passage time are given by

$$Var[t(x_0)] = \frac{1}{6D^2}(L^4 - x_0^4), \tag{4.45}$$

and

$$Var[t(x_0)] = \frac{1}{6D^2}(L^4 - x_0^4) - \frac{2L^3}{3\theta D^2} - \frac{3L^2}{\theta^2 D^2}, \tag{4.46}$$

respectively.

Fig. 4.2 shows a comparison between the data on the variance of the first-passage time from the simulation of the stochastic SRW model, and the theoretical predictions made by equations (4.45) and (4.46) for various initial locations. The validity of these predictions is reinforced by the good agreement with the simulation data. We see that the further away the initial point of release from the absorbing boundary at $x = L$ and closer to the origin, the larger the variance by an extra factor that is equal to the fourth power of the distance to $x = L$. As expected the variance is larger at initial locations further away from the absorbing boundary. If a particle is released close to the boundary, we intuitively expect a higher probability that it will be absorbed fast. However, a more interesting quantity is the relative difference between the size of the mean and the variance of the first-passage time. Fig. 4.3 shows a comparison between the first two moments of the first-passage time probability distribution and, as is evident, their size is similar closer to the absorbing boundary. At the other end of the domain, the variance is smaller in comparison to the MFPT. Hence, in the SRW model the variance of the first-passage time becomes more significant a

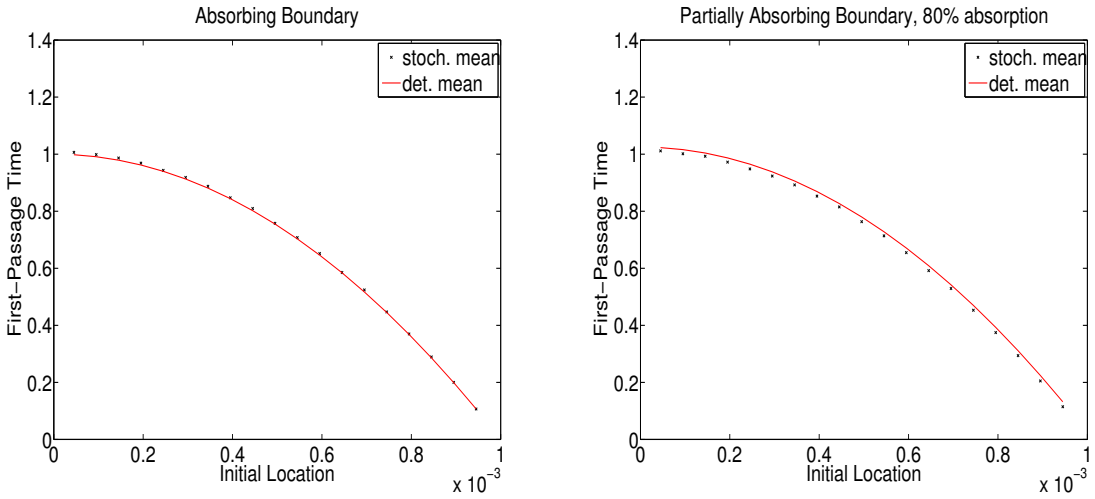


Figure 4.1: Plot of the mean first-passage time, $< t(x_0) >$, versus the initial position, x_0, for the SRW model. The left and right panels show the results of the stochastic simulation (black crosses) for a fully and a partially absorbing boundary (with a probability of absorption, $p_{absorb} = 0.8$), respectively. The analytical expressions, obtained from the deterministic model and given by equations (4.31) and (4.32), respectively, are depicted by the red solid line. We performed 100000 simulations and have taken $D = 5 \cdot 10^{-7}$ and $L = 10^{-3}$.

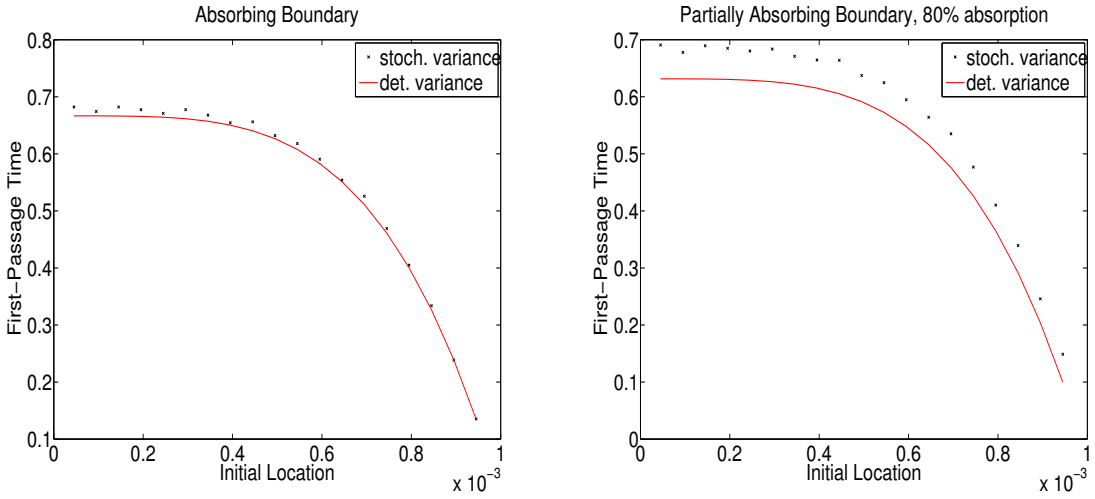


Figure 4.2: Plot of the variance of the first-passage time, $Var[t(x_0)]$, versus the initial position, x_0, for the SRW model. The left and right panels show the results of the stochastic simulation (black crosses) for a fully and a partially absorbing boundary (with a probability of absorption, $p_{absorb} = 0.8$), respectively. The analytical expressions, obtained from the deterministic model and given by equations (4.45) and (4.46), respectively, are depicted by the red solid line. We performed 100000 simulations and have taken $D = 5 \cdot 10^{-7}$ and $L = 10^{-3}$.

quantity the closer the point of release to the absorbing boundary at the right-hand of the domain.

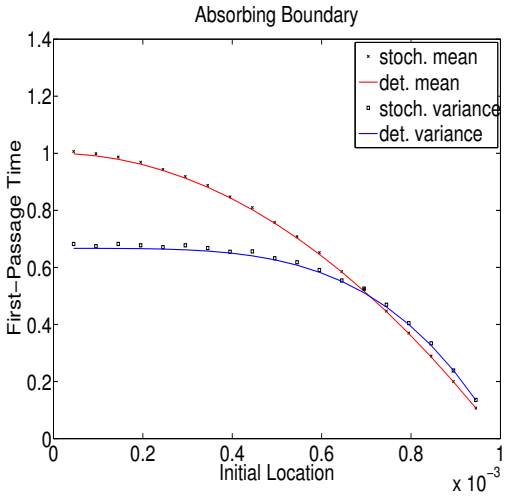


Figure 4.3: Plot of the mean and the variance of the first-passage time versus the initial position, x_0, for the SRW model. The analytical expressions, obtained from the deterministic model and given by equations (4.31) and (4.45), respectively, are depicted by the red solid line. We performed 100000 simulations and have taken $D = 5 \cdot 10^{-7}$ and $L = 10^{-3}$.

4.3.2 Biased Random Walk

As in the previous section, we begin by integrating the governing equation satisfied by the occupation probability with respect to time in order to obtain an ODE. In the BRW model, this corresponds to integrating the advection-diffusion equation (3.16) from $t = 0$ to $t = \infty$ to obtain

$$D\frac{d^2P_0}{dx^2} - u\frac{dP_0}{dx} = -\delta(x - x_0) \tag{4.47}$$

as $p(x, 0) = \delta(x - x_0)$ and $\lim_{t\to\infty} p(x, t; x_0) = 0$. We split the solution of equation (4.47) into two parts to address the presence of the discontinuity in the derivative at

$x = x_0$ and so the system of ODEs that we need to solve is

$$\begin{aligned} D\frac{d^2P_0^-}{dx^2} - u\frac{dP_0^-}{dx} = 0, \quad x < x_0, \\ D\frac{d^2P_0^+}{dx^2} - u\frac{dP_0^+}{dx} = 0, \quad x > x_0. \end{aligned} \tag{4.48}$$

In order to solve this, we consider the boundary conditions at $x = 0, L$ and two extra conditions at the point x_0. Recall that for a reflective boundary at $x = 0$, the appropriate condition for the occupation probability in the BRW is the zero-flux condition $D\frac{\partial p}{\partial x}(0,t) - up(0,t) = 0$. This implies

$$D\frac{dP_0^-}{dx}(0) - uP_0^-(0) = 0. \tag{4.49}$$

At $x = L$, the appropriate condition for an absorbing boundary is $p(L,t) = 0$, so we have

$$P_0^+(L) = 0, \tag{4.50}$$

or in the case of a partially absorbing boundary, where the boundary condition reads $\frac{\partial p}{\partial x}(L,t) - up(L,t) = -\theta p(L,t)$, the condition we need is given by

$$D\frac{dP_0^+}{dx}(L) - uP_0^+(L) = -\theta DP_0^+(L). \tag{4.51}$$

We require that the solution is continuous at $x = x_0$ so our third condition is the same as in the SRW model, namely

$$P_0^-(x_0) = P_0^+(x_0). \tag{4.52}$$

Finally, we integrate equation (4.47) with respect to x from x_0^- to x_0^+ to obtain the

last condition, which is also the same as in the SRW model,

$$\frac{dP_0^+}{dx}(x_0) - \frac{dP_0^-}{dx}(x_0) = -\frac{1}{D}, \tag{4.53}$$

as the terms $\pm u P_0^{\pm}(x_0)$ cancel each other out due to condition (4.52). Solving the system (4.83) with boundary conditions given by (4.49), (4.50), (4.52) and (4.53) in the case of an absorbing boundary at $x = L$, we obtain

$$P_0(x) = \frac{1}{u}(e^{\frac{u}{D}(x^*-x_0)} - e^{\frac{u}{D}(x-L)}), \tag{4.54}$$

where $x^* = \min(x, x_0)$. Replacing condition (4.50) by (4.51) to model a partially absorbing boundary at $x = L$, we obtain

$$P_0(x) = \frac{1}{u}(e^{\frac{u}{D}(x^*-x_0)} - e^{\frac{u}{D}(x-L)}) + \frac{1}{\theta D}e^{\frac{u}{D}(x-L)}. \tag{4.55}$$

The corresponding expressions for the MFPT are given by

$$< t(x_0) >= \frac{(L-x_0)}{u} + \frac{D}{u^2}(e^{-\frac{u}{D}L} - e^{-\frac{u}{D}x_0}), \tag{4.56}$$

and

$$< t(x_0) >= \frac{(L-x_0)}{u} + \frac{D}{u^2}(e^{-\frac{u}{D}L} - e^{-\frac{u}{D}x_0}) + \frac{1-e^{-\frac{u}{D}L}}{\theta u}, \tag{4.57}$$

respectively. As $u \to \infty$, $< t(x_0) > \to \frac{L-x_0}{u}$, while as $u \to 0$, we have

$$\begin{aligned}\lim_{u\to 0} < t(x_0) > &= \frac{(L-x_0)}{u} + \frac{D}{u^2}\left(1 - \frac{u}{D}L + \frac{u^2}{2D^2}L^2 - 1 + \frac{u}{D}x_0 - \frac{u^2}{2D^2}x_0^2 + O(u^3)\right) \\ &= \frac{L^2 - x_0^2}{2D},\end{aligned}$$

as expected from the results of the SRW model.

Fig. 4.4 shows a comparison between the analytical expression for the MFPT in the

BRW model and the results of the stochastic model for an absorbing and a partially absorbing boundary (left and right panel, respectively). In this model, the MFPT reduces faster as the initial location is chosen closer to the absorbing barrier at $x = L$. The effect of the parameter θ is similar to that for the SRW case and in the limits $\theta \to 0$ and $\theta \to \infty$ such that $\theta \Delta x \to 1$, we obtain the familiar expressions for a fully reflecting and a fully absorbing boundary, namely the MPFT tends to infinity in the former case, while it tends to the expression (4.56) in the latter case.

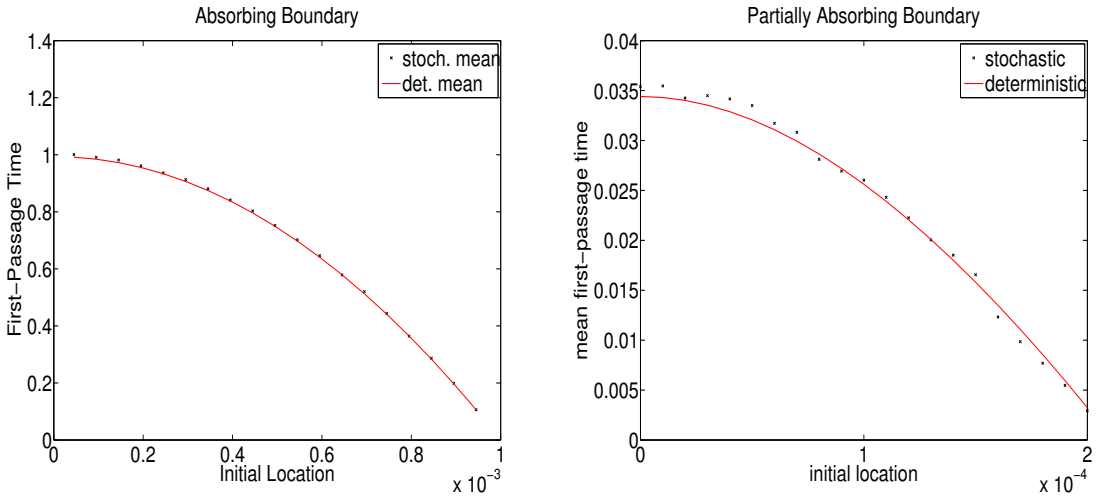


Figure 4.4: Plot of the mean first-passage time, $< t(x_0) >$, versus the initial position, x_0, for the BRW model. The left and right panels show the results of the stochastic simulation (black crosses) for a fully and a partially absorbing boundary (with a probability of absorption, $p_{absorb} = 0.8$), respectively. The analytical expressions, obtained from the deterministic model and given by equations (4.56) and (4.57), respectively, are depicted by the red solid line. We performed 100000 simulations and have taken $D = 5 \cdot 10^{-7}$, $u = 10^{-5}$ and $L = 10^{-3}$ in the case of the fully absorbing boundary and $u = 2 \cdot 10^{-3}$, $L = 2 \cdot 10^{-4}$ in the case of the partially absorbing boundary.

In the BRW model, the ODE governing the spatial distribution of $P_1(x)$ is given by

$$D\frac{d^2P_1}{dx^2} - u\frac{dP_1}{dx} = -P_0. \tag{4.58}$$

As in the case of the SRW model, the solution is not straightforward due to the discontinuity in the derivative at $x = x_0$. We therefore have to split it into two parts, $P_1^-(x)$ for $x < x_0$ and $P_1^+(x)$ for $x > x_0$, as previously, and substitute into equation

(4.58) to obtain

$$\begin{aligned} D\frac{d^2P_1^-}{dx^2} - u\frac{dP_1}{dx} &= \frac{1}{u}(e^{-\frac{u}{D}L} - e^{-\frac{u}{D}x_0})e^{\frac{u}{D}x}, \quad x < x_0, \\ D\frac{d^2P_1^+}{dx^2} - u\frac{dP_1}{dx} &= \frac{1}{u}(e^{\frac{u}{D}(x-L)} - 1), \quad x > x_0. \end{aligned} \tag{4.59}$$

The boundary and matching conditions are given by

$$\begin{aligned} D\frac{dP_1^-}{dx}(0) - uP_1^-(0) &= 0, \\ P_1^+(L) &= 0, \\ P_1^-(x_0) &= P_1^+(x_0), \\ \frac{dP_1^-}{dx}(x_0) &= \frac{dP_1^+}{dx}(x_0). \end{aligned} \tag{4.60}$$

The solution of the above ODE boundary-value problem is given by

$$\begin{aligned} P_1(x) = \frac{D}{u^3}(e^{-\frac{u}{D}x_0} - e^{-\frac{u}{D}L})(e^{\frac{u}{D}(x-L)} - 1) + \frac{1}{u^2}\left(x + x_0 - 2L - 2\frac{D}{u}\right)e^{\frac{u}{D}(x-L)} \\ + \frac{1}{u^2}\left[|x - x_0| + 2\frac{D}{u}\right)e^{\frac{u}{D}(x^*-x_0)}, \end{aligned} \tag{4.61}$$

where $x_* = \min(x, x_0)$. The corresponding expressions for the variance of the first-passage time are given by

$$\begin{aligned} Var[t(x_0)] = 2\frac{D}{u^3}\left(L - x_0 + 2Le^{-\frac{u}{D}L} - x_0e^{-\frac{u}{D}L} - x_0e^{-\frac{u}{D}x_0}\right) \\ + (e^{-\frac{u}{D}L} - e^{-\frac{u}{D}x_0})\left(\frac{4D^2}{u^4} + \frac{2D}{u^3}x_0 + \frac{D^2}{u^4}e^{-\frac{u}{D}L} + \frac{D^2}{u^4}e^{-\frac{u}{D}x_0}\right). \end{aligned} \tag{4.62}$$

The left panel of Fig. 4.5 shows a comparison between the data on the variance of the first-passage time from the simulation of the stochastic BRW model, and the theoretical predictions of equation (4.62) for various initial locations. The validity of the equations is confirmed by the good agreement with the simulation data. We see that the further away the initial point of release from the absorbing boundary

at $x = L$ and closer to the origin, the larger the variance as in the case of the SRW model. As expected, the variance is again larger at initial locations further away from the absorbing boundary. Additionally, the difference in size between the first two moments of the first-passage time is smaller closer to the absorbing boundary and larger at the other end of the domain, as shown by the right panel of Fig. 4.5. Hence, the variance of the first-passage time in the BRW model becomes less significant, as previously, if we release a particle far from the absorbing boundary.

4.3.3 Correlated Random Walk

We begin by integrating the telegrapher's equation (A.37) with respect to t from $t = 0$ to $t = \infty$ to obtain the ODE satisfied by the time-integrated probability

$$\frac{d^2 P_0}{dx^2} = -\frac{2\lambda}{v^2}\delta(x - x_0). \tag{4.63}$$

As usual, we split the solution into two parts and attempt to solve the system

$$\begin{aligned} \frac{d^2 P_0^-}{dx^2} &= 0, \quad x < x_0, \\ \frac{d^2 P_0^+}{dx^2} &= 0, \quad x > x_0, \end{aligned} \tag{4.64}$$

subject to the appropriate boundary conditions for the CRW model. At the reflecting boundary at $x = 0$, the boundary condition in terms of the occupation probability is a zero Neumann condition, hence the condition we seek, in terms of the time-integrated probability, is

$$\frac{dP_0^-}{dx}(0) = 0. \tag{4.65}$$

At the absorbing, or partially absorbing, boundary, the appropriate, respective, conditions for $P_0(L)$ are given by

$$v\frac{dP_0^+}{dx}(L) + 2\lambda P_0^+(L) = 0, \tag{4.66}$$

and

$$(2-\theta)v\frac{dP_0^+}{dx}(L) + 2\lambda\theta P_0^+(L) = 0. \tag{4.67}$$

We also require a matching condition at x_0, which represents the continuity of the solution. Finally, the fourth condition, which is obtained by estimating the size of the discontinuity of the derivative at x_0, is given by

$$\frac{dP_0^+}{dx}(x_0) - \frac{dP_0^-}{dx}(x_0) = -\frac{2\lambda}{v^2}. \tag{4.68}$$

Solving the system using the characteristic polynomials of the two ODEs, we obtain

$$P_0(x) = \frac{2\lambda}{v^2}(L - x^*) + \frac{1}{v}, \tag{4.69}$$

where $x^* = \max(x, x_0)$ in the case of a fully absorbing boundary and

$$P_0(x) = \frac{2\lambda}{v^2}(L - x^*) + \frac{2-\theta}{\theta v}, \tag{4.70}$$

in the case of a partially absorbing one. Upon substitution of the time-integrated occupation probability into equation (4.21), we derive an analytical expression for the MFPT of the CRW model, given by

$$< t(x_0) >= \frac{\lambda}{v^2}(L^2 - x_0^2) + \frac{L}{v}, \tag{4.71}$$

or

$$< t(x_0) >= \frac{\lambda}{v^2}(L^2 - x_0^2) + \frac{2-\theta}{\theta}\frac{L}{v}, \tag{4.72}$$

respectively.

Fig. 4.6 shows a plot of the MFPT for a fully and a partially absorbing barrier (left and right panel, respectively) from the results of the simulation of the stochastic model representing a CRW versus the analytical expressions given by (4.71) and (4.72), respectively. There is good agreement between the two types of models as in the previous cases, which shows the effectiveness of estimating the MFPT of velocity-jump processes through the time-integrated probability formulation. A higher velocity implies that the particle needs less time to reach the boundary, as expected, while with a higher turning rate, the motion is completely random since there is no persistence and so more time is necessary. As was the case in the SRW model, the MFPT reduces quadratically with the initial position of the particle, but the proportionality constant is $\frac{\lambda}{v^2}$ instead of $\frac{1}{2D}$. Finally, the MFPT will decrease as $\theta \to 1$, i.e. as the boundary at $x = L$ becomes fully absorbing and for $\theta = 1$ in particular, the MFPT reduces to the expression given by (4.71).

In the CRW model, the ODE obeyed by the first moment of the occupation probability with respect to time, $P_1(x)$, is given by

$$\frac{d^2 P_1}{dx^2} = -\frac{2\lambda}{v^2}P_0 + \frac{1}{v^2}\delta(x - x_0). \tag{4.73}$$

Again the solution is not straightforward due to the discontinuity in the derivative at $x = x_0$. We therefore have to split it into two parts, $P_1^-(x)$ for $x < x_0$ and $P_1^+(x)$ for

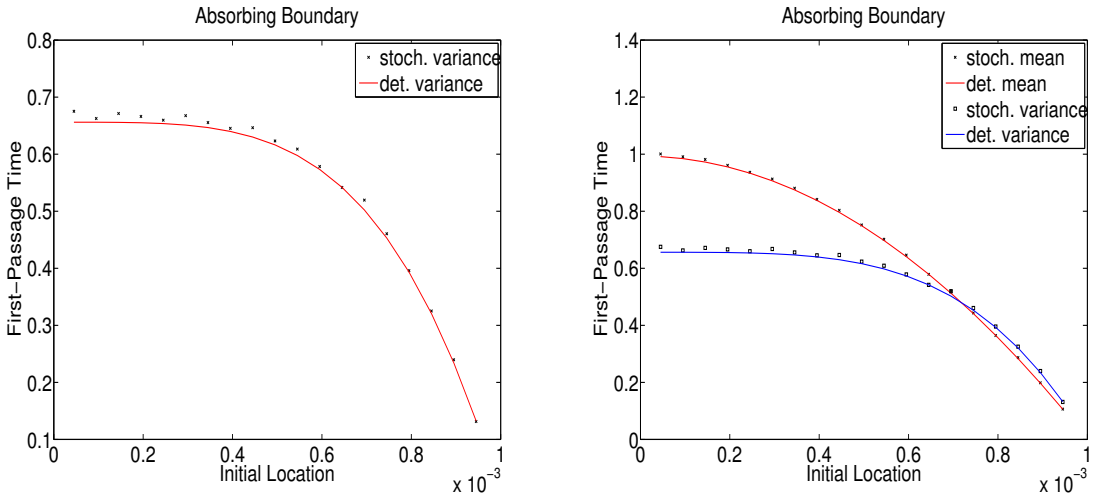


Figure 4.5: Plot of the variance first-passage time, $< t(x_0) >$, versus the initial position, x_0, for the BRW model in the left panel. The analytical expressions, obtained from the deterministic model are depicted by the red solid line. We performed 100000 simulations and have taken $D = 5 \cdot 10^{-7}$, $u = 10^{-5}$ and $L = 10^{-3}$ and a fully absorbing boundary at $x = L$. The right panel shows a comparison between the mean and the variance of the first-passage time.

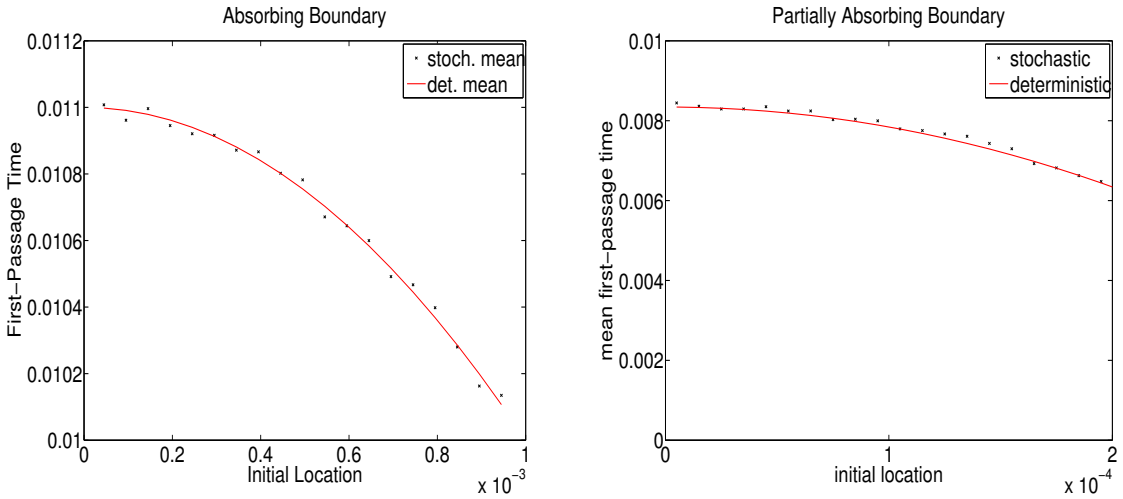


Figure 4.6: Plot of the mean first-passage time, $< t(x_0) >$, versus the initial position, x_0, for the CRW model. The left and right panels show the results of the stochastic simulation (black crosses) for a fully and a partially absorbing boundary (with a probability of absorption, $p_{absorb} = 0.85$), respectively. The analytical expressions, obtained from the deterministic model and given by equations (4.71) and (4.72), respectively, are depicted by the red solid line. We performed 100000 simulations and have taken $v = 10^{-1}$, $\lambda = 10$ and $L = 10^{-3}$ in the case of the fully absorbing boundary and $L = 2 \cdot 10^{-4}$ in the case of the partially absorbing boundary.

$x > x_0$, as previously, and substitute into equation (4.73) to obtain

$$\begin{aligned} \frac{d^2P_1^-}{dx^2} &= \frac{4\lambda^2}{v^4}(x_0 - L) - \frac{2\lambda}{v^3}, \quad x < x_0, \\ \frac{d^2P_1^+}{dx^2} &= \frac{4\lambda^2}{v^4}(x - L) - \frac{2\lambda}{v^3}, \quad x > x_0. \end{aligned} \tag{4.74}$$

The ODE system for the case of a partially absorbing boundary at $x = L$ is, on the other hand, given by

$$\begin{aligned} \frac{d^2P_1^-}{dx^2} &= \frac{4\lambda^2}{v^4}(x_0 - L) - \frac{2-\theta}{\theta}\frac{2\lambda}{v^3}, \quad x < x_0, \\ \frac{d^2P_1^+}{dx^2} &= \frac{4\lambda^2}{v^4}(x - L) - \frac{2-\theta}{\theta}\frac{2\lambda}{v^3}, \quad x > x_0. \end{aligned} \tag{4.75}$$

The boundary and matching conditions are given by

$$\begin{aligned} \frac{dP_1^-}{dx}(0) &= 0, \\ v\frac{dP_1^+}{dx}(L) + 2\lambda P_1^+(L) &= P_0(L), \\ P_1^-(x_0) &= P_1^+(x_0), \\ \frac{dP_1^-}{dx}(x_0) - \frac{dP_1^+}{dx}(x_0) &= \frac{1}{v^2}. \end{aligned} \tag{4.76}$$

The second of these four conditions is replaced by

$$(2-\theta)v\frac{dP_1^+}{dx}(L) + 2\lambda\theta P_1^+(L) = \theta P_0(L), \tag{4.77}$$

in the case of a partially absorbing boundary at $x = L$. Solving the above ODE boundary-value problem, we obtain

$$P_1(x) = \frac{4\lambda^2L^3}{3v^4} + \frac{2\lambda L^2}{v^3} - \left(\frac{2\lambda^2 L}{v^4} + \frac{\lambda}{v^3}\right)(x^2 + x_0^2) + \frac{2\lambda^2}{3v^4}x_+^3 + \frac{2\lambda^2}{v^4}x_0x_-x + \frac{1}{v^2}x_+, \tag{4.78}$$

where $x_- = \min(x, x_0)$ and $x_+ = \max(x, x_0)$. In the case of a partially absorbing

boundary at $x = L$ we have

$$P_1(x) = \frac{4\lambda^2 L^3}{3v^4} + \frac{2-\theta}{\theta}\frac{2\lambda L^2}{v^3} - \left(\frac{2\lambda^2 L}{v^4} + \frac{2-\theta}{\theta}\frac{\lambda}{v^3}\right)(x^2 + x_0^2) + \frac{2\lambda^2}{3v^4}x_+^3 + \frac{2\lambda^2}{v^4}x_0 x_- x + \frac{1}{v^2}x_+ + \left[\left(\frac{2-\theta}{\theta}\right)^2 - 1\right]\frac{L}{v^2}. \tag{4.79}$$

The corresponding expressions for the variance of the first-passage time are given by

$$Var[t(x_0)] = \frac{2\lambda^2}{3v^4}(L^4 - x_0^4) + \frac{2-\theta}{\theta}\frac{4\lambda}{3v^3}L^3 + \frac{1}{v^2}x_0^2, \tag{4.80}$$

and

$$Var[t(x_0)] = \frac{2\lambda^2}{3v^4}(L^4 - x_0^4) + \frac{4\lambda}{3v^3}L^3 + \frac{1}{v^2}x_0^2 + \left[\left(\frac{2-\theta}{\theta}\right)^2 - 1\right]\frac{L^2}{v^2}, \tag{4.81}$$

respectively.

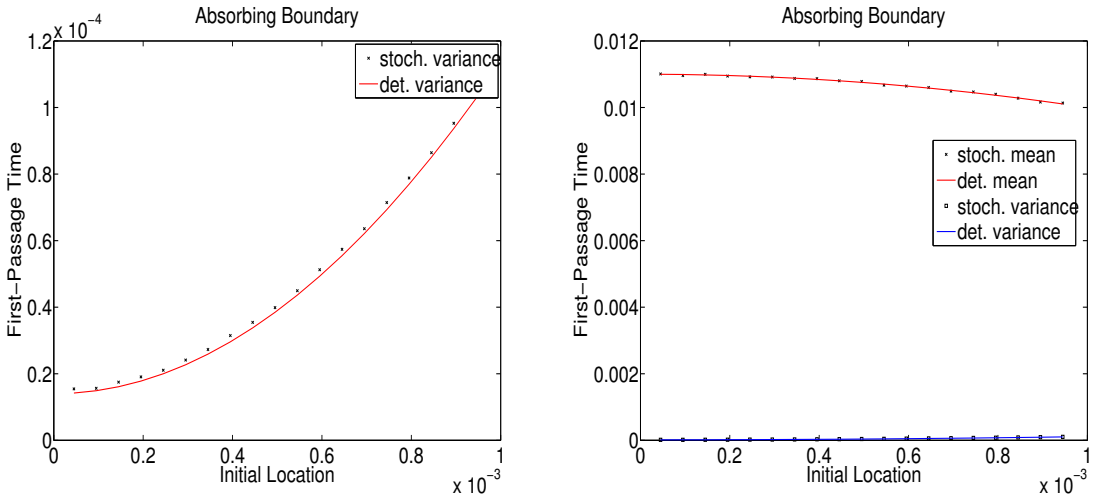


Figure 4.7: Plot of the variance first-passage time, $< t(x_0) >$, versus the initial position, x_0, for the CRW model in the left panel. The analytical expressions, obtained from the deterministic model are depicted by the red solid line. We performed 100000 simulations and have taken $v = 10^{-1}$, $\lambda = 10$ and $L = 10^{-3}$ and a fully absorbing boundary at $x = L$. The right panel shows a comparison between the mean and the variance of the first-passage time.

The left panel of Fig. 4.7 shows a comparison of the variance of the first-passage time between the data obtained from the simulation of the CRW model and the theoretical

predictions given by equation (4.80). In contrast to the corresponding results for the position-jump processes, the variance of the first-passage time in the CRW model is much greater if the point of release is closer to the absorbing boundary at $x = L$. This is not expected intuitively. It can be explained, however, if we consider carefully what happens in a CRW. If a particle is released close to $x = L$, it has an equal chance of jumping to the right and to the left initially. Its correlation coefficient is quite high (as the turning probability is equal to $\lambda\Delta t \simeq \lambda\frac{\Delta}{v} = 10^{-3}$ in this case, which is an extremely low probability of changing direction). Thus, the FPT of the particle depends heavily on the initial direction it takes. On the other hand, a particle released close to the other end of the domain will either go right and strongly persist in its direction or go left, persist again in its direction but be reflected quite soon at the boundary at $x = 0$. After being reflected, it will strongly persist in a rightward direction. Therefore, there is not such a significant variance in the time it will take to be absorbed at $x = L$. Consequently, after a careful consideration of the mechanism of a velocity-jump process, the variance of the first-passage time should be expected to be higher if the particle is released close to the absorbing boundary, given a high persistence in direction. This effect will be reversed given a low persistence in direction (high turning ratio) as the first-passage time will not depend strongly on the initial direction of the particle. The motion will start resembling a simple unbiased random walk and hence there will be a higher variance of the time until capture for particles released further away from the absorbing boundary.

The right panel of Fig. 4.7 shows a comparison between the size of the MFPT and the variance of the first-passage time for various initial locations. Again, we notice an effect which is quite different from the results obtained in the case of the position-jump processes. The variance is significantly lower - in fact two orders of magnitude lower - than the MFPT. The reason is the high persistence rate in the previous direction of motion which ensures that the first-passage time will not vary significantly between

the different realisations.

4.3.4 Biased and Correlated Random Walk

Following the usual approach, the ODE satisfied by the time-integrated probability can be shown to be

$$v^2\frac{d^2P_0}{dx^2} + v(\lambda_1 - \lambda_2)\frac{dP_0}{dx} = -(\lambda_1 + \lambda_2)\delta(x - x_0). \tag{4.82}$$

Splitting the solution into two parts, we need to solve the system

$$\begin{aligned} v\frac{d^2P_0^-}{dx^2} + (\lambda_1 - \lambda_2)\frac{dP_0^-}{dx} = 0, \quad x < x_0, \\ v\frac{d^2P_0^+}{dx^2} + (\lambda_1 - \lambda_2)\frac{dP_0^+}{dx} = 0, \quad x > x_0, \end{aligned} \tag{4.83}$$

subject to the following conditions

$$\begin{aligned} &v\frac{dP_0^-}{dx}(0) + (\lambda_1 - \lambda_2)P_0^-(0) = 0, \\ &v\frac{dP_0^+}{dx}(L) + 2\lambda_1 P_0^+(L) = 0, \quad \text{or} \\ &v\frac{dP_0^+}{dx}(L) + \frac{2(\lambda_1 + (\theta - 1)\lambda_2)}{2 - \theta}P_0^+(L) = 0, \\ &P_0^-(x_0) = P_0^+(x_0), \\ &\frac{dP_0^+}{dx}(x_0) - \frac{dP_0^-}{dx}(x_0) = -\frac{\lambda_1 + \lambda_2}{v^2}. \end{aligned} \tag{4.84}$$

The respective solutions P_0, for the cases of a fully and a partially absorbing barrier, are given by

$$P_0(x) = \frac{(\lambda_1 + \lambda_2)e^{\frac{\lambda_2 - \lambda_1}{v}(x^* - x_0)} - 2\lambda_1 e^{\frac{\lambda_2 - \lambda_1}{v}(x - L)}}{v(\lambda_2 - \lambda_1)}, \tag{4.85}$$

and

$$P_0(x) = \frac{(\lambda_1 + \lambda_2)e^{\frac{\lambda_2 - \lambda_1}{v}(x^* - x_0)} + 2((1 - \theta)\lambda_2 - \lambda_1)e^{\frac{\lambda_2 - \lambda_1}{v}(x - L)}}{v(\lambda_2 - \lambda_1)}, \tag{4.86}$$

where $x^* = \min(x, x_0)$. The respective expressions for the MFPT can be shown to be

$$< t(x_0) >= \frac{\lambda_1 + \lambda_2}{v(\lambda_2 - \lambda_1)}(L - x_0) + \frac{1}{\lambda_2 - \lambda_1} + \frac{2\lambda_1 e^{-\frac{\lambda_2 - \lambda_1}{v}L} - (\lambda_1 + \lambda_2)e^{-\frac{\lambda_2 - \lambda_1}{v}x_0}}{(\lambda_2 - \lambda_1)^2}, \quad (4.87)$$

and

$$\begin{aligned} < t(x_0) > = & \frac{\lambda_1 + \lambda_2}{v(\lambda_2 - \lambda_1)}(L - x_0) + \frac{(3 - 2\theta)\lambda_2 - \lambda_1}{(\lambda_2 - \lambda_1)^2} \\ & + \frac{2(\lambda_1 - (1 - \theta)\lambda_2)e^{-\frac{\lambda_2 - \lambda_1}{v}L} - (\lambda_1 + \lambda_2)e^{-\frac{\lambda_2 - \lambda_1}{v}x_0}}{(\lambda_2 - \lambda_1)^2}. \end{aligned} \quad (4.88)$$

Fig. 4.8 shows a plot of the MFPT for a fully and a partially absorbing boundary (left and right panel, respectively) from the results of the simulation of the stochastic model representing a BCRW versus the analytical expressions given by equations (4.87) and (4.88), respectively. The bias towards the right makes the time to reach the boundary considerably smaller than in the CRW case. The effect of the parameter θ representing the permeability of the boundary is the same as in all other cases.

Summary

In this chapter, we introduced the notion of the first-passage time and its first moment in order to rigorously define the concept of a 'mean time scale' for processes, such as diffusion, that require an infinite amount of time to reach an equilibrium state. The MFPT can be used as a quantitative tool that enables a comparison between the different invasion processes considered in the four cellular-level hypotheses we investigate regarding the mechanism behind PNI.

As we saw, implementing one-dimensional models of stochastic processes and performing simulations to record the MFPT is not difficult. However, obtaining analytical

results is significantly harder and there exists a variety of techniques, each with its own merits and drawbacks. In particular, we applied two techniques for calculating the MFPT of the migration models introduced in Chapter 3 and also briefly mentioned the MAT approach. We chose to proceed with the MFPT approaches in the ensuing analysis for several reasons. Firstly, the two MFPT approaches are formulated through an initial consideration of the stochastic model representing a process, whereas the MAT approach considers the equivalent deterministic model directly. As aforementioned, and as will become more obvious in the next chapter where branching processes are incorporated into the models, a discrepancy may exist between the two modelling regimes as deterministic models are often formulated phenomenologically rather than derived from the microscopic behaviour of the underlying discrete components of a system. Furthermore, the approximation is only valid in certain limits. Thus, it is more appropriate to treat the stochastic models as the basis of our analysis. Secondly, the MFPT approaches have significantly wider applications than the MAT approach and the literature on the MFPT is vast, as opposed to the existing literature on the MAT. Thirdly, the MFPT is intuitively easier to formulate and the definitions involved are more rigorous than in the case of the MAT (see the McNabb series of papers for instance), where concepts are harder to define and understand. Finally, boundary conditions can be easily derived through an MFPT approach, whereas for the MAT approach phenomenological arguments and assumptions are required.

First, we applied the direct MFPT approach by McKenzie et al. [2009], which is very powerful when considering a general position-jump process and can be used to derive the governing equation satisfied by the MFPT through the Fokker-Planck equation corresponding to the process. This technique, however, is limited when considering velocity-jump processes. Consequently, we applied the time-integrated occupation probability formulation, due to the fundamental work on first-passage processes by Redner [2001]. We thereby managed to derive analytical results for

the random walk models we considered in Chapter 3, which are consistent with the results of the direct method, as far as position-jump processes are concerned, and agree well with the results of the stochastic simulation for all jump processes, in general. We considered both the case of a fully and a partially absorbing boundary as the target for cells, representing a nerve biologically. Note also that both of these techniques can be applied to migration models that incorporate spatial inhomogeneity and chemical signalling profiles which affect the migration rates, two of the main limitations of the simplistic models that we have so far considered (see Chapter 7 for a discussion). The following table summarises the stochastic processes, equivalent deterministic models and mean first-passage times (for a fully absorbing boundary) we have considered.

Stochastic Process	Deterministic Model	Mean First-Passage Time
SRW	$\frac{\partial p}{\partial t} = D\frac{\partial^2 p}{\partial x^2}$	$< t(x_0) >= \frac{1}{2D}(L^2 - x_0^2)$
BRW	$\frac{\partial p}{\partial t} = -u\frac{\partial p}{\partial x} + D\frac{\partial^2 p}{\partial x^2}$	$< t(x_0) >= \frac{(L-x_0)}{u} + \frac{D}{u^2}(e^{-\frac{u}{D}L} - e^{-\frac{u}{D}x_0})$
CRW	$\frac{\partial^2 p}{\partial t^2} + 2\lambda\frac{\partial p}{\partial t} = v^2\frac{\partial^2 p}{\partial x^2}$	$< t(x_0) >= \frac{\lambda}{v^2}(L^2 - x_0^2) + \frac{L}{v}$
BCRW	$\frac{\partial^2 p}{\partial t^2} + (\lambda_1 + \lambda_2)\frac{\partial p}{\partial t} + v(\lambda_2 - \lambda_1)\frac{\partial p}{\partial x} = v^2\frac{\partial^2 p}{\partial x^2}$	$< t(x_0) >= \frac{\lambda_1+\lambda_2}{v(\lambda_2-\lambda_1)}(L - x_0) + \frac{1}{\lambda_2-\lambda_1} + \frac{2\lambda_1 e^{-\frac{\lambda_2-\lambda_1}{v}L} - (\lambda_1+\lambda_2)e^{-\frac{\lambda_2-\lambda_1}{v}x_0}}{(\lambda_2-\lambda_1)^2}$

In addition, we saw that the variance of the first-passage time has to be taken into account in order to assess how useful a quantity the MFPT is. Our analysis consisted of solving similar ODE boundary-value problems as in the case of the MFPT, but for the first, instead of the zeroth, moment of the occupation probability with respect to time. It showed that in the case of the position-jump processes, the variance of the first-passage time is larger if the point of release is further away from the absorbing boundary. However, it is also smaller in size compared to the MFPT and hence the MFPT is a more useful and informative quantity in such cases.

In the case of velocity-jump processes, the variance of the first-passage time is highly dependent on the degree of persistence in the previous direction of motion. The higher it is, the lower the variance of the first-passage time compared to the size of the MFPT. Therefore, conclusions drawn from the consideration of the MPFT are stronger. However, the closer the point of release to the absorbing boundary, the higher the variance as opposed to the results obtained from simulating the position-jump models.

The work of this chapter allows us to evaluate the 'migration-only' hypotheses regarding the mechanism behind PNI. In particular, the analytical results we obtained enable an investigation in the entire range of parameter values in order to identify the regime under which invasion occurs within the observed timeframe. Furthermore, these analytical results can be used for comparison to models that incorporate branching and annihilation processes, especially if we can only rely on the results from the stochastic simulations.

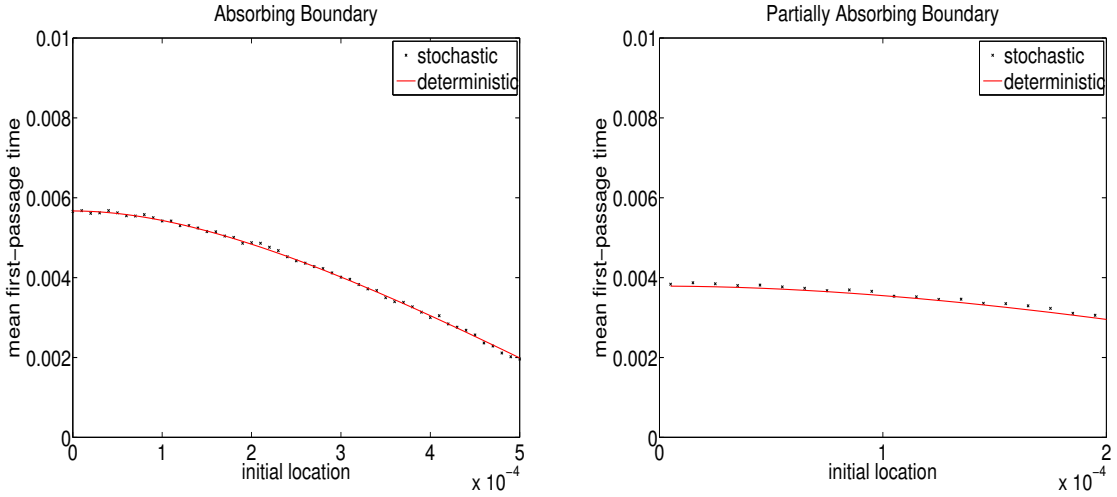


Figure 4.8: Plot of the mean first-passage time, $< t(x_0) >$, versus the initial location, x_0, for the BCRW model. The left and right panels show the results of the stochastic simulation (black crosses) for a fully and a partially absorbing boundary (with a probability of absorption, $p_{absorb} = 0.85$), respectively. The analytical expressions, obtained from the deterministic model and given by equations (4.87) and (4.88), respectively, are depicted by the red solid line. We performed 10000 simulations and have taken $\Delta x = 10^{-5}$, $\Delta t = 10^{-4}$ ($v = 10^{-1}$), $\lambda_1 = 10$, $\lambda_2 = 100$ and $L = 5 \cdot 10^{-4}$ in the case of the fully absorbing boundary and $L = 2 \cdot 10^{-4}$ in the case of the partially absorbing boundary.

Chapter 5

Incorporating Cell Proliferation and Death

Overview

Proliferation and death are two very important processes at the cellular level, which are highly regulated in order to maintain the homeostasis of an organism. Cell proliferation normally occurs in order to fulfil the void resulting from tissue damage. For instance, in the case of human muscle tissue, this damage may be a result of an external injury or physical exercise. In response to this loss of cells, other cells begin dividing and the tissue grows. Cell death, on the other hand, may be a consequence of several factors. Firstly, it may occur as a result of external factors, such as a physical injury. Secondly, it may take the form of programmed cell death (apoptosis), which occurs if the loss of a certain number of cells is favourable to the survival of the entire organism. Thirdly, it may result from lack of nutrients or space and, finally, it may be due to the immune response of the organism if a cell is identified as dangerous to the surrounding tissue. Since some of the biological hypotheses regarding the mechanism

behind PNI include the up- or down-regulation of cell division and apoptosis, we shall extend our modelling approach in order to incorporate these processes.

The first mathematical models that considered population growth and decay, in addition to migration, followed a deterministic approach and were derived phenomenologically, i.e. according to certain physical assumptions whose validity was usually taken for granted without any justification, at least *a priori*. The classical textbooks by Okubo and Levin [2001], Murray [2002] and Edelstein-Keshet [2005] show several examples of the derivation of ODEs or PDEs from matter or energy conservation laws and other less obvious or more approximate assumptions about the underlying physical problem. These assumptions make the models simpler and more tractable analytically, but they may hide certain aspects of the actual process.

Continuing in the same fashion as before, we intend to begin our study by examining the stochastic models first. Microscopic interactions may lead to global behaviour that may possibly be described by equivalent deterministic models. In this chapter, however, it will become evident that an equivalence between a stochastic process and a deterministic model is often the exception, rather than the norm.

Fisher [1937] and Kolmogorov et al. [1937] were among the first to study models of migration and proliferation in their work on the spread of advantageous genes among a population. They independently considered the famous *Fisher-KPP* equation, a PDE, in order to investigate the nonlinear stochastic process describing the spread and growth of a gene population. Despite the importance of their work, it also created a lot of misconceptions about the equivalence of the stochastic process they were studying with the deterministic model. McKean [1975] was the first to show that the Fisher-KPP equation is not, in fact, equivalent (in some limit) to the nonlinear stochastic process that the early workers considered, but rather to a simpler linear stochastic process. Mollison [1977] reviewed different types of branching models and

discussed the importance of demographic stochasticity in population processes and the equivalence of deterministic models to stochastic processes (see also the essay by Mollison [1981]).

We are going to consider two different models of proliferation. The first model, presented in Section 5.1, treats particle birth as a linear stochastic process, i.e. the probability of a birth occurring will be proportional to the size of the population. In the second model, presented in Section 5.2, we introduce a probability of failure in the birth that represents lack of nutrients and space. We consider a linear death rate, representing cell loss due to apoptosis and an immune response, in both models. Finally, we present a first passage-time analysis in Section 5.3.

5.1 Linear Stochastic Model

Upon consideration of processes such as cell proliferation, it becomes evident that the population approach we followed in Section 3.2 is more practical and less involved to implement than a single individual approach. We shall thus follow the compartment-based approach that we used before.

There are various ways of modelling the birth of individuals. The probability of a birth may be proportional to the size of the population, in which case the stochastic model is termed 'linear', or it may take a more complicated form if other aspects such as the available space are taken into account, in which case we are faced with 'nonlinear' stochastic models. We intend to study the linear model first and then examine its differences from the simplest nonlinear model. We shall then discuss the equivalence of these two stochastic processes to deterministic models.

The linear stochastic model is termed a *diffusion birth process* (DBP), as defined by Mollison [1977], since it consists of a random birth process where particles spread

through a spatial domain. Mollison [1977] showed that this process is an example of a more general process, termed a *contact birth process* (CBP). A CBP model does not consider diffusion at all; it consists of a random birth process with a prescribed ('contact') distribution that determines the location of daughter particles with respect to their parents. In this model, daughter particles are obviously not restricted to dividing within the compartment their parents inhabit.

The probability that a birth of an individual, in the DBP model, occurs in the i-th compartment of the domain within the time interval $(t, t + \Delta t)$ is proportional to the total number of particles, u_i, in the compartment. We can formally define this probability by

$$P\{u_i \to u_i + 1 \ \text{ in } \ (t, t + \Delta t)\} = \gamma_i(t)\Delta t, \tag{5.1}$$

where the propensity function γ is given by

$$\gamma_i(t) = k_B u_i(t), \tag{5.2}$$

and $k_B > 0$ denotes the division rate of a particle.

Recall from Chapter 3 the reaction scheme (3.7) which was used to represent a position-jump process on the discretised domain [0,L] of N compartments. In a similar fashion, we can represent the occurrence of a division in the i-th compartment in order to obtain the schematic of the DBP model

$$\begin{aligned} &u_1 \underset{d}{\overset{d}{\rightleftharpoons}} u_2 \underset{d}{\overset{d}{\rightleftharpoons}} \ldots \underset{d}{\overset{d}{\rightleftharpoons}} u_{i-1} \underset{d}{\overset{d}{\rightleftharpoons}} u_i \underset{d}{\overset{d}{\rightleftharpoons}} u_{i+1} \underset{d}{\overset{d}{\rightleftharpoons}} \ldots \underset{d}{\overset{d}{\rightleftharpoons}} u_{N-1} \underset{d}{\overset{d}{\rightleftharpoons}} u_N \xrightarrow{d} u_{N+1}, \\ &u_i \xrightarrow{k_B} u_i, \quad i = 1, ..., N. \end{aligned} \tag{5.3}$$

The master equation corresponding to the DBP model is given by

$$\begin{aligned}\frac{\partial P}{\partial t}(\mathbf{n},t) &= \sum_{i=1}^{N} d[(n_i+1)P(R_i\mathbf{n},t) - n_i P(\mathbf{n},t)] \\ &+ \sum_{i=2}^{N} d[(n_i+1)P(L_i\mathbf{n},t) - n_i P(\mathbf{n},t)] \\ &+ \sum_{i=1}^{N} k_B[(n_i-1)P(J_i^{-}\mathbf{n},t) - n_i P(\mathbf{n},t)],\end{aligned} \tag{5.4}$$

obtained by considering the state probability in a forward step in time, which is equal to the sum of all possible transitions to the right, all possible transitions to the left and all possible births minus the probability that no reaction occurs within the specified time interval.

If we define the stochastic mean number of particles, $\mathbf{M}(t)$, as in equation (3.12), we can use a similar method as with the previous models we considered to obtain the system of ODEs it satisfies, given by

$$\begin{aligned}\frac{\partial M_1}{\partial t} &= d(M_2 - M_1) + k_B M_1, \\ \frac{\partial M_i}{\partial t} &= d(M_{i+1} - 2M_i + M_{i-1}) + k_B M_i, \quad i = 2, ..., N-1, \\ \frac{\partial M_N}{\partial t} &= d(M_{N-1} - 2M_N) + k_B M_N.\end{aligned} \tag{5.5}$$

For $d = \frac{D}{\Delta x^2}$, this system of equations forms a discretised version of the diffusion equation with an additional linear reaction term representing the growth of the population,

$$\frac{\partial u}{\partial t} = D\frac{\partial^2 u}{\partial x^2} + k_B u, \tag{5.6}$$

with a zero-flux Neumann boundary condition at $x = 0$ and a zero Dirichlet boundary condition at $x = L$. Fig. 5.1 shows a plot of the temporal evolution of the stochastic mean of the DBP model over the spatial domain. The results of the stochastic model, represented by the histogram, seem to agree quite well with the solution of the

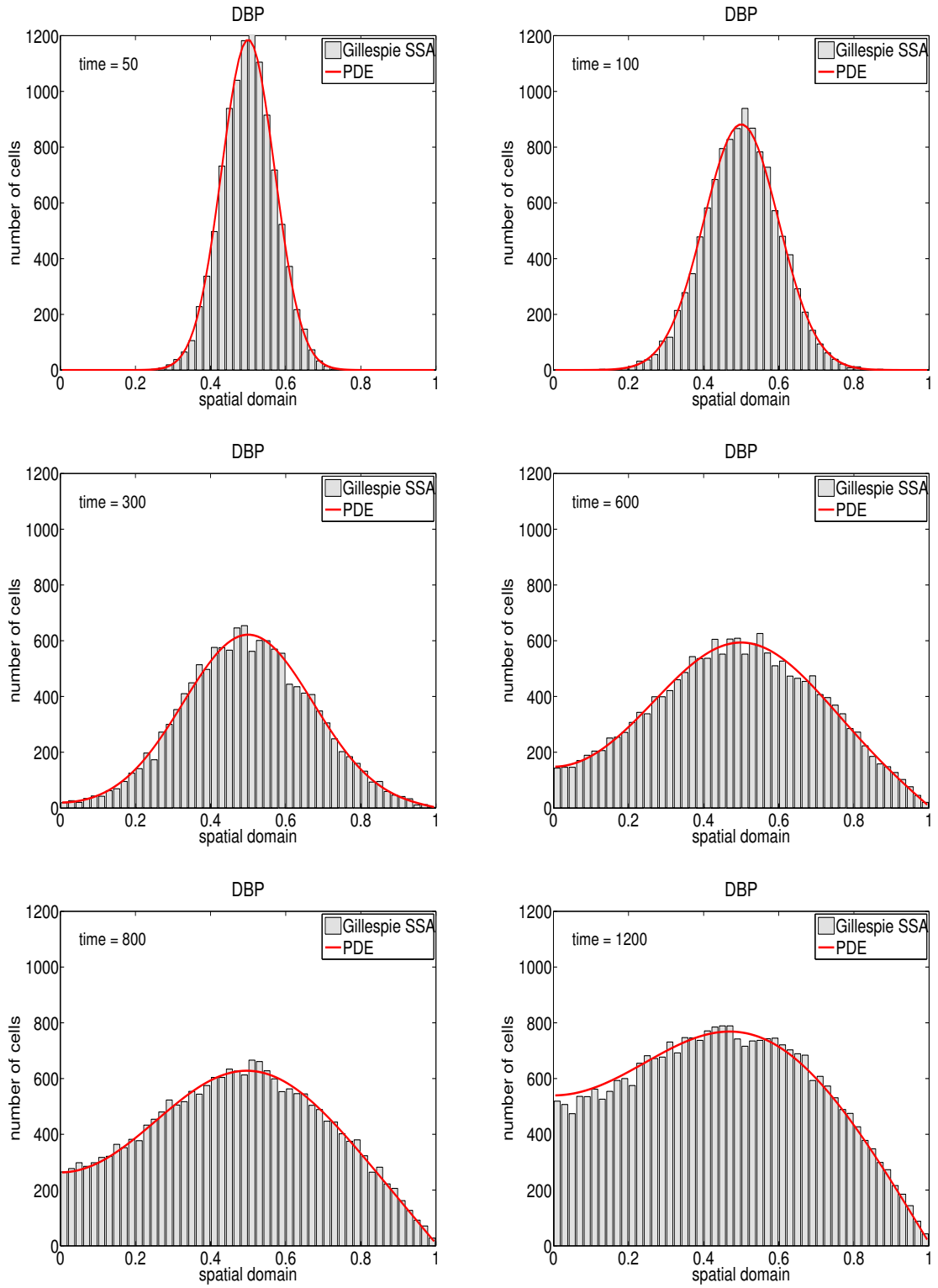


Figure 5.1: Plot of the temporal evolution of the stochastic mean number of particles, $\mathbf{M}(t)$, in the linear DBP model (in black dots) versus the numerical solution of the corresponding PDE (5.6) (red solid line). One stochastic realisation is shown for times $t = 50, 100, 300, 600, 800$ and 1200. The domain $[0, 1]$ is discretised into 50 compartments and 10000 particles are released at $t = 0$ at the point $x = 0.5$ with diffusion coefficient $D = 5 \cdot 10^{-5}$ and proliferation rate $k_B = 10^{-3}$.

deterministic model (red solid line) defined by equation (5.6). It is also evident that the total number of particles over the entire domain increases and does not gradually reduce to zero, as would be the case with the SRW model due to the particles escaping the domain at the absorbing boundary. Particles still escape but even more particles are born inside the domain because the proliferation rate is greater than the diffusion coefficient. Note also that as expected, a linear proliferation rate gives rise to an exponentially growing population, as Fig. 5.2 shows. This is an unrealistic model of proliferation, even in the case of neoplastic epidermal tissue. However, exponential growth can be regarded as an upper bound of the actual mode of tumour growth, which is useful if we try to eliminate this mechanism from consideration as unlikely (see Chapters 6 and 7 for a more extensive discussion of this argument).

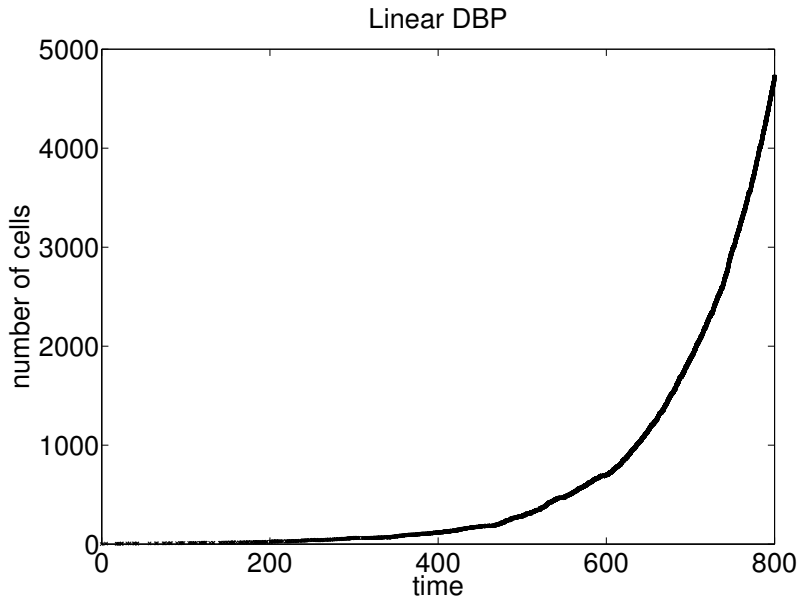


Figure 5.2: Plot of the temporal evolution of the number of particles in one of the two middle compartments, $x = 0.5 + \frac{\Delta x}{2}$, in the linear DBP model. A single stochastic realisation is shown. Initially 10 particles are released at the point $x = 0.5$ with a diffusion coefficient equal to $D = 5 \cdot 10^{-5}$ and a proliferation rate equal to $k_B = 10^{-3}$.

One may also formulate a *Diffusion Death Process* (DDP) or a *Diffusion Birth Death Process* (DBDP) in the exact same manner as for the DBP model by specifying a death rate $k_D > 0$. In the former case, the reaction represented by the last line of the

schematic (5.3) will be replaced by

$$u_i \xrightarrow{k_D} u_i, \quad i = 1, ..., N, \tag{5.7}$$

while in the latter case both reactions are necessary. The resulting PDEs are given by

$$\frac{\partial u}{\partial t} = D\frac{\partial^2 u}{\partial x^2} - k_D u, \tag{5.8}$$

and

$$\frac{\partial u}{\partial t} = D\frac{\partial^2 u}{\partial x^2} + k_B u - k_D u, \tag{5.9}$$

respectively. Fig. 5.3 shows a plot of the results of the stochastic simulation for the DDP model compared to the solution of equation (5.8). Evidently, particle density approaches the equilibrium solution faster than the SRW model, as some particles die before being in position to escape the domain.

In the following section we consider the corresponding nonlinear stochastic process and determine the validity of the Fisher-KPP equation.

5.2 Nonlinear Stochastic Model

In the case of a linear birth process, the particle population grows exponentially. A more realistic model should consider the effect of the size of the population and the available space or nutrients on the birth rate. If we modify the DBP by introducing a probability that a birth might fail as the size of the population increases, we obtain the *simple epidemic* model of Mollison [1977]. In this model the propensity function is given by

$$\gamma_i(t) = k_B u_i(t) \left(1 - \frac{u_i(t)}{K}\right), \tag{5.10}$$

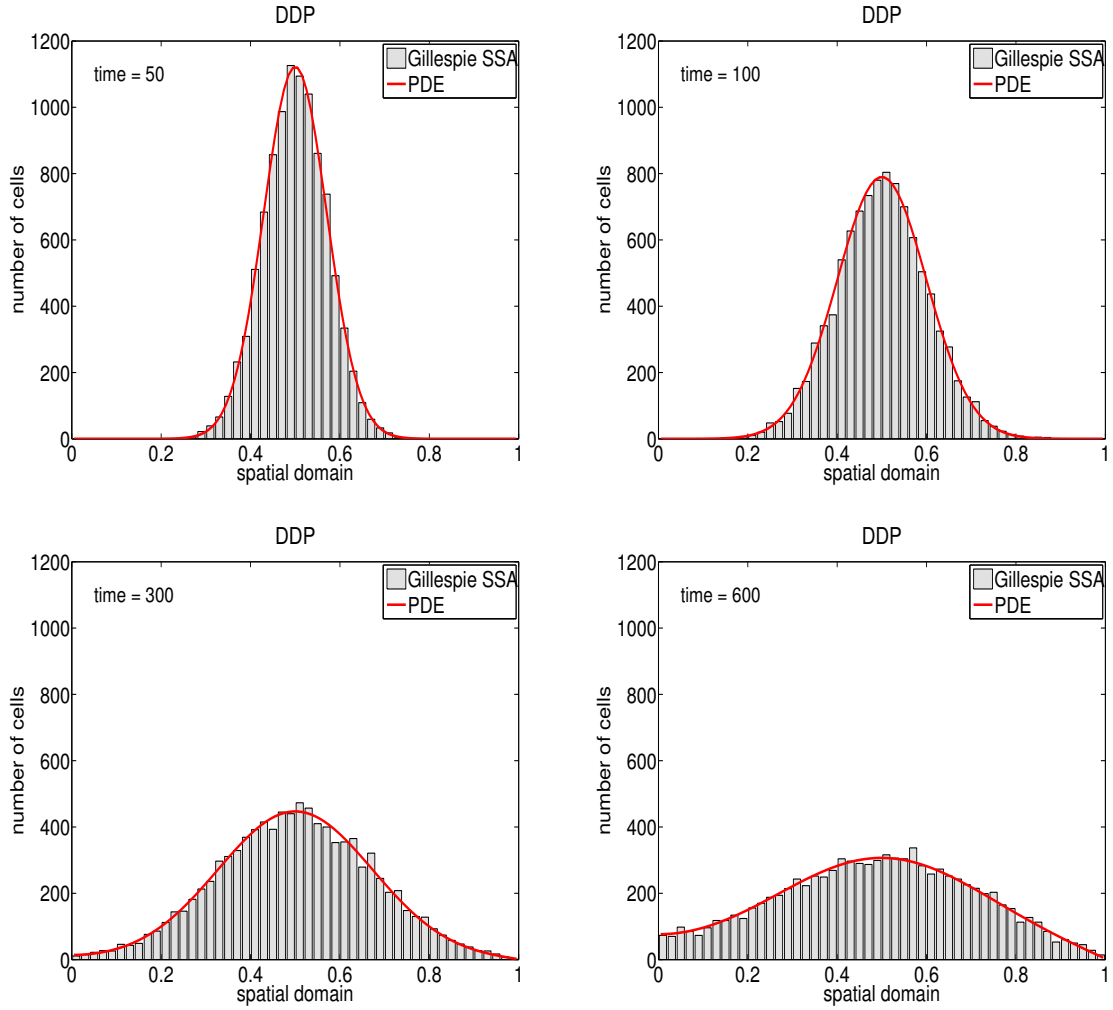


Figure 5.3: Plot of the evolution of the stochastic mean number of particles, $\mathbf{M}(t)$ over time in the DDP model (in black dots) versus the numerical solution of the corresponding PDE (5.8) (red solid line). One stochastic realisation is shown for times $t = 50, 100, 300$ and 600. The domain $[0, 1]$ is discretised into 50 compartments and 10000 particles are released at $t = 0$ at the point $x = 0.5$ with diffusion coefficient $D = 5 \cdot 10^{-5}$ and death rate $k_D = 10^{-4}$.

where $K \in \mathbb{N}$ denotes the carrying capacity of each compartment. As the number of particles in any compartment approaches K, the probability of a birth occurring within the compartment approaches zero.

Early work on stochastic phenomena, especially that by Fisher [1937] and Kolmogorov et al. [1937] who studied the way of advance of genes undergoing mutations within a population, resulted in the famous deterministic model, the *Fisher-KPP equation*,

$$\frac{\partial u}{\partial t} = D\frac{\partial^2 u}{\partial x^2} + k_B u\left(1 - \frac{u}{K}\right). \tag{5.11}$$

McKean [1975] showed that this PDE is actually related to the linear stochastic process if one is tracking the leading individual. In other words, if S_t denotes the location of the leading particle at time t, then the function $h(s,t) = Pr\{S_t > s\}$ obeys the Fisher-KPP equation. The particle density, on the other hand, cannot be described by equation (5.11). The reason is obvious once we look at the master equation of the system and try to derive ODEs for the stochastic mean particle density. The stochastic mean of the term $u(1 - \frac{u}{K})$ over all possible states of $\mathbf{u}$, $\mathbf{n}$, does not equal the product of the means of the respective terms in general, i.e.

$$< u\left(1 - \frac{u}{K}\right) > \neq < u > \cdot < 1 - \frac{u}{K} > . \tag{5.12}$$

Fig. 5.4 shows how the particle density evolves over time for the nonlinear DBP model (in black dots). We have also plotted the numerical solution of the linear and nonlinear deterministic models in red (solid line) and green (dotted), respectively. The former works as an upper bound for the nonlinear DBP model, while the latter, the solution to the Fisher-KPP equation, is the corresponding phenomenological model. It is evident that there is not good agreement between the deterministic models and the actual nonlinear stochastic process, as expected.

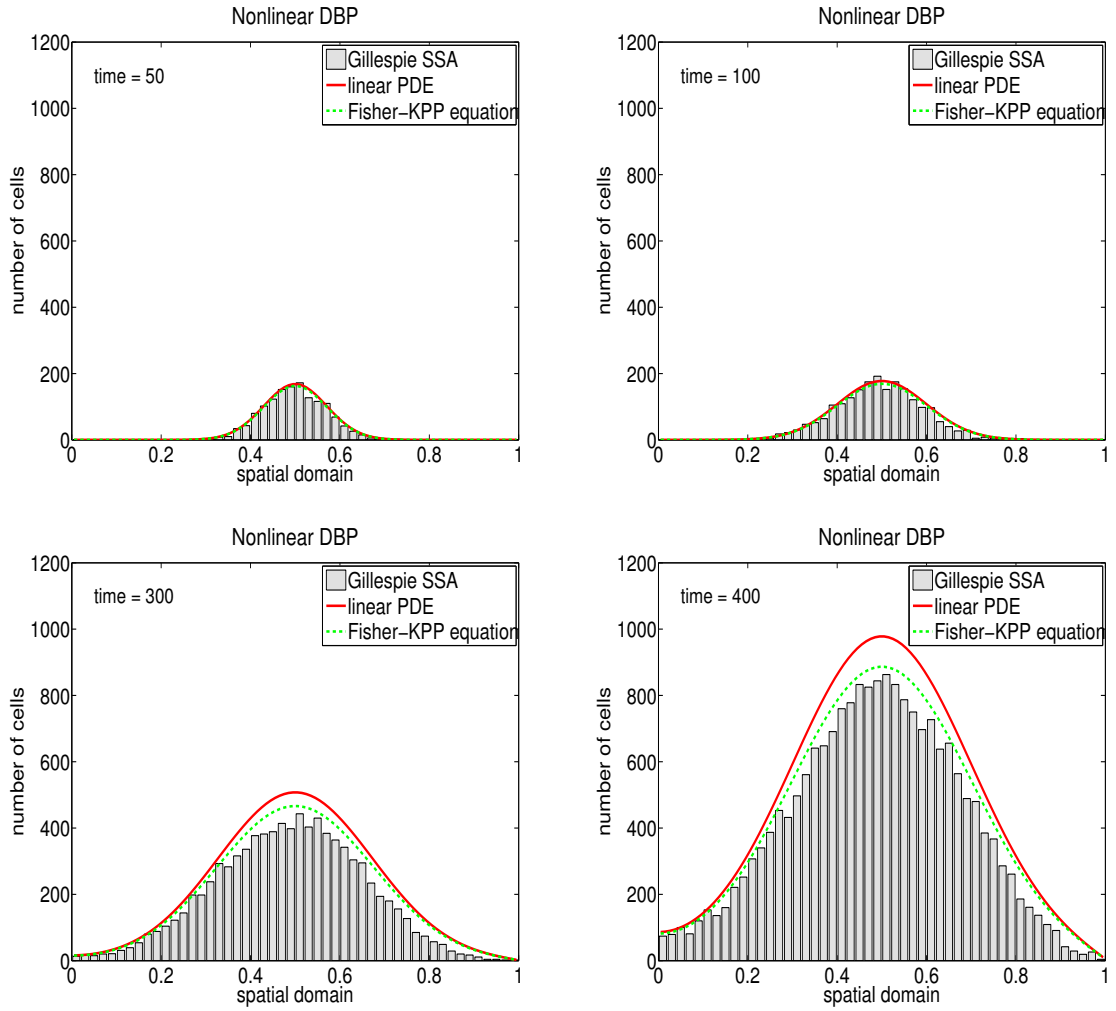


Figure 5.4: Plot of the evolution of the stochastic mean, $\mathbf{M}(t)$, over time for the nonlinear DBP model (in black dots) versus the numerical solution of the linear PDE (5.6) (red solid line) and the nonlinear Fisher-KPP equation (5.11) (green dotted line). One stochastic realisation is shown for times $t = 50, 100, 300, 600, 800$ and 1200. The domain $[0, 1]$ is discretised into 50 compartments and 10000 particles are released at $t = 0$ at the point $x = 0.5$ with diffusion coefficient $D = 5 \cdot 10^{-5}$, death rate $k_D = 10^{-4}$ and carrying capacity $K = 10000$ particles.

Note that, as opposed to the case of linear birth rate, the number of cells in the nonlinear DBP model obey what roughly resembles a logistic growth, as Fig. 5.5 shows from the results of a single realisation. If we were to plot the average of several realisations, then the graph would show a curve that bears an even stronger resemblance to logistic growth although it would not exactly be logistic growth. This is expected from the fact that the Fisher-KPP equation is a reasonable approximation (even if not the actual governing PDE) to the mean-field behaviour of the stochastic model. The number of cells in each compartment can never exceed the carrying capacity (100 cells in Fig. 5.5). This is a more realistic mode of growth than the one in the linear DBP model as spatial limitations are taken into consideration.

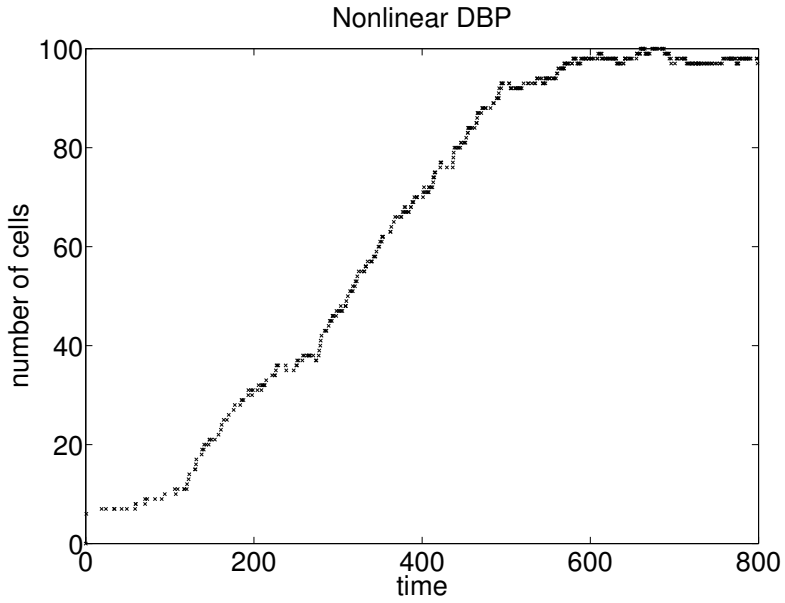


Figure 5.5: Plot of the temporal evolution of the number of particles in one of the two middle compartments, $x = 0.5 + \frac{\Delta x}{2}$, in the nonlinear DBP model. A single stochastic realisation is shown. Initially 10 particles are released at the point $x = 0.5$ with a diffusion coefficient equal to $D = 5{\cdot}10^{-5}$, a proliferation rate equal to $k_B = 10^{-3}$ and a carrying capacity equal to $K = 100$.

In the following section, we show the results obtained for the mean first-passage time of each of these two models through stochastic simulations. We also discuss the difficulties in obtaining an analytical expression for the MFPT of models that include branching.

5.3 Mean First-Passage Time

In order to consider a first-passage process for the models that include branching, we must first establish a framework so as to compare its results to the migration-only models of Chapter 3. In Chapter 4 we introduced the notion of a first-passage time and derived a relation to the occupation probability of a single individual performing a position- or a velocity-jump process. The idea can be easily extended to jump processes performed by several individuals at the same time due to the fact that the latter are not interacting with each other. Therefore, allowing a single individual to perform the process over, $S > 0$ say, simulations and recording the time it takes to hit the absorbing boundary for the first time is exactly the same as allowing S non-interacting individuals to perform the process simultaneously and recording the respective times it takes to hit the boundary [Gardiner, 1985]. In order to check this, we simulated the SRW model using Gillespie's SSA, recorded the first-passage time for each of the 10000 particles and then compared the average to the analytical expression obtained through the single-individual approach. Fig. 5.6 shows that there is excellent agreement between the results of the stochastic realisation (black dots) and the theoretical prediction (in red).

In the DBP model, however, particle creation and annihilation are interactions that need to be taken into account. Fig. 5.7 shows a comparison between the simulation of a single realisation of the DBP model with 1000 initial particles and the simulation of 1000 realisations of the DBP model with one initial particle using Gillespie's SSA. The MFPT was recorded for various values of the initial location, x_0, and it is clear that the results between the two different methods of simulation vary significantly. It is evident that the former method yields lower values for the MFPT. The reason is that if we consider several particles performing a diffusion-birth process simultaneously, there is a good chance that progeny of a single particle (the leading cell most likely)

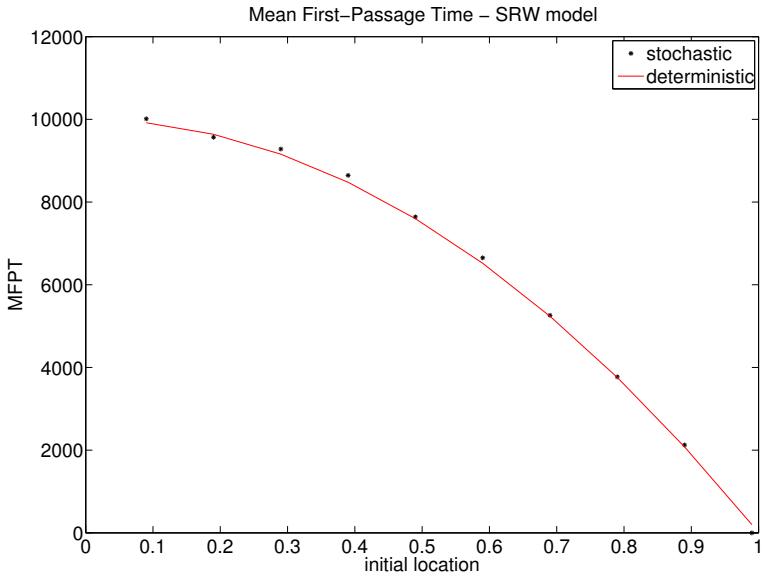


Figure 5.6: Plot of the mean first-passage time, $< t(x_0) >$, versus the initial position, x_0, for the SRW model (in black dots) using Gillepie's SSA versus the analytical expression from the deterministic model (4.31) (red solid line). We performed 10000 realisations.

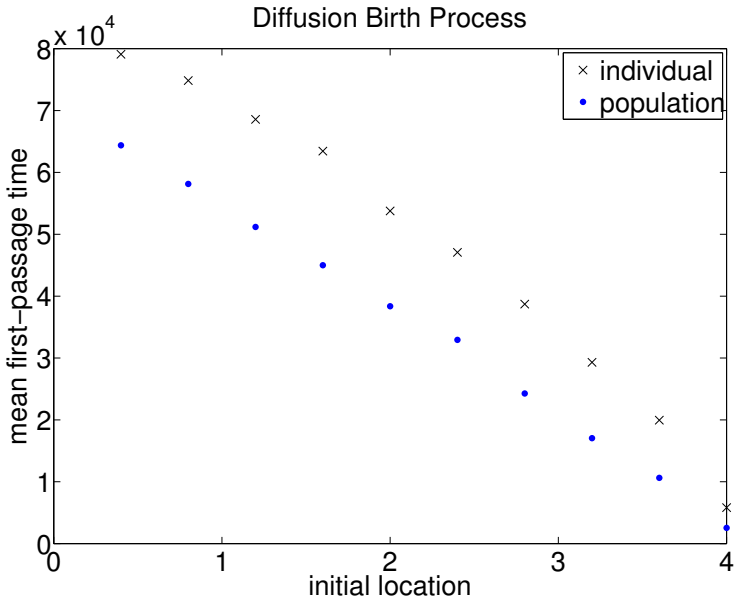


Figure 5.7: Plot of the mean first-passage time, $< t(x_0) >$, versus the initial position, x_0, in the DBP model using Gillespie's SSA through two different methods; the individual method, depicted in black crosses, which considers 1000 realisations of the DBP model where a single particle is initially released, and the population method, depicted in blue dots, where 1000 particles are released and the MFPT of the first 1000 to reach the boundary is recorded.

might reach the boundary before their counterparts. As a result, we simulate the process 10000 times using Gillespie's SSA with a single particle released at the start of the process.

Fig. 5.8 shows the MFPT results obtained by the stochastic simulation of the DBP (black asterisks) and the nonlinear DBP (blue dots) models. For comparison purposes we have also plotted the theoretical MFPT of the SRW model.

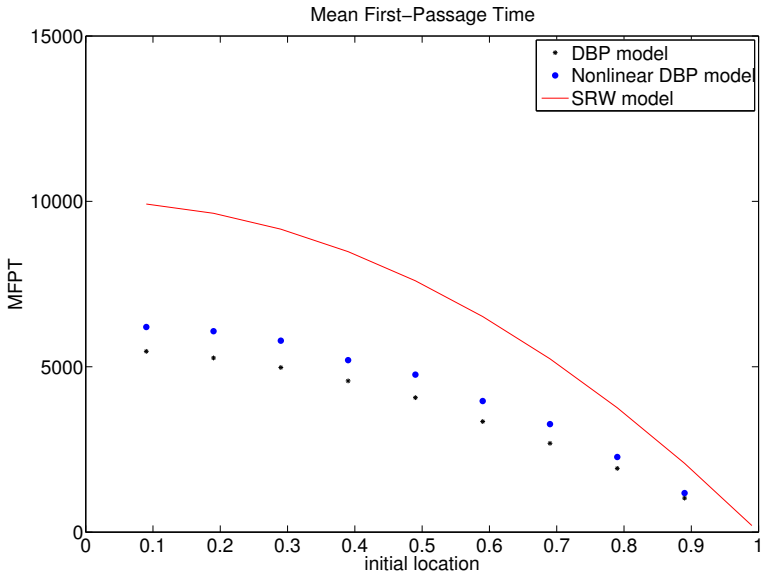


Figure 5.8: Plot of the mean first-passage time, $< t(x_0) >$, obtained from 10000 stochastic realisations versus the initial position, x_0, for the DBP model (in black asterisks), the nonlinear DBP model (blue dots) and the analytical expression of the SRW model (4.31) (red solid line) for comparison purposes.

As expected, the MFPT of the DBP model is smaller compared to the MFPT of the SRW model, i.e. proliferation makes the invasion wave faster. The MFPT of the nonlinear DBP is also small compared to MFPT of the SRW model but greater than the MFPT of the DBP model as particles are born at a slower rate; the population growth is not exponential with respect to time in this case.

Ideally, in order to obtain theoretical predictions for the MFPT of the stochastic processes under examination, we would like to exploit the analytical tractability of the corresponding deterministic models as before. An instant difficulty in the case

of the nonlinear DBP model is the fact that we do not have a deterministic model that accurately describes the collective behaviour of the particles as produced by the simulation of the stochastic process. Even in the case of the DBP model, however, the application of the techniques we used in Chapter 4 is quite complicated due to the extra reaction term and does not lead to a solution in closed form.

Summary

In this chapter, we introduced cell proliferation and death into our models. We only considered simplistic models, where the rate of particle creation takes a linear or a simple nonlinear form and the rate of particle loss is linear. The reason is twofold. Firstly, our model-building approach dictates that we consider as simple as possible a model, whose behaviour can be fully understood, at first, and then incorporate additional features incrementally, so that the effect of the additions on the observed behaviour is evident. Secondly, linear proliferation and death rates produce exponential growth and decay, respectively, which can be considered as upper and lower bounds of more realistic descriptions, respectively. As such, we can determine the maximum parameter rates required for invasion to occur within the observed timeframe and compare them to realistic values so that we eliminate possible mechanisms from consideration as unlikely.

The importance of considering the stochastic model of a random process first, instead of the usual phenomenological deterministic description, and then deriving the appropriate deterministic approximation (highlighted by Mollison's work and by McKean [1975]) became evident in the case of the nonlinear DBP model. The deterministic approximation of the linear stochastic process was very easy to obtain through a master equation approach, whereas a corresponding approximation in the nonlin-

ear model, which is clearly more realistic as we saw from the temporal evolution of the number of cells, in closed form, is not possible through this approach. We also determined from the results of the simulations that considering a stochastic process from the perspective of an individual and performing multiple realisations is the same as considering the process from the perspective of an entire population of particles performing the process simultaneously, as long as particles are non-interacting.

Then, we considered the MFPT of the DBP models and concluded that both of the techniques presented in the previous chapter are inadequate for deriving analytical solutions for the MFPT of a branching process. Consequently, we shall have to rely on the results of the stochastic simulations in order to evaluate the hypotheses that include up-regulated proliferation and reduced apoptosis as potential mechanisms behind PNI. In addition, we saw the importance of Gillespie's SSA upon consideration of branching and annihilation processes as it is not only significantly more efficient than a Monte Carlo method, but also the latter is considerably more involved to implement in this case and more costly, computationally, both time-wise and in terms of computer memory. Finally, we determined that in order to record the correct MFPT in the stochastic simulations, we need to consider an individual performing a process over multiple realisations and not a population of particles simultaneously as there is a possibility that the progeny of a single ancestor are faster than their counterparts.

Chapter 6

Parameter Regimes For Invasion

Overview

In previous chapters we considered some basic models of cell migration, cell proliferation and cell death in order to build a simple mathematical framework of tumour invasion. This framework enables a formal definition of the notion of a 'mean first-passage time', which, physically, may be connected to the concept of an 'average time scale'. We used this framework in order to make a quantitative comparison between models of invasion processes representing the different hypotheses regarding the mechanism behind PNI.

In this chapter, we perform a parameter investigation and identify the range in which invasion occurs in under 42 days for each hypothesis. We shall then show where realistic parameter values lie with respect to this range and thereby assess the validity of the four biological hypotheses about the mechanism behind PNI. We use analytical results, wherever possible, in order to make a full parameter investigation. In the models that include particle creation and loss, we rely on the results of the stochastic simulations solely.

In previous chapters we considered a one-dimensional domain $[0, L]$ in order to model tumour invasion. Biologically this domain represents a portion of tissue from the edge of the skin towards the dermo-epidermal junction and the deepest layers thereafter, where nerve endings lie. The choice of one dimension for the spatial domain instead of a more realistic three-dimensional setup is made for three reasons. Firstly, a straight line is the fastest route for a tumour cell that is migrating from the outer layers of the skin towards the deepest. Therefore, if we observe that a certain mechanism is not sufficient to produce invasion within the observed timeframe in one dimension, we can be certain that this is the case in three-dimensional space as well. Secondly, a one-dimensional domain may often provide a good approximation to a three-dimensional space so that the important aspects remain. For instance, the volume of a three-dimensional space may be modelled through the specification of a carrying capacity so that the spatial limitations are evident in the one-dimensional approximation. A stable chemotactic profile in two or three dimensions may retain its important aspects if we consider the appropriate dimension from the two or three possibilities, respectively. Finally, working in one dimension is less involved both analytically and computationally. Furthermore, the one-dimensional case can provide a reference frame for comparison to more complicated higher-dimensional models in the future.

In the ensuing parameter investigation we pick $L = 4$mm and choose x_0, the initial location of a tumour cell, to be the origin since PNI associated with NMSC is usually a result of squamous cell carcinomas, a type of tumour that arises in the outermost layers of the epidermis.

6.1 Diffusion-only Scenario

Hypothesis 1 'Random motion alone is sufficient to produce perineural invasion up to 4mm deep within 42 days.'

In order to test this first hypothesis we initially employ the SRW model. We use the analytical results regarding the mean first-passage time to test whether a diffusion process is capable of producing invasion within the observed timeframe. After this first comparison, we use the results for the MPFT of the CRW model to see if random motion with a certain degree of persistence in the motion is sufficient as a mechanism for invasion to occur within the observed timeframe.

We compare the range of values of the diffusion coefficient required for invasion to occur within 42 days, which may be determined through the analytical expression for the MFPT in the SRW model, given by equation (4.31), substituting for x_0,

$$< t(0) >= \frac{L^2}{2D},$$

with realistic values from the literature.

Fig. 6.1 shows a plot of the MFPT as a function of the diffusion coefficient. There is a threshold value, say D_{crit}, above which invasion occurs within the observed timeframe. This value is given by

$$D_{\text{crit}} = 2.205 \cdot 10^{-6} \text{mm}^2\text{s}^{-1}. \tag{6.1}$$

The hypothesis under consideration can only be valid if cells associated with PNI tumours have an effective diffusion coefficient greater than or equal to D_{crit}. Otherwise, a tumour cell would *on average* be unable to cover 4mm of deeper tissue within the expected timeframe, simply through random motion alone (even when constrained to move on a straight path, which is the case with our one-dimensional models). There-

fore, in higher-dimensional space, a tumour cell would need even more time to cover the same distance due to the extra degrees of freedom characterising its motion.

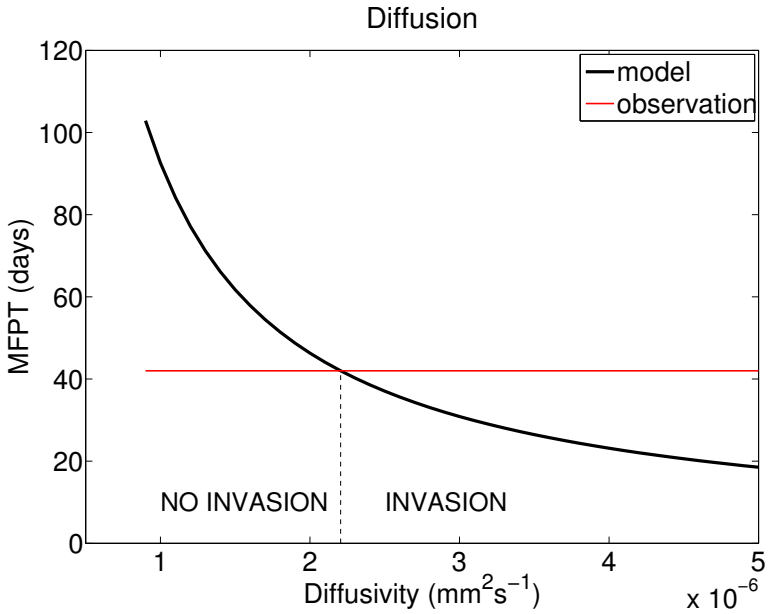


Figure 6.1: Plot of the mean first-passage time, $< t(x_0) >$, in the SRW model, for $x_0 = 0$ and $L = 4$mm as a function of the diffusion coefficient of tumour cells in the critical regime under which invasion occurs. There is a critical value, D_{crit}, above which invasion occurs within the expected timeframe of 42 days.

The process of finding realistic values for the parameters used in a model is quite difficult, in general, especially if few biochemical studies have been performed on the topic. Here, we seek a biologically realistic value for the diffusion coefficient of squamous carcinoma cells of the epidermal tissue. Since this is quite hard to find, we are faced with a choice between using values found in mathematical modelling papers on tumour growth (and invasion) and values for the diffusion coefficient of non-neoplastic epidermal tissue. From the latter category in particular, we picked studies on epidermal wound healing as it is an example of a process characterised by a very rapidly migrating healthy cell population. In their review on tumour cell migration, Friedl and Wolf [2003] describe the mechanisms behind tumour cell migration and they show that the basic strategy behind the movement of tumour cells is the same as in the case of healthy cells. Hence, it is not unreasonable to assume that the effective

diffusion coefficients of healthy cells and tumour cells do not vary by a significant amount, at least in terms of the order of magnitude, and, as such, we can use the values of the former as realistic values for the latter.

Dale et al. [1994b,a] proposed a reaction-diffusion model of corneal epithelial wound healing and used experimental data to determine a value for the diffusion coefficient of the order of $10^{-7}\text{mm}^2\text{s}^{-1}$. Similar values were quoted by Sherratt and Murray [1990], who used a specific value of $3 \cdot 10^{-7}\text{mm}^2\text{s}^{-1}$ in their model of epidermal wound healing, while Sherratt and Murray [1991] used a value of $3.5 \cdot 10^{-8}\text{mm}^2\text{s}^{-1}$, based on a best-fit analysis on wound healing data presented by Murray [2002]. Gatenby and Gawlinski [1996], on the other hand, used a value of $2 \cdot 10^{-8}\text{mm}^2\text{s}^{-1}$ for the diffusion coefficient of cells in their model of tumour growth, but theirs was also an average estimate of values obtained from studies on wound healing.

Regardless of the exact value of the diffusion coefficient of cells in the epidermal tissue, it is evident that the order of magnitude of realistic values is considerably lower than the order of magnitude of D_{crit}. Even if tumour cells move faster than epidermal cells during wound healing, it is very unlikely that their diffusion coefficient is two orders of magnitude greater than that of healthy epidermal cells. This suggest that random motion alone is probably not sufficient as the main mechanism behind perineural spread. However, in order to safely discard this hypothesis, we should also consider the scenario in which random motion is modelled as a velocity-jump process.

In this case, we use the results for the MFPT of a CRW from Section 4.3.3 to obtain a range of values for the velocity of tumour cells and their turning rate, in which invasion occurs within 42 days. Recall the analytical expression for the MFPT of a CRW, given by equation (4.71), substituting for $x_0 = 0$,

$$< t(0) >= \frac{\lambda L^2}{v^2} + \frac{L}{v}.$$

We require that this expression is less than 42 days for realistic values of the velocity of tumour cells and their turning rate. For ease of notation, we shall use $T_i = 42$ days, to denote the time scale of invasion and so in mathematical terms we require that $< t(0) > \leq T_i$. Re-arranging this inequality in terms of a polynomial of v, and considering only $v \in \mathbb{R}^+$ since v is the speed of a cell, we obtain

$$f(v) = T_i v^2 - Lv - \lambda L^2 \geq 0. \tag{6.2}$$

If v_1 and v_2 denote the roots of the equation $f(v) = 0$, then the condition (6.2) may be written as

$$v \leq v_1 \quad \text{or} \quad v \geq v_2. \tag{6.3}$$

To obtain the two roots we look at equation $f(v) = 0$, the discriminant of which is given by

$$\Delta = (1 + 4\lambda T_i)L^2, \tag{6.4}$$

and require that $\Delta \geq 0$ for real roots, which is always satisfied since $1 + 4\lambda T_i \geq 0$ $\forall \lambda \in \mathbb{R}$. The two roots are given by

$$v_{1,2} = \frac{L}{2T_i}\left(1 \pm \sqrt{1 + 4\lambda T_i}\right). \tag{6.5}$$

We only consider the condition on the positive root and are led to a relation that provides us with a lower bound for the velocity of a cell given a fixed turning rate, λ, given by

$$v \geq v_{min} = \frac{L}{2T_i}\left(1 + \sqrt{1 + 4\lambda T_i}\right). \tag{6.6}$$

Since experimental data on the velocity of tumour cells are easier to obtain than data on the turning rate, we can re-arrange this expression to obtain an upper bound for

the turning rate of cells, given a fixed velocity. This is given by

$$\lambda \leq \lambda_{max} = \frac{v}{L}\left(\frac{T_i v}{L} - 1\right). \tag{6.7}$$

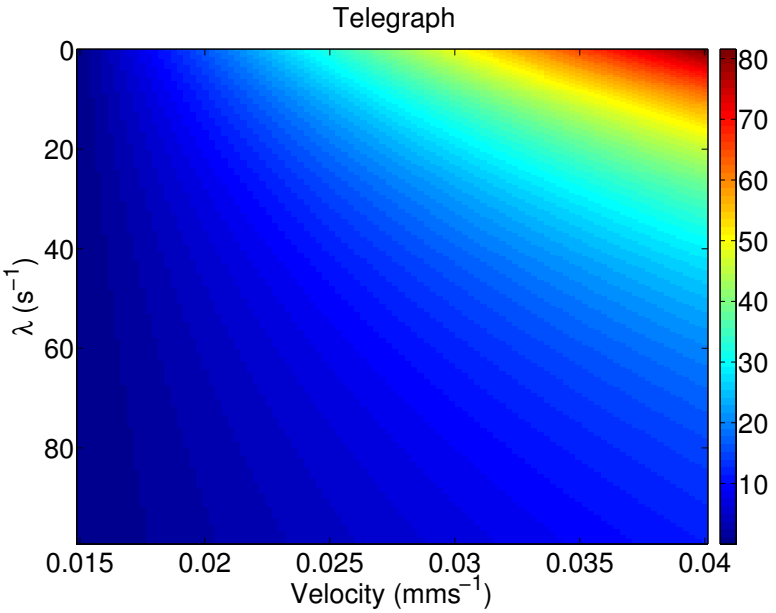


Figure 6.2: Plot of the mean first-passage time, $< t(x_0) >$, in the CRW model, for $x_0 = 0$ and $L = 4$mm as a function of the velocity of tumour cells and the rate of changing direction, λ, in the critical regime under which invasion occurs. The colour bar on the right represents the MFPT in days.

Fig. 6.2 shows the mean first-passage time obtained from the analytical expression (4.71) for a range of values of v and λ. The colour bar on the right represents the values of the MFPT in days. We see that for a fixed speed and small turning rates the MFPT is small because the persistence in the previous direction of motion is higher and hence a cell will reach a fixed boundary faster than just by random motion alone. As the turning rate increases, on the other hand, the motion becomes more random and approaches a diffusive process rather than a telegraph process and so the MFPT is higher.

From the left panel of Fig. 6.3 we can see that for small values of the speed of tumour cells, even of the order of $0.001 - 0.01\text{mms}^{-1}$, which is probably quite high realistically,

one needs a very small turning rate, in other words, a very strong persistence in the previous direction of motion.

The right panel of Fig. 6.3, on the other hand, shows that if the value of the velocity of tumour cells is extremely small, of the order of 10^{-6}mms^{-1}, then invasion does not occur for any positive turning rate, no matter how low. This is to be expected since

$$\lim_{\lambda \to 0} v_{min} = \frac{L}{T_i} \simeq 1.103 \cdot 10^{-6}\text{mms}^{-1},$$

as is evident from the graph.

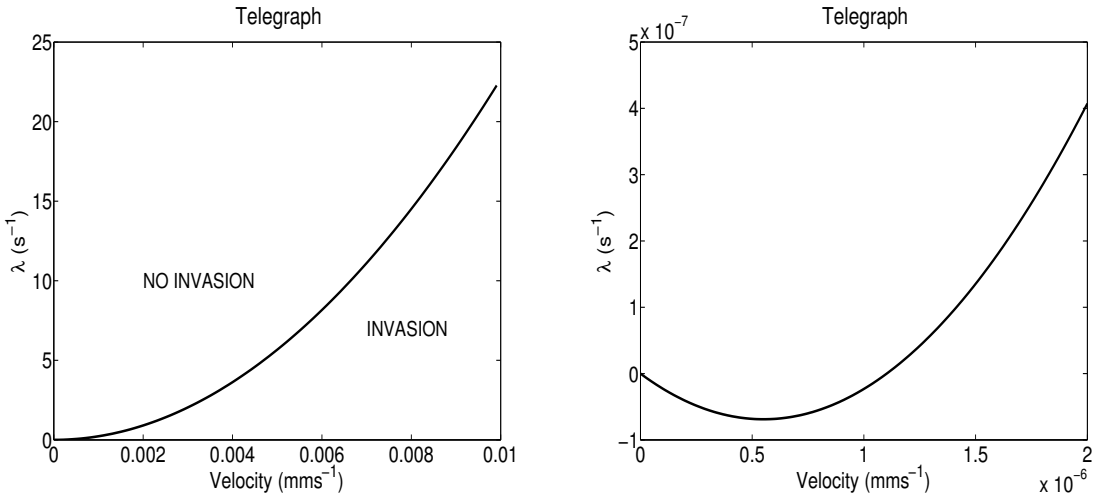


Figure 6.3: Plot of the rate of changing direction, λ, versus the velocity of tumour cells in the CRW model for a mean first-passage time, $< t(x_0) >= 42$ days, $x_0 = 0$ and $L = 4$mm. The critical parameter regime under which invasion occurs for the range $v = 0 - 0.01\text{mms}^{-1}$ is shown on the left panel. The right panel shows the more realistic range $v = 0 - 2 \cdot 10^{-6}\text{mms}^{-1}$. There is a critical value, $v_{\min}$, below which invasion occurs within the expected timeframe of 42 days only if λ is negative, which is meaningless physically.

Friedl and Wolf [2003] report values in the range from 0.1 to $1\mu\text{m}h^{-1}$ for the migration velocity of tumour cells exhibiting mesenchymal movement[1]. This means that tumour cells of the epidermal tissue have an average speed in the range $2.778{\cdot}10^{-8} - 2.778{\cdot}10^{-8}$ mms^{-1}. Clearly, invasion cannot occur within the expected timeframe simply due to this process for any positive turning rate. Consequently, random motion, whether

[1]Type of movement predominantly found in specific types of tissue, including epithelial cancers.

assisted by a strong persistence in the previous direction or not, is not a sufficient mechanism to produce tumour invasion within the observed time scale. We thus need to consider if migration assisted by a possibly up-regulated proliferation rate can produce invasion within 42 days.

6.2 Diffusion-Proliferation Scenario

Hypothesis 2 'Up-regulation of the tumour cell proliferation rate is necessary and sufficient for tumour invasion to occur within the expected timeframe, while random motion alone cannot produce such rapid invasion.'

This hypothesis may be tested through the DBP model. To the best of our knowledge, there is no analytical expression for the MFPT of a DBP so in this case we rely completely on the results of the stochastic model for our parameter investigation. We simulate the diffusion birth process for different values of the diffusivity, in the range $10^{-6}\text{mm}^2\text{s}^{-1} < D < 10^{-5}\text{mm}^2\text{s}^{-1}$, and various values of the proliferation rate.

Fig. 6.4 shows a plot of the MFPT (in days) of the linear DBP model as a function of the diffusivity and the proliferation rate. It is evident that for low values of the diffusion coefficient, invasion can occur within 42 days only if the proliferation rate is of order 10^{-3}s^{-1} or greater. This means an average cell cycle of approximately 16.6 minutes, which seems unrealistic even for cells of rapidly proliferating tissues. We also simulated the process for lower values of the diffusion coefficient, within the experimentally observed range $10^{-8} - 10^{-7}\text{mm}^2\text{s}^{-1}$, but we omit the simulation results because the model is producing a completely unrealistic behaviour. The reason is that we need extremely high proliferation rates for tumour cells to achieve invasion within 42 days. As a consequence, at the left end of the domain, where cells are released, the total number of cells grows exponentially to millions before one reaches the absorbing

boundary representing the nerve. Clearly, a high proliferation rate along with a small diffusion coefficient produces a tumour that grows in size and thereby expands as a single mass towards the nerve sheath, whereas a high diffusion coefficient with a low proliferation rate produces a pattern with very few leading cells reaching the boundary individually. The latter scenario is consistent with clinical observations regarding PNI.

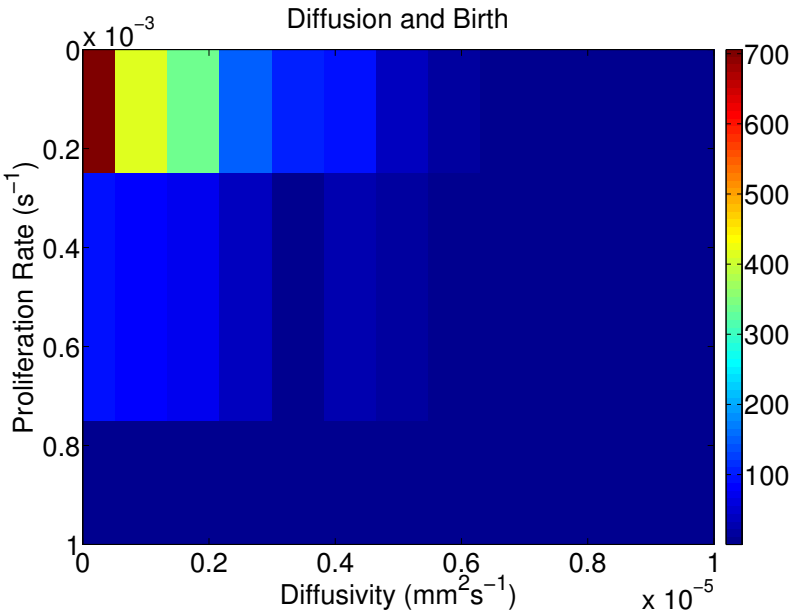


Figure 6.4: Plot of the mean first-passage time, $< t(x_0) >$, in the linear DBP model, for $x_0 = 0$ and $L = 4$mm as a function of the diffusion coefficient and the proliferation rate, k_B, in the critical regime under which invasion occurs. The colour bar on the right represents the MFPT in days. For the parameter range depicted in this figure, invasion occurs within the expected timeframe of 42 days only at the right-hand corner of the panel.

Due to this limitation of the linear DBP model, we need to consider the nonlinear DBP model so as to examine a more realistic range of values for the diffusion coefficient. The left and right panels of Fig. 6.5 show a plot of the MFPT of the nonlinear DBP, for values of the diffusivity in the range $10^{-7} - 10^{-6}\text{mm}^2\text{s}^{-1}$ and $10^{-8} - 10^{-7}\text{mm}^2\text{s}^{-1}$, respectively, with a carrying capacity $K = 10$ and for various values of the proliferation rate. It is evident from the results that the proliferation rate required for invasion to occur within 42 days is unrealistic.

As in the case for the diffusion coefficient, kinetic parameter values for carcinomas are hard to obtain. In this case there is an extensive literature from numerous studies on the cell cycle of tumour cells. The difficulty lies in the fact that kinetic parameters vary markedly among different tissues, carcinomas and extracellular environmental conditions. As a result, we considered various biochemical studies on the cell cycle of tumour cells of the epidermoid epithelium.

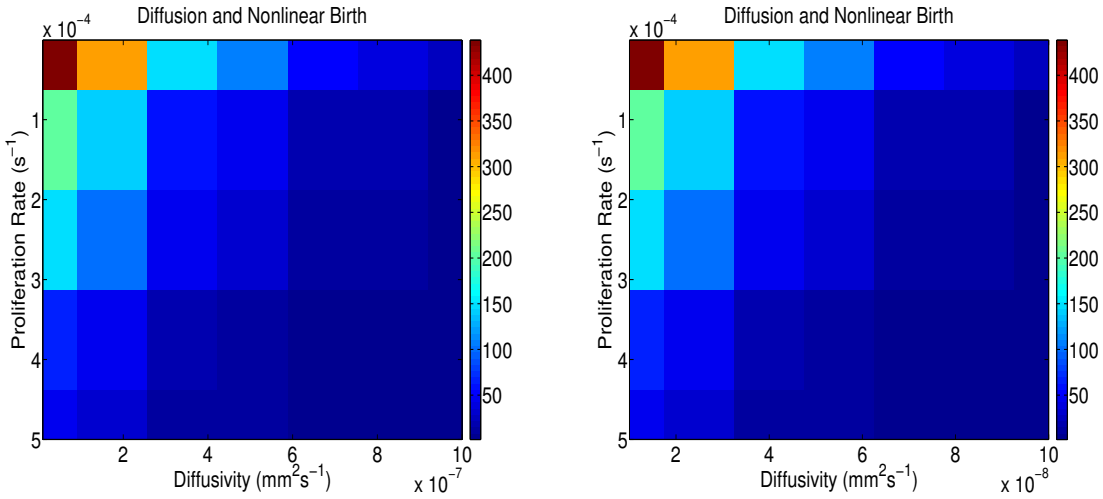


Figure 6.5: Plot of the mean first-passage time, $< t(x_0) >$, in the nonlinear DBP model, for $x_0 = 0$ and $L = 4$mm as a function of the diffusion coefficient and the proliferation rate, k_B, in the critical regime under which invasion occurs. The carrying capacity is equal to $K = 10$cells. The colour bar on the right represents the MFPT in days. The left panel shows the range $10^{-7}\text{mm}^2\text{s}^{-1} < D < 10^{-6}\text{mm}^2\text{s}^{-1}$ whereas the right panel shows the more realistic range $10^{-8}\text{mm}^2\text{s}^{-1} < D < 10^{-7}\text{mm}^2\text{s}^{-1}$. For the parameter ranges depicted in this figure, invasion occurs within the expected timeframe of 42 days only at the right-hand corner of the panels.

Shirakawa et al. [1970], in one of the early works on the subject, studied human melanoma cells and report an average cell cycle of 2-3 days. This means that the proliferation rate, k_B, is in the range $3.86 \cdot 10^{-6} - 5.79 \cdot 10^{-6}\text{s}^{-1}$ according to the authors. Some of the highest estimates for the cell cycle duration are reported by Straus and Moran [1977], who studied epidermal tumours of the head and neck and measured a time greater than 100 hours, i.e. $k_B = 2.78 \cdot 10^{-6}\text{s}^{-1}$. Another one of the early studies, on the other hand, Tannock [1970] report a cell cycle time of 13 hours upon studying mammary tumours, one of the lowest estimates. This implies a value

for k_B equal to $2.14 \cdot 10^{-5}\text{s}^{-1}$. Two other studies that report values in a similar range are those by Terz et al. [1971], who measured a mean time of 25 to 27 hours and Young and DeVita [1970], who report a time of 23 hours. Steel [1972] reported a cell cycle time of 38 hours for epidermoid epitheliomas. Frindel et al. [1968] suggest a cell cycle time of 97 hours upon studying basal cell carcinomas and Bennington [1969] report an average time of 60 hours upon examining epidermoid epitheliomas as well. Finally, Bresciani et al. [1974], who reviewed several studies, suggest that intermitotic time ranges from 52 to 88 hours. To compare, healthy epidermal tissue is characterised by a cell cycle of 311 hours [Weinstein et al., 1984], which indicates that tumour cells in the epidermis have a considerably up-regulated proliferation rate.

All of these findings indicate that even the combination of random motion with an up-regulated proliferation rate, within a realistic range, do not suffice for invasion to occur within 42 days. As such, it is unlikely that this is the driving mechanism behind PNI.

6.3 Diffusion-Proliferation-Reduced Apoptosis Scenario

Hypothesis 3 'A combination of an up-regulated proliferation rate and a reduced apoptotic rate is required to produce the observed invasion rate.'

In order to test this hypothesis, we only need to consider the effect of particle loss on the MFPT of a process and use the information obtained in Chapter 5 along with the arguments made to assess the previous hypothesis.

Considering a DDP process from the perspective of an individual, we see that cell death, or more generally particle loss, does not affect the FPT of a single particle.

If the particle dies at some stage before reaching the specified absorbing boundary, then we simply do not have a recording. If, on the other hand, the particle reaches the boundary before dying, then the FPT is simply the FPT of a particle performing a simple random walk. As a result, the effects of particle loss on the MFPT of a process may only be observed if we look at the macroscopic behaviour.

Recall the governing PDE of the stochastic mean cell density for a linear DBP from Section 5.1, given by equation (5.9),

$$\frac{\partial u}{\partial t} = D\frac{\partial^2 u}{\partial x^2} + (k_B - k_D)u.$$

From this point of view, it is evident that the effect of the death rate, k_D, is to reduce the effective birth rate, k_B, to $k_B - k_D$.

In the nonlinear model, we can use the Fisher-KPP equation, with an additional term representing a linear death rate, as an approximation to the correct equations for the stochastic mean cell density to obtain a scaled Fisher-KPP equation with no death rate. One can thereby show that the effect of the death rate in the nonlinear model is also an effective reduced proliferation rate and a smaller carrying capacity. We do not really need to consider the exact expressions for two reasons. First of all, as we have already noted, the Fisher-KPP equation is only an upper bound and not the correct governing equation of the mean cell density. More importantly, however, we are only interested in the fact that the death rate reduces the effective birth rate in the nonlinear model, just as in the case of the linear model, to a certain degree.

As such, and using the results we obtained in the consideration of a 'proliferation-only' scenario in the second hypothesis, we can make the argument that a reduced apoptotic rate is unlikely to be the extra trigger to a 'random motion with increased proliferation' mechanism that produces sufficiently rapid invasion. Even if the death rate of tumour cells is zero, their proliferation rate is not high enough for invasion to

occur within 42 days. Despite this, by considering realistic values for the apoptotic rates of epidermoid tumour cells and the degree of the immune response in the epidermis and the dermis, we can determine realistic values for the effective birth rate, $k_B - k_D$. However, it seems likely that a bias towards the nerve sheath is necessary for cells to cover a distance of 4mm so fast.

6.4 Advection-Diffusion Scenario

Hypothesis 4 'A strong bias towards the nerve sheath, possibly due to the existence of some chemical attractant, is required in order to produce the observed invasion rate.'

This hypothesis cannot be tested directly through the BRW model as was the case with the other hypotheses. The reason is that our chemoattractant is hypothetical at this point and hence we cannot search in the literature for realistic values. However, we can use the fact that passive migration with an up-regulated proliferation rate and a reduced apoptotic rate cannot induce invasion in the expected timeframe, in order to make an argument for this hypothesis. Furthermore, we can use the results on the MFPT of a BRW to estimate the advection coefficient of the chemical gradient we are looking for.

Fig. 6.6 shows how the MFPT (in days) varies a function of the diffusion and advection coefficients in the range $10^{-8}\text{mm}^2\text{s}^{-1} < D < 10^{-6}\text{mm}^2\text{s}^{-1}$. As expected, the stronger the bias, the smaller the diffusion coefficient required for invasion to occur within the clinically observed timeframe.

Fig. 6.7 shows that for a diffusion coefficient of the order $10^{-7}\text{mm}^2\text{s}^{-1}$, a constant bias of $1.1 \cdot 10^{-6}\text{mm}^2\text{s}^{-1}$ is necessary for invasion to proceed in exactly 42 days. In order to put this value into perspective, we searched the literature for realistic values

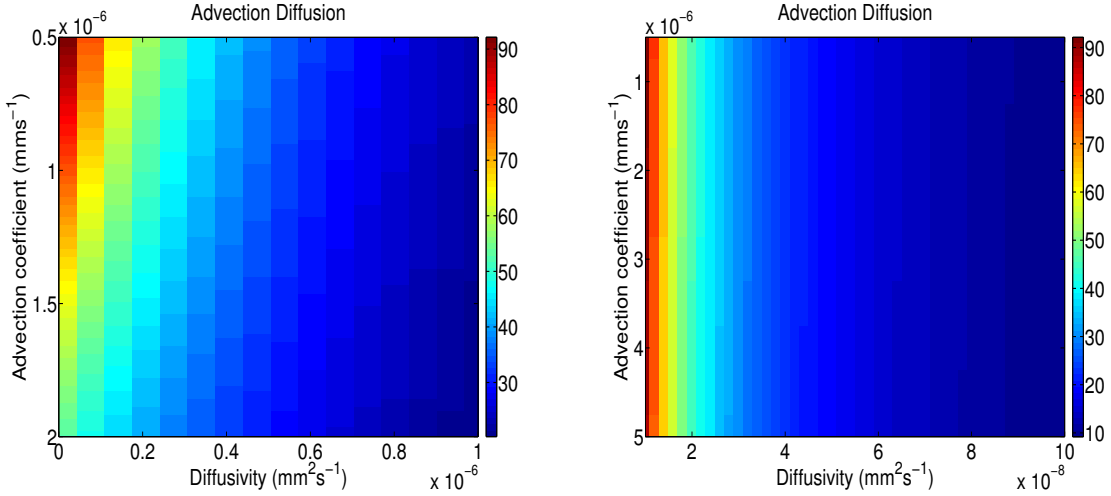


Figure 6.6: Plot of the mean first-passage time, $< t(x_0) >$, in the BRW model, for $x_0 = 0$ and $L = 4$mm as a function of the diffusion coefficient of tumour cells and the advection coefficient of the bias present in the critical regime under which invasion occurs. The left panel shows the range $10^{-7}\text{mm}^2\text{s}^{-1} < D < 10^{-6}\text{mm}^2\text{s}^{-1}$ whereas the right panel shows the more realistic range $10^{-8}\text{mm}^2\text{s}^{-1} < D < 10^{-7}\text{mm}^2\text{s}^{-1}$. The colour bar on the right represents the MFPT in days.

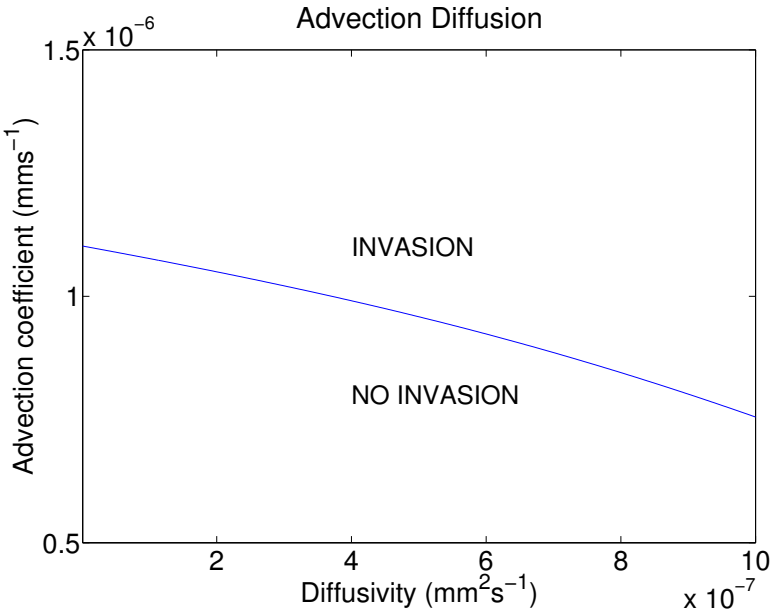


Figure 6.7: Plot of the advection coefficient versus the diffusivity of tumour cells in the BRW model for a mean first-passage time, $< t(x_0) >= 42$ days, $x_0 = 0$ and $L = 4$mm in the critical parameter regime under which invasion occurs. There is a critical value, u_{crit}, below which invasion cannot occur within the expected timeframe of 42 days, which is of the order 10^{-6}mms^{-1} for realistic values of the diffusivity.

of the coefficient of a chemical gradient due to a directional bias for the case of acidic Fibroblast Growth Factor (aFGF) and Vascular Endothelial Growth Factor (VEGF). Stokes and Lauffenburger [1991] quote a value of $2.6 \cdot 10^{-5}\text{mm}^2\text{s}^{-1}$ for the chemotactic coefficient of aFGF. The continuum deterministic model they consider is an example of the classical Patlak-Keller-Segel-Alt (PKSA) chemotaxis model [Patlak, 1953, Keller and Segel, 1971, Alt, 1980], where the chemotactic coefficient is a phenomenological parameter that describes the drift in the migration of a cell population due to the existence of a chemical directional bias. The value quoted above corresponds to the maximum chemotactic response in concentrations of aFGF [Anderson and Chaplain, 1998, Stokes and Lauffenburger, 1991]. In the case of VEGF, Chaplain and Stuart [1993] quote the same value as Stokes and Lauffenburger [1991] for the chemotactic coefficient, while Plank and Sleeman [2004] use a value of approximately $6.8 \cdot 10^{-5}\text{mm}^2\text{s}^{-1}$.

Summary

In this chapter, we considered each of the four cellular-level hypotheses regarding the mechanism behind PNI separately in order to identify the parameter regimes under which invasion occurs within the clinically observed timeframe. We then compared these regimes with realistic parameter values from the literature so that we can assess the validity of each hypothesis.

Our results suggest that random motion, either alone or in combination with up-regulated proliferation and/or reduced apoptosis, is insufficient to exhibit invasion within the expected timeframe. Therefore, these processes are unlikely to be the driving mechanism behind PNI, even if they have an effect on its progression. In particular, we established that the migration and the effective proliferation rate of

tumour cells required for invasion are two to three orders of magnitude greater than realistic values, which were drawn from the literature from data on neoplastic epidermal tissue. This type of tissue, especially if neoplastic but also if healthy, is among the most rapidly migrating and proliferating in the human body. Thus, the value of the MFPT predicted by the models using these parameter values may be regarded as an upper bound (with respect to the limitations of the models, see Chapter 7) for the mean time of the actual invasion process, a fact which reinforces our conclusions. Finally, the fourth hypothesis surrounding the mechanism behind PNI, the existence of a chemical signal attracting tumour cells towards the nerve sheath, cannot be eliminated from consideration. We managed, however, to establish a lower bound for the advection coefficient required to produce invasion within the observed timeframe.

This analysis concludes an initial evaluation of the different hypotheses, through simplified mathematical models, using the mean time of invasion as a measure for comparison. The choice of working in one dimension enabled us to determine certain mechanisms as even more unlikely in more realistic two- or three-dimensional geometries. The framework we have created in our exploration of the cellular-level mechanisms behind PNI, through the use of the notion of the first-passage time, can be extended to consider the incidence rates predicted by each model. This can be used as a second measure of comparison between the different hypotheses regarding PNI. However, before proceeding to this next step, the limitations in our models (for instance spatial homogeneity) need to be addressed.

Chapter 7

Discussion

PNI is a type of tumour spread associated with very high mortality rates. By entering a perineural space, tumour cells migrate towards the CNS through a path of minimal resistance as there is no immune response. There are various hypotheses, both at the cellular and at the subcellular level, regarding the mechanism behind PNI and the reason why tumour cells are particularly attracted to the nerve sheath. At the cellular level, possible hypotheses include: random motion as the sole mechanism behind PNI; random in combination with an up-regulated proliferation rate and a reduced apoptotic rate; or directed motion due to the existence of a chemoattractant. At the subcellular level, four different scenarios have been proposed in the literature as potential subcellular mechanisms behind PNI. Firstly, neurotrophins, and in particular NGF and its Trk receptors, have been connected to PNI. Secondly, a correlation between NCAM and PNI has been observed. Thirdly, the over-expression of nuclear factor NFκB has been suggested as the potential mechanism driving PNI. Finally, evidence relating MMPs to the progression of PNI has been found.

PNI exhibits certain characteristics that distinguish it from other modes of tumour spread. In particular, the first stage of PNI, i.e. the migration of tumour cells from

their initial site, in the epidermis, to the point they enter the nerves of deeper tissue, is a very fast process (within six weeks deeper tissue of up to 4mm may be invaded [Gilmore et al., 2009]). The 'finger-like' or 'disconnected island' patterns observed are another distinguishing characteristic of PNI. By exploiting these features, one can create a mathematical framework that may shed light on the different hypotheses regarding the mechanism behind PNI.

Traditional mathematical modelling approaches were mainly driven by experimental data. However, more recent approaches, which focus on the qualitative aspects of a system and explore all the possible behaviours of the system, are particularly suitable for assessing the validity of the hypotheses surrounding PNI. There are various modelling regimes that describe processes, such as cell migration, proliferation and apoptosis, which can be used to test the cellular-level hypotheses regarding PNI. A basic dichotomy exists between continuum models, which describe population-level characteristics of a tumour, and discrete models, which represent the interactions between individual tumour cells. These models may or may not consider the inherent randomness characterising these processes, so another dichotomy exists between a stochastic and a deterministic approach. Each modelling approach has its own merits and drawbacks and there is more to gain if they are used in combination, in order to exploit their complementary strengths towards developing a multi-scale model of tumour invasion.

7.1 Conclusion

Throughout this thesis, we attempt to connect a discrete stochastic modelling regime to a continuum deterministic description in order to build simplified models of PNI. These models, along with the notion of a 'first-passage time', are the tools we employ

in order to make a first assessment of the four cellular-level hypotheses regarding PNI, outlined in Section 1.3 of Chapter 1. We always begin with an individual-level description of tumour cells, as this is more appropriate, and try to derive the deterministic behaviour exhibited by tumour cells collectively rather than model the latter phenomenologically. Furthermore, we work in a one-dimensional domain as a straight line is the fastest route to a specified destination and we are only concerned with an upper bound for the mean time of invasion in order to suggest that a certain hypothesis is unlikely.

The short-term objective of our approach is to predict the mean time of invasion of each potential mechanism behind PNI and then compare the results to the clinically observed time scale. This can be achieved through a first-passage time analysis, which provides a natural framework for studying the time it takes for a particle which performs a stochastic process to reach a specified boundary. In Chapter 4, we showed that in the context of migration alone, analytical results may be obtained from equivalent deterministic models. However, once branching and annihilation processes are incorporated into the model, the techniques employed earlier do not suffice to derive analytical results. Consequently, we relied on the results of the stochastic simulations only in order to establish the MFPT of such processes.

Our first hypothesis, namely that random motion alone is sufficient to produce invasion within the expected timeframe, was assessed through both a position- and a (more realistic) velocity-jump process. In both models, realistic parameter values lie outside the range required for invasion to occur sufficiently fast. Both the value of the diffusion coefficient and the velocity of tumour cells required are at least two orders of magnitude greater than the values measured experimentally. As a result, this hypothesis seems unlikely because a cell cannot reach 4mm within six weeks, on average. Some of the limitations of the SRW model, a model of a position-jump

process, are accounted for by the CRW model, an example of a velocity-jump process, which is more realistic (the former class may be regarded as a good approximation of the latter class of jump processes at large time scales [Othmer, 1988]). However, the conclusion reached on this hypothesis needs to be assessed with respect to a limitation shared by both of these simple models, namely the assumption that invasion occurs in a spatially homogeneous environment (see Section 7.2). However, even if the parameters of the models are allowed to be spatially-dependent instead of constant, only an upper bound of realistic values is necessary in order to logically infer that this process is insufficient to produce sufficiently rapid invasion.

Our second and third hypotheses suggest that while random motion alone may be unlikely as a potential mechanism behind PNI, a combination with an up-regulated proliferation rate and/or a reduced apoptotic rate (both common characteristics of tumour cells) may be sufficient to produce invasion within the observed time scale. Both of these scenarios were addressed through employing the results of the simulation of discrete stochastic models. Although analytical results would have been more helpful in highlighting the exact dependence of the mean time of invasion on model parameters, we could not find any techniques in the literature that enable us to derive an analytical expression for the MFPT of branching processes. However, the results of the stochastic simulation are clearly very suggestive. Even in the case of exponential growth without cell loss, the proliferation rate required is two to three orders of magnitude greater than the highest estimates of experimentally observed values. Furthermore, the kinetic parameters we considered were estimated from carcinomas of the epidermis, which is the type of tissue characterised by the highest proliferation rates. The fact that PNI is also associated with other types of tissue, where cell division generally occurs at a slower pace in comparison to epidermal tissue, reinforces the argument that both of these hypotheses seem unlikely. While an up-regulated proliferation rate and a reduced apoptotic rate may have an effect on

PNI, they cannot be the driving mechanisms behind it. The main limitation of the branching models we considered is the fact that the cell cycle does not depend on the extracellular environment or the density of tumour cells (for an extension see Section 7.2).

Our final hypothesis suggests that some kind of bias towards the nerves (for instance due to a chemoattractant) is necessary to produce invasion within the observed timeframe. Our results show that this hypothesis does indeed seem likely if a constant bias of the order of $10^{-6}\text{mm}^2\text{s}^{-1}$ is present, which is not unrealistic for the directional bias created by growth factors such as aFGF or VEGF, for instance. As with the other models of cell migration, spatial homogeneity is a severe limitation that needs to be addressed. Considering a constant chemical gradient is not realistic as the substance will diffuse in space. However, the required value of the advection coefficient can be used as a lower bound.

One other severe limitation in the conclusions reached by our analysis is the fact that we rely heavily on the notion of an average time scale as a means for comparison. However, as we saw in Chapter 4, the variance of the first-passage time can be very large and of considerable magnitude with respect to the size of the MFPT, especially for the position-jump processes. Consequently, although the average time of invasion predicted by our models is much larger, in the investigation of the first three hypotheses, than the expected timeframe of invasion, we cannot eliminate the possibility of invasion completely. Invasion may occur through isolated tumour cells, or very small islands of cells, that do not obey the mean and reach the boundary much faster than a cell would on average. The possibility of spreading inside perineural spaces is, of course, lower than if a bulk of tumour cells reached the neural structures of the dermis in time. However, tumour cells are faced with a path of minimal resistance and almost no immune response once inside a perineural space. Thus, even islands of few

cells may be able to cause PNI. This leads us to consider incidence rates (see Section 7.2 for a discussion) as another means for comparison between the different possible mechanisms behind PNI

In conclusion, one can see that evaluating different hypotheses regarding the mechanism behind a complicated biological problem requires various modes of comparison and an extensive analysis from many angles. In this thesis, we reviewed the problem of perineural invasion, a particularly aggressive and rapid type of invasion, from the point of view of various biological observations. We then examined some simplistic models of cell migration, proliferation and annihilation. We created a framework for comparing average time scales of first-passage processes in the two major categories of models of migration, position- and velocity-jump models. We also derived a method to assess the strength and validity of our conclusions. Finally, we applied this modelling framework in order to investigate the possible mechanism behind PNI for the first time, to the best of our knowledge.

7.2 Future Work

Our strategy for assessing the four cellular-level hypotheses regarding PNI through a first-passage time analysis in one dimension suggests that three of the four hypotheses seem highly unlikely. However, there are several areas that can be extended in order to make even more conclusive arguments and obtain further insight about the mechanism behind PNI.

One of the main limitations of all the simplified models we considered is the assumption of spatial homogeneity. In the position-jump models, this is reflected by the fact that the transition probabilities are constant with respect to the spatial position. In the velocity-jump models, spatial homogeneity is reflected by the spatially-

independent rate of changing direction. In the equivalent deterministic models this translates to a spatially-independent diffusion coefficient or velocity, respectively. As far as branching and annihilation processes are concerned, spatial homogeneity is evident in the spatially-independent birth and death rates.

The assumption that PNI progresses within a spatially homogeneous environment is unrealistic for several reasons. First of all, the earliest stage of PNI, i.e. migration from the initial tumour site up to a 4mm depth of subcutaneous tissue, occurs within two different skin layers, the epidermis (0.1-1mm thick) and the dermis (0.6-3mm thick). The epidermis (outer layer) is mainly composed of rapidly migrating and proliferating epithelial tissue, whereas the dermis mainly consists of cells of connective (fibroblasts) and adipose (energy-storing) tissue, and of macrophages (from various types of tissue). Hence, the journey of PNI cells from their initial location towards deeper tissue occurs within significantly different environments. As such, the migration rate of tumour cells does not remain constant throughout the entire journey. However, it is sensible to assume that these rates are greater in the epidermis than in deeper tissue. Since the experimental values we have used may be regarded as average kinetic parameter values of epidermal tissue, the estimated mean time of invasion is indeed an upper bound of the actual duration, which is extremely important for assessing the validity of our conclusions.

In order to achieve a more realistic description of migration, we need to consider a spatially inhomogeneous environment where the transition rules in the jump process depend on the spatial location of a cell. Johnson et al. [1992] studied population dynamics in heterogeneous landscapes and propose three different theoretical approaches based on random walk theory on percolation clusters (partitions of the environment). McKenzie et al. [2009] provide analytical solutions for the MFPT of one- and two-dimensional position-jump processes where the migration rate is spatially-dependent.

A more general approach for calculating the MFPT of stochastic processes in complex scale-invariant media is that by Condamin et al. [2007]. The authors derived analytical results which show the dependence of the MFPT on the volume of confined media and the source-target distance and agree well with Monte Carlo simulations. Noh and Rieger [2004] and Tejedor et al. [2009] followed a similar approach for estimating the MFPT and the global MFPT (averaged over the initial location), respectively, of processes occurring on complex networks. The case of anomalous diffusion (nonlinear dependence of the MSD on time) was considered by Gitterman [2000]. Finally, another extension is to consider density-dependent migration rates since it is sensible to assume that the rate of movement of tumour cells depends on the available space. The techniques for estimating the MFPT analytically by Redner [2001] are still applicable in this case [Yates, 2011].

Another reason why spatial homogeneity is an unrealistic assumption is the fact that the duration of the cell cycle is utterly dependent on the extracellular environment and the amount of available nutrients. The epidermis is an avascular environment with a scarce supply of nutrients. The dermis, on the contrary, is full of lymphatic and blood vessels. As such, it may seem odd that the epidermal tissue is among the most highly proliferating in a human body. However, these dermal vessels provide nourishment for both dermal and epidermal cells. In addition, dead squamous cells at the surface of the skin, i.e. in the epidermis, are constantly shed and replaced by basal cells being pushed toward the outer layers by a vigorous underlying mitotic activity. Therefore, given the experimental studies we have used, the estimated mean time of invasion may be regarded as an upper bound of the actual time scale in the case of branching, as well. A more realistic way of incorporating cell proliferation (and death) is by assigning a cell cycle model to each cell, for instance in the form of a set of ODEs. Proliferation rates can then be determined by the internal cell cycle dynamics [van Leeuwen et al., 2009], signals from the extracellular environment

[Pitt-Francis et al., 2009, van Leeuwen et al., 2009] and the spatial constraints due to the increasing size of the cell population (density-dependent configuration).

Finally, it is also unrealistic to assume that the death rate of tumour cells is constant as the immune response of the organism will vary considerably among the different skin layers and the apoptotic rate of cells also depends on the extracellular environment. Biologically, we expect the immune response to be milder in the epidermis, stronger in the dermis and non-existent once tumour cells have entered the perineural space. The apoptotic rate is higher in the epidermis due to the constant shedding and replacement of cells. As was the case with proliferation and migration, however, the assumption of spatial homogeneity does not alter our conclusion regarding the 'reduced apoptosis' hypothesis, which is unlikely as a mechanism behind PNI.

The assumption of a spatially homogeneous environment becomes important when considering the last hypothesis regarding the existence of a chemoattractant. Since we cannot eliminate this hypothesis from consideration as unlikely and can only determine a lower bound for the advection coefficient necessary for invasion to proceed within the expected timeframe, it is essential that we extend this model to consider a diffusing chemical gradient. Othmer and Stevens [1997] considered the movement of organisms in response to diffusible signals by building on the classical chemotaxis model by Patlak [1953]. The authors classified the PDEs they derived depending on how transition rules in a jump process are affected by the signalling profile and then investigated the various dynamics that arise. Hillen and Othmer [2000] and Othmer and Hillen [2002] studied the transport equations arising from velocity-jump processes and derived the resulting PDEs in the diffusion limit under a variety of external biases. They then showed that the classical PKSA chemotaxis model [Patlak, 1953, Alt, 1980, Keller and Segel, 1971] is, in fact, the appropriate continuum deterministic approximation only if the bias is sufficiently small. A large variety of

chemical signalling profiles that may affect the migration rate of cells was also studied by Berg and Purcell [1977] and more recently by Parent and Devreotes [1999] and Levine et al. [2006]. These models are amenable to the time-integrated occupation probability technique by Redner [2001] in order to find an analytical expression for the MFPT [Yates, 2011].

The first-passage time approach we have followed can also be used in order to predict the incidence rate of PNI. So far, we have only looked at the first moment of the first-passage time probability distribution as we only considered the average time scale of an invasion process. Clinical observations suggest that PNI cells often create disconnected tumour islands in the nerve, as opposed to a diffusely infiltrating tumour wave. This indicates that even if a process is insufficient to produce invasion within a certain timeframe, on average, there is still a probability that few tumour cells manage to reach the nerve sheath faster than the average cell. An estimate of this probability, which is given by the FPT distribution, can be used to predict the incidence rate for each of the processes we considered in this thesis. As such, we can use the clinically observed incidence rates as an additional measure of comparison between the different models and a tool for the evaluation of the four cellular-level hypotheses regarding the mechanism behind PNI.

Another biological observation that can prove helpful in identifying the mechanism behind PNI is that of the irregular spatial patterns and shapes that PNI tumour cells exhibit. Tohya et al. [1998] considered a two-dimensional continuum chemotaxis model of BCC in order to produce the finger-like structures observed in PNI. Their results cannot be reproduced in one dimension, so we have to extend our analysis to higher dimensions in order to predict the patterns produced by each of the invasion processes we considered. Since Tohya et al. [1998] considered a phenomenological model only, it would be interesting to see if these PDEs can be derived by the two-

dimensional stochastic processes, which is not at all trivial, if at all possible [Codling et al., 2008].

Finally, another limitation of our simplified models that needs to be addressed is the interaction of tumour cells with the healthy cell population. In our analysis this interaction is only evident in the nonlinear DBP model where spatial constraints or limited nutrient supply are considered by means of the carrying capacity. These additional spatial constraints can only increase the mean time of invasion so our conclusions would not be altered, but a more realistic approach, such as the 'ghost vs folks' model by Simpson et al. [2009], should consider the effect of the healthy cell population, especially if one is interested in the resulting spatial patterns.

Appendix A

Appendices for Chapter 3.

A.1 Simple Random Walk

A.1.1 Occupation Probability in Discrete Space and Time

The first objective is to find the probability that a particle will be found at a position $x = m\Delta x$ $(m > 0)$ after n time steps. Without loss of generality, assume that n and m are even. Suppose further that the particle has moved α steps to the right and β steps to the left, so

$$n = \alpha + \beta, \;\; m = \alpha - \beta, \;\; \alpha = \frac{n+m}{2}, \;\; \beta = \frac{n-m}{2}.$$

The particle under consideration will have performed n independent steps at time $t = n\Delta t$, so the probability of its following a specific path will be equal to the product of the probabilities of performing a single step. Since the probability of moving to either direction is $\frac{1}{2}$, the probability of moving n steps is equal to $\left(\frac{1}{2}\right)^n$. Now, in order to find the probability that the particle will be found at a specific site after n steps, we need to count all the possible paths through which it can reach this site.

We know from combinatorial theory that the number of ways of choosing k elements from a set of n objects is given by

$$C_n^k = \binom{n}{r} = \frac{n!}{k!(n-k)!}.$$

Given that our particle has taken α steps to the right, the number of possible paths to reach $x = m\Delta x$ is equal to the number of ways of choosing α elements from a set of n, i.e.

$$\binom{n}{\alpha} = \frac{n!}{\alpha!(n-\alpha)!}.$$

Note that we can make the same argument by picking β elements from a set of n objects and as expected the number of possible paths is the same,

$$\binom{n}{\beta} = \frac{n!}{\beta!(n-\beta)!} = \frac{n!}{(n-\alpha)!\alpha!} = \binom{n}{\alpha}.$$

Consequently, the probability of finding our particle at a distance $m\Delta x$ from the origin after n time steps is given by equation (3.1)

$$p(m,n) = \left(\frac{1}{2}\right)^n \cdot \binom{n}{\frac{n+m}{2}} = \frac{n!}{2^n(\frac{n-m}{2})!(\frac{n+m}{2})!}, \tag{A.1}$$

with $n \pm m$ even since n, m are even.

A.1.2 Occupation Probability Approximation as $n \to \infty$

Stirling's approximation for large factorials is given by

$$n! = \sqrt{2\pi n}\left(\frac{n}{e}\right)^n, \tag{A.2}$$

as $n \to \infty$. If we take logarithms[1], equation (A.2) becomes

$$\log n! = n \log n - n + \frac{1}{2} \log (2\pi n). \tag{A.3}$$

Then, from equation (3.1) we obtain

$$\log p(m,n) = \log n! - n \log 2 - \log \left[\left(\frac{n+m}{2} \right)! \right] - \log \left[\left(\frac{n-m}{2} \right)! \right].$$

By substituting each of the three factorials with simplified expressions using Stirling's approximation and rewriting

$$\log \left(\frac{n \pm m}{2} \right) = \log \left[\frac{n}{2} \left(1 \pm \frac{m}{n} \right) \right] = \log n - \log 2 + \log \left(1 \pm \frac{m}{n} \right),$$

we obtain

$$\begin{aligned} \log p(m,n) = & \frac{1}{2} \log (2\pi n) - \frac{1}{2} \log (n^2 - m^2) \\ & - \left(\frac{n+m}{2} \right) \log \left(1 + \frac{m}{n} \right) \\ & - \left(\frac{n-m}{2} \right) \log \left(1 - \frac{m}{n} \right) - \log \pi. \end{aligned} \tag{A.4}$$

In the limit $n \to \infty$, $m \ll n$ and using a series expansion,

$$\log \left(1 \pm \frac{m}{n} \right) = \pm \frac{m}{n} - \frac{m^2}{2n^2} + O\left(\frac{m^3}{n^3} \right),$$

and

$$\log (n^2 - m^2) = 2 \log n - \frac{m^2}{n^2} + O\left(\frac{m^4}{n^4} \right).$$

[1] the natural logarithm of x denoted by $\log x$

By substituting these expressions into (A.4), we arrive at

$$\lim_{n\to\infty} \log p(m,n) = \frac{1}{2}\log\left(\frac{2}{\pi n}\right) - \frac{m^2}{2n} + O\left(\frac{m^2}{n^2}\right). \tag{A.5}$$

Therefore,

$$\lim_{n\to\infty} p(m,n) = \sqrt{\frac{2}{\pi n}}\exp\left(-\frac{m^2}{2n}\right).$$

A.1.3 Statistical Measures

We shall now define some useful standard statistical measures in order to examine the behaviour of the process further. The general k-th moment of the occupation probability is defined as

$$E(X_t^k) = \int_{-\infty}^{\infty} x^k \cdot p(x,t)dx, \ \forall k \in \mathbb{N}. \tag{A.6}$$

Some special cases are the zero-th moment, defined as

$$E(X_t^0) = \int_{-\infty}^{\infty} p(x,t)dx = 1, \tag{A.7}$$

which is one of the three defining properties of a probability space. The first moment, the *expected location*, is defined as

$$E(X_t) = \int_{-\infty}^{\infty} x \cdot p(x,t)dx, \tag{A.8}$$

and describes the mean location of the walker if the process is simulated several times. The second moment, the *mean squared displacement* (MSD), defined as

$$E(X_t^2) = \int_{-\infty}^{\infty} x^2 \cdot p(x,t)dx, \tag{A.9}$$

describes the mean dispersal about the origin $x = 0$. However, a related statistic, the variance, defined as

$$\sigma_t^2 = E([X_t - E(X_t)]^2) = \int_{-\infty}^{\infty} [x - E(X_t)]^2 \cdot p(x,t)dx, \tag{A.10}$$

measures the dispersal about the mean location and may be more useful in models where the mean is non-zero. Note that the variance is related to the MSD by the formula

$$\begin{aligned} \sigma_t^2 &= \int_{-\infty}^{\infty} [x^2 - 2xE(X_t) + E(X_t)^2] \cdot p(x,t)dx \\ &= E(X_t^2) - 2E(X_t) \cdot E(X_t) + E(X_t)^2 \\ &= E(X_t^2) - E(X_t)^2, \end{aligned} \tag{A.11}$$

since the mean $E(X_t)$ is a function of time only. It is usually easier and faster to calculate the difference of the MSD from the square of the mean than the variance itself from first principles.

A.1.4 Gillespie's SSA - Compartment-based Diffusion

In the context of the SRW, the algorithm is as follows. We start with initial condition $u_i = \frac{n_0}{2}$ for $i = \frac{N}{2}, \frac{N}{2} + 1$ and $u_i = 0$ otherwise, which corresponds to n_0 particles being released at $x = 0.5$. Then we perform six steps:

(1) Generate two random numbers r_1, r_2 uniformly distributed in (0,1).

(2) Compute the propensity functions $\alpha_i = d \cdot u_i(t)$ for $i = 1, 2, ..., N$ and the expression

$$\alpha_0 = \sum_{i=1}^{N} \alpha_i + \sum_{i=2}^{N} \alpha_i, \tag{A.12}$$

i.e. we first consider all possible transitions to the right and then all possible transitions to the left.

(3) Compute the time at which the next transition will occur as $t + \Delta t$ by

$$\Delta t = \frac{1}{\alpha_0} \log \frac{1}{r_1}. \tag{A.13}$$

(4) If $r_2 < \sum_{i=1}^{N} \frac{\alpha_i}{\alpha_0}$, find $j \in 1, 2, ..., N$ such that

$$r_2 \geq \sum_{i=1}^{j-1} \frac{\alpha_i}{\alpha_0} \text{ and } r_2 < \sum_{i=1}^{j} \frac{\alpha_i}{\alpha_0}.$$

Then,

$$\begin{aligned} u_j(t + \Delta t) &= u_j(t) - 1, \\ u_{j+1}(t + \Delta t) &= u_{j+1}(t) + 1, \\ u_i(t + \Delta t) &= u_i(t), \forall i \neq j, i \neq j + 1. \end{aligned} \tag{A.14}$$

(5) If $r_2 \geq \sum_{i=1}^{N} \frac{\alpha_i}{\alpha_0}$, find $j \in 2, ..., N$ such that

$$r_2 \geq \sum_{i=1}^{N} \frac{\alpha_i}{\alpha_0} + \sum_{i=1}^{j-1} \frac{\alpha_i}{\alpha_0} \text{ and } r_2 < \sum_{i=1}^{N} \frac{\alpha_i}{\alpha_0} + \sum_{i=1}^{j} \frac{\alpha_i}{\alpha_0}.$$

Then,

$$\begin{aligned} u_j(t + \Delta t) &= u_j(t) - 1, \\ u_{j-1}(t + \Delta t) &= u_{j-1}(t) + 1, \\ u_i(t + \Delta t) &= u_i(t), \forall i \neq j, i \neq j - 1. \end{aligned} \tag{A.15}$$

(6) Go to step (1) and repeat the process for $t + \Delta t$.

A.2 Biased Random Walk

A.2.1 Derivation of PDE

By expanding the following terms about x and t, using Taylor's theorem, we obtain

$$p(x \pm \Delta x, t) = p(x,t) \pm \Delta x \frac{\partial p}{\partial x} + \frac{1}{2!}\Delta x^2 \frac{\partial^2 p}{\partial x^2} + O(\Delta x^3),$$

and

$$p(x, t + \Delta t) = p(x,t) + \Delta t \frac{\partial p}{\partial t} + \frac{1}{2!}\Delta t^2 \frac{\partial^2 p}{\partial t^2} + O(\Delta t^3).$$

Substituting into equation (3.14) we arrive at

$$\begin{aligned} p(x,t) + \Delta t \frac{\partial p}{\partial t} + \frac{1}{2!}\Delta t^2 \frac{\partial^2 p}{\partial t^2} + O(\Delta t^3) = \\ \alpha p(x,t) - \alpha \Delta x \frac{\partial p}{\partial x} + \frac{1}{2!}\alpha \Delta x^2 \frac{\partial^2 p}{\partial x^2} + \\ \beta p(x,t) + \beta \Delta x \frac{\partial p}{\partial x} + \frac{1}{2!}\beta \Delta x^2 \frac{\partial^2 p}{\partial x^2} + \\ (1 - \alpha - \beta) p(x,t) + O(\Delta x^3), \end{aligned}$$

which upon simplification, in the limit as $\Delta t \to 0$ and $\Delta x \to 0$, reduces to

$$\frac{\partial p}{\partial t} = -(\alpha - \beta)\frac{\Delta x}{\Delta t}\frac{\partial p}{\partial x} + (\alpha + \beta)\frac{\Delta x^2}{2\Delta t}\frac{\partial^2 p}{\partial x^2} + O\left(\frac{\Delta x^3}{\Delta t}\right) + O(\Delta t^2). \tag{A.16}$$

In the appropriate limits, as defined by (3.15), this relation becomes the advection-diffusion equation

$$\frac{\partial p}{\partial t} = -u\frac{\partial p}{\partial x} + D\frac{\partial^2 p}{\partial x^2}. \tag{A.17}$$

A.2.2 Derivation of the Mean Location and Variance of the BRW

Multiply the governing PDE of the BRW model, the advection-diffusion equation given by (3.16), by x and integrate with respect to x from $-\infty$ to $+\infty$ to obtain

$$\int_{-\infty}^{\infty} x\frac{\partial p}{\partial t}dx = -u\int_{-\infty}^{\infty} x\frac{\partial p}{\partial x}dx + D\int_{-\infty}^{\infty} x\frac{\partial^2 p}{\partial x^2}dx. \tag{A.18}$$

The LHS of equation (A.18) can be written as

$$\frac{d}{dt}[E(X_t)],$$

since the limits are independent of t and so we can interchange the integration and differentiation operations. Integration by parts of the RHS of equation (A.18) yields

$$-u\cdot([xp(x,t)]_{-\infty}^{\infty} - \int_{-\infty}^{\infty} p(x,t)dx) + D\cdot\left([x\frac{\partial p}{\partial x}(x,t)]_{-\infty}^{\infty} - \int_{-\infty}^{\infty}\frac{\partial p}{\partial x}dx\right)$$

By noting that

$$\int_{-\infty}^{\infty} p(x,t) = 1, \tag{A.19}$$

by definition of the probability space and that

$$\lim_{|x|\to\infty} p(x,t) = 0, \quad \lim_{|x|\to\infty}\frac{\partial p}{\partial x} = 0, \tag{A.20}$$

as the probability of finding a particle at a specific point at some specified finite time becomes smaller the further away the point is from the origin (or in general the release point x_0 if $x_0 \neq 0$) and it is reasonable to assume its first derivatives with respect to

x tend to zero, we obtain

$$\frac{d}{dt}[E(X_t)] = u, \tag{A.21}$$

along with the initial condition $E(X_0) = 0$ since at $t = 0$ the walker is located at the origin. The solution of this ODE is given by (3.18).

In order to derive an expression for the MSD, we repeat the procedure but this time by multiplying equation (3.16) by x^2. Integrating by parts twice and applying the same limits as in the case of the mean leads to the linear first-order ODE

$$\frac{d}{dt}[E(X_t^2)] = 2u^2t + 2D, \tag{A.22}$$

along with initial condition $E(X_0^2) = 0$. Integration with respect to t yields the desired result given by (3.19). We then use the relation (A.11) to find that the variance equals $2Dt$.

A.2.3 Derivation of the Zero-flux Boundary Condition given by Equation 3.22

Recall that the occupation probability at the left boundary of the domain is given by equation (3.21),

$$p(0, t + \Delta t) = \beta p(\Delta x, t) + (1 - \alpha)p(0, t),$$

which, after a Taylor's expansion about the origin, leads to

$$\begin{aligned} &p(0,t) + \Delta t \frac{\partial p}{\partial t}(0,t) + \frac{\Delta t^2}{2}\frac{\partial^2 p}{\partial t^2}(0,t) + O(\Delta t^3) \\ &\quad = (1 - \alpha + \beta)p(0,t) + \beta \Delta x \frac{\partial p}{\partial x}(0,t) + \beta \frac{\Delta x^2}{2}\frac{\partial^2 p}{\partial x^2} + O(\Delta x^3), \end{aligned} \tag{A.23}$$

where $\Delta x^2, \Delta t^2$ denote the squares of the spatial and temporal steps, $(\Delta x)^2, (\Delta t)^2$, respectively. By multiplying the above equation by Δx, then dividing by Δt and after

cancelling the $p(0,t)$ term from both sides of the equation, we obtain

$$\begin{aligned}\Delta x\frac{\partial p}{\partial t}(0,t)+\frac{\Delta x\Delta t}{2}\frac{\partial^2 p}{\partial t^2}+O(\Delta x\Delta t^2)\\ =\frac{\Delta x(\beta-\alpha)}{\Delta t}p(0,t)+\frac{\beta\Delta x^2}{\Delta t}\frac{\partial p}{\partial x}(0,t)+\frac{\beta\Delta x^3}{2\Delta t}\frac{\partial^2 p}{\partial x^2}(0,t)+O\left(\frac{\Delta x^4}{\Delta t}\right),\end{aligned} \tag{A.24}$$

If we let $\Delta x, \Delta t$ tend to zero in such a way that $\frac{\Delta x^2}{2\Delta t}$ and $\epsilon\frac{\Delta x}{\Delta t}$ are finite, then $\Delta x \sim O(\Delta t^{\frac{1}{2}})$ and $\epsilon \sim O(\Delta t^{\frac{1}{2}})$ so we need $\epsilon \to 0$ for the continuum approximation to be valid. We now set

$$u=\lim_{\epsilon,\Delta x,\Delta t\to 0}\frac{\epsilon\Delta x}{\Delta t},\quad \text{and}\quad D=\lim_{\Delta x,\Delta t\to 0}k\frac{\Delta x^2}{2\Delta t}$$

and observe that

$$\begin{aligned}\lim_{\Delta x,\Delta t\to 0}\Delta x\Delta t&=0,\\ \lim_{\Delta x,\Delta t\to 0}\beta\Delta x\Delta t^2&=0,\\ \lim_{\Delta x,\Delta t\to 0}\frac{\beta\Delta x^3}{2\Delta t}=\lim_{\Delta x,\Delta t\to 0}\beta\Delta x\frac{\Delta x^2}{2\Delta t}&=0,\\ \lim_{\Delta x,\Delta t\to 0}\frac{\beta\Delta x^4}{2\Delta t}=\lim_{\Delta x,\Delta t\to 0}\beta\Delta x^2\frac{\Delta x^2}{2\Delta t}&=0.\end{aligned} \tag{A.25}$$

Hence, after the cancellations, we obtain

$$\lim_{\Delta x,\Delta t\to 0}\left[\frac{\Delta x(\beta-\alpha)}{\Delta t}p(0,t)+\frac{\beta\Delta x^2}{\Delta t}\frac{\partial p}{\partial x}(0,t)\right]=0. \tag{A.26}$$

By setting $\epsilon=\alpha-\beta$ in the first term of the left-hand side of the above equation and expressing β in the form

$$\frac{2\beta}{2}=\frac{\beta+\beta}{2}=\frac{(\beta+\alpha)}{2}+\frac{(\beta-\alpha)}{2}$$

in the second term of the left-hand side, leads to

$$\lim_{\Delta x,\Delta t\to 0}\left[-\frac{\epsilon\Delta x}{\Delta t}p(0,t)+(\alpha+\beta)\frac{\Delta x^2}{2\Delta t}\frac{\partial p}{\partial x}(0,t)+(\beta-\alpha)\frac{\Delta x^2}{2\Delta t}\frac{\partial p}{\partial x}(0,t)\right]=0. \quad \text{(A.27)}$$

Since $\epsilon\frac{\Delta x}{\Delta t}$ is finite in this limit, we obtain

$$D\frac{\partial p}{\partial x}(0,t)-up(0,t)+\lim_{\Delta x,\Delta t,\epsilon\to 0}u\frac{\Delta x}{2}\frac{\partial p}{\partial x}(0,t)=0. \quad \text{(A.28)}$$

The last term of the left-hand side of the above equation tends to zero as $\Delta x\to 0$ so we obtain the familiar zero-flux boundary condition given by (3.22).

Finally, notice that the usefulness of this approach is limited by the constraint that ϵ needs to be of order $O(\Delta t^{\frac{1}{2}})$ and tend to zero as both Δx and Δt tend to zero. In other words, the transition probabilities α and β vary with Δx and Δt to ensure that the continuum approximation is valid. There are, however, different derivations where the condition $\epsilon\to 0$ is not required. Two such examples are due to the work of Okubo and Levin [2001] and Othmer [1988].

Okubo and Levin [2001] present a derivation of the Fokker-Planck equation which governs the motion in a biased random walk by considering the population density $S(x,t)$ and taking the limits of the first two moments of the displacement as $\Delta t\to 0$. The equation here takes the form

$$\frac{\partial S}{\partial t}=-\frac{\partial}{\partial x}\left[M_1(x,t)\right]S+\frac{\partial^2}{\partial x^2}\left[\frac{1}{2}M_2(x,t)S\right], \quad \text{(A.29)}$$

where

$$\begin{aligned}M_1(x,t)&=\lim_{\Delta t\to 0}\frac{1}{\Delta t}\int_{-\infty}^{\infty}(x'-x)\phi(x,t;x',t+\Delta t)dx',\\ M_2(x,t)&=\lim_{\Delta t\to 0}\frac{1}{\Delta t}\int_{-\infty}^{\infty}(x'-x)^2\phi(x,t;x',t+\Delta t)dx'.\end{aligned} \quad \text{(A.30)}$$

In the above system of equations, $\phi(x,t;x',t+\Delta t)$ denotes the probability that a population between points x and $x+\Delta x$ at time t will move to x' by time $t+\Delta t$.

A more general (but similar in many aspects to Okubo and Levin [2001]) derivation is that due to Othmer [1988]. The authors generalised the framework within which one can analyse all types of position-jump processes. The restriction $\epsilon \to 0$ is not required in this approach as both the diffusion coefficient and the drift are specified in terms of a single limit that is independent of the difference between the transition probabilities. The governing equation takes the form

$$\frac{\partial p}{\partial t} = -u\frac{\partial p}{\partial x} + D\frac{\partial^2 p}{\partial x^2}, \tag{A.31}$$

where u and D are given by

$$\begin{aligned} u &= \lim_{\Delta t\to 0,\lambda\to\infty} \lambda\frac{\Delta x^2}{2}\int_R T(r,\Delta x)r^2 dr, \\ D &= \lim_{\Delta t\to 0,\lambda\to\infty} \lambda\frac{\Delta x^2}{2}\int_R \frac{T(r,\Delta x)}{\Delta x} r dr, \end{aligned} \tag{A.32}$$

where $T(r,\Delta x) = T(\frac{x-y}{\Delta x},\Delta x)$ denotes the transition probability from point x to point y and λ denotes the intensity of an exponentially distributed waiting time distribution.

A.3 Correlated Random Walk

Recall the system of equations (3.31)

$$\begin{aligned}\alpha(x,t+\Delta t) &= (1-\lambda\Delta t)\cdot\alpha(x-\Delta x,t)+\lambda\Delta t\cdot\beta(x-\Delta x,t),\\ \beta(x,t+\Delta t) &= \lambda\Delta t\cdot\alpha(x+\Delta x,t)+(1-\lambda\Delta t)\cdot\beta(x+\Delta x,t).\end{aligned} \tag{A.33}$$

Consider the first of these equations initially. Through a Taylor expansion about x and t we obtain

$$\frac{\partial\alpha}{\partial t}=\lambda(\beta-\alpha)-(1-\lambda\Delta t)\frac{\Delta x}{\Delta t}\frac{\partial\alpha}{\partial x}-\lambda\Delta x\frac{\partial\beta}{\partial x}-\frac{1}{2!}\Delta t\frac{\partial^2\alpha}{\partial t^2}+\frac{1}{2!}\Delta x^2(1-\lambda\Delta t)\frac{\partial^2\alpha}{\partial x^2}+O(\Delta t^2)+O\left(\frac{\Delta x^3}{\Delta t}\right).$$

If $\Delta t\to 0$ and $\Delta x\to 0$ such that the limit,

$$v=\lim_{\Delta t\to 0,\Delta x\to 0}\frac{\Delta x}{\Delta t}\neq 0,$$

is finite, then the PDE for the right-moving individuals reads

$$\frac{\partial\alpha}{\partial t}=\lambda(\beta-\alpha)-v\frac{\partial\alpha}{\partial x}. \tag{A.34}$$

In a similar fashion, we obtain the PDE for the left-moving population

$$\frac{\partial\alpha}{\partial t}=-\lambda(\beta-\alpha)+v\frac{\partial\beta}{\partial x}, \tag{A.35}$$

i.e. the system of equations given by (3.33). Adding and subtracting the equations in (3.33) we obtain

$$\begin{aligned}\frac{\partial(\alpha+\beta)}{\partial t} &= v\frac{\partial(\beta-\alpha)}{\partial x},\\ \frac{\partial(\beta-\alpha)}{\partial t} &= v\frac{\partial(\alpha+\beta)}{\partial x}-2\lambda(\beta-\alpha).\end{aligned} \tag{A.36}$$

By differentiating the first equation with respect to t and the second one with respect to x, we have

$$\frac{\partial^2(\alpha+\beta)}{\partial t^2} = v\frac{\partial^2(\beta-\alpha)}{\partial t \partial x},$$
$$\frac{\partial^2(\beta-\alpha)}{\partial x \partial t} = v\frac{\partial^2(\alpha+\beta)}{\partial x^2} - 2\lambda\frac{\partial(\beta-\alpha)}{\partial x}.$$

We substitute $p = \alpha + \beta$, the unconditional occupation probability, in the LHS of the first equation and use the second equation to replace the RHS and arrive at the governing PDE given by (A.37),

$$\frac{\partial^2 p}{\partial t^2} + 2\lambda\frac{\partial p}{\partial t} = v^2\frac{\partial^2 p}{\partial x^2}, \tag{A.37}$$

which is the telegrapher's equation.

A.3.1 Derivation of the Mean Location and Variance of the CRW

Multiply equation (A.37) by x and integrate with respect to x from $-\infty$ to $+\infty$ to obtain

$$\frac{\partial^2}{\partial t^2}\left[\int_{-\infty}^{\infty} xp(x,t)dx\right] + 2\lambda\frac{\partial}{\partial t}\left[\int_{-\infty}^{\infty} xp(x,t)dx\right] = v^2\int_{-\infty}^{\infty} x\frac{\partial^2 p}{\partial x^2}.$$

Integration of the RHS by parts, the application of the normalisation condition (A.19) and an assumption about $p(x,t)$ and its derivatives, as in (A.20), leads to the equation

$$\frac{d^2}{dt^2}[E(X_t)] + 2\lambda\frac{d}{dt}[E(X_t)] = 0. \tag{A.38}$$

The general solution of this linear second-order ODE is given by $A + Be^{-2\lambda t}$, which for initial conditions $E(X_0) = 0$, $\frac{d}{dt}[E(X_0)] = 0$ reduces to $E(X_t) = 0$.

In a similar fashion, one can obtain a linear second-order ODE for the MSD, namely

$$\frac{d^2}{dt^2}[E(X_t^2)] + 2\lambda \frac{d}{dt}[E(X_t^2)] - 2v^2 = 0. \tag{A.39}$$

Integrating once with respect to t and then using an integrating factor to solve the linear first-order ODE, along with initial conditions $E(X_0^2) = 0,\ \frac{d}{dt}[E(X_0^2)] = 0$, leads to the expression (3.37)

$$E(X_t^2) = \frac{v^2}{\lambda}\left(t - \frac{1}{2\lambda}(1 - e^{-2\lambda t})\right), \tag{A.40}$$

which is also equal to the variance since the mean is zero.

A.4 Biased and Correlated Random Walk

To obtain the governing PDE for $p(x,t)$, recall the PDEs describing the evolution of the conditional probabilities given by

$$\begin{aligned} \frac{\partial \alpha}{\partial t} &= -\lambda_1 \alpha + \lambda_2 \beta - v\frac{\partial \alpha}{\partial x}, \\ \frac{\partial \beta}{\partial t} &= \lambda_1 \alpha - \lambda_2 \beta + v\frac{\partial \beta}{\partial x}. \end{aligned} \tag{A.41}$$

We add and subtract the equations of this system to obtain

$$\begin{aligned} \frac{\partial(\alpha+\beta)}{\partial t} &= v\frac{\partial(\beta-\alpha)}{\partial x}, \\ \frac{\partial(\beta-\alpha)}{\partial t} &= v\frac{\partial(\alpha+\beta)}{\partial x} + 2\lambda_1\alpha - 2\lambda_2\beta, \end{aligned} \tag{A.42}$$

two equations which will also be useful in the determination of the boundary conditions later. By differentiating the first equation with respect to t and the second one with respect to x,

$$\begin{aligned} \frac{\partial^2(\alpha+\beta)}{\partial t^2} &= v\frac{\partial^2(\beta-\alpha)}{\partial t \partial x}, \\ \frac{\partial^2(\beta-\alpha)}{\partial x \partial t} &= v\frac{\partial^2(\alpha+\beta)}{\partial x^2} + 2\lambda_1\frac{\partial \alpha}{\partial x} - 2\lambda_2\frac{\partial \beta}{\partial x}, \end{aligned}$$

and combining them, we arrive at the governing PDE for the unconditional occupation probability of the BCRW model, given by (3.54),

$$\frac{\partial^2 p}{\partial t^2} + (\lambda_1+\lambda_2)\frac{\partial p}{\partial t} + v(\lambda_2-\lambda_1)\frac{\partial p}{\partial x} = v^2\frac{\partial^2 p}{\partial x^2}, \tag{A.43}$$

which is the biased telegrapher's equation.

To obtain the correct boundary conditions in terms of $p(x,t)$, consider the second equation of the system (A.42) at the points $x = 0, L$ and substitute for $p(0,t) = 2\alpha(0,t) = 2\beta(0,t)$, in the former case, and $p(L,t) = \alpha(L,t)$ (or for a partially absorb-

ing barrier $p(L,t) = (2-\theta)\alpha(L,t)$), in the latter case. The resulting conditions are given by

$$\begin{aligned} &v\frac{\partial p}{\partial x}(0,t) + (\lambda_1 - \lambda_2)p(0,t) = 0, \\ &\frac{\partial p}{\partial t}(L,t) + v\frac{\partial p}{\partial x}(L,t) + 2\lambda_1 p(L,t) = 0, \quad \text{or,} \\ &\theta\frac{\partial p}{\partial t}(L,t) + (2-\theta)v\frac{\partial p}{\partial x}(L,t) + (2\lambda_1 - 2\lambda_2 + 2\lambda_2\theta)p(L,t) = 0. \end{aligned} \tag{A.44}$$

A.4.1 Derivation of the Mean Location and Variance of the BCRW

Multiply equation (3.54) by x and integrate by parts with respect to x from $-\infty$ to $+\infty$ to obtain

$$\begin{aligned} &\frac{\partial^2}{\partial t^2}\left[\int_{-\infty}^{\infty} xp(x,t)dx\right] + (\lambda_1+\lambda_2)\frac{\partial}{\partial t}\left[\int_{-\infty}^{\infty} xp(x,t)dx\right] = \\ &= v(\lambda_1-\lambda_2)\left[[xp(x,t)]_{-\infty}^{\infty} - \int_{-\infty}^{\infty} p(x,t)dx\right] + v^2\left[[x\frac{\partial p}{\partial x}]_{-\infty}^{\infty} - \int_{-\infty}^{\infty}\frac{\partial p}{\partial x}dx\right]. \end{aligned}$$

The application of the normalisation condition (A.19) and the assumptions on $p(x,t)$ and its derivatives, as in (A.20), leads to the equation

$$\frac{d^2}{dt^2}[E(X_t)] + (\lambda_1+\lambda_2)\frac{d}{dt}[E(X_t)] + v(\lambda_1-\lambda_2) = 0. \tag{A.45}$$

The solution of this linear second-order ODE, subject to initial conditions $E(X_0) = 0$, $\frac{d}{dt}[E(X_0)] = 0$, can be found by integrating once to obtain a linear first-order ODE and then using the integrating factor $e^{(\lambda_1+\lambda_2)t}$ to solve the latter. The solution is given by

$$E(X_t) = \frac{v(\lambda_2-\lambda_1)}{\lambda_1+\lambda_2}\left(t - \frac{1}{\lambda_1+\lambda_2}(1-e^{-(\lambda_1+\lambda_2)t})\right). \tag{A.46}$$

In a similar fashion, but by multiplying equation (3.54) with x^2 instead of x, one can

obtain a linear second-order ODE satisfied by the MSD

$$\frac{d^2}{dt^2}[E(X_t)]+(\lambda_1+\lambda_2)\frac{d}{dt}[E(X_t)]-2v^2-2v^2\frac{(\lambda_1-\lambda_2)^2}{(\lambda_1+\lambda_2)}\left(t-\frac{1}{\lambda_1+\lambda_2}(1-e^{-(\lambda_1+\lambda_2)t})\right)=0. \tag{A.47}$$

Using the relation (A.11), the analytical expression for the evolution of the variance of a BCRW is given by

$$\begin{aligned}\sigma_t^2 = &\frac{2v^2}{\lambda_1+\lambda_2}\left(1-\frac{(\lambda_2-\lambda_1)^2}{(\lambda_1+\lambda_2)^2}\right)t \\ &+\frac{(\lambda_2-\lambda_1)^2v^2}{(\lambda_1+\lambda_2)^4}(2e^{-(\lambda_1+\lambda_2)t}-e^{-2(\lambda_1+\lambda_2)t}) \\ &+\frac{5(\lambda_2-\lambda_1)^2v^2}{(\lambda_1+\lambda_2)^4}-\frac{2v^2}{(\lambda_1+\lambda_2)^2}.\end{aligned} \tag{A.48}$$

A.5 Derivation of the Stochastic Mean Equations of a Position-Jump Process from the Master Equation

In order to find the mean density of individuals, we multiply the master equation of the BRW model (the SRW model is just the special case $d^- = d^+ = d$), given by (3.29), by n_j, $j = 1, 2, ..., N$, to get a system of N equations and sum over all possible states $\mathbf{n}$ of the density $\mathbf{u}$ to obtain

$$\begin{aligned}\sum_{\mathbf{n}=0}^{\infty} n_j \frac{\partial P}{\partial t}(\mathbf{n}, t) = \\ = d^+ \sum_{i=1}^{N} \left[\sum_{\mathbf{n}=0}^{\infty} n_j (n_i + 1) P(R_i \mathbf{n}, t) - \sum_{\mathbf{n}=0}^{\infty} n_j n_i P(\mathbf{n}, t) \right] \\ + d^- \sum_{i=2}^{N} \left[\sum_{\mathbf{n}=0}^{\infty} n_j (n_i + 1) P(L_i \mathbf{n}, t) - \sum_{\mathbf{n}=0}^{\infty} n_j n_i P(\mathbf{n}, t) \right].\end{aligned} \tag{A.49}$$

Split the sums of the RHS of equation (A.49) into two parts and consider them separately. For $j \neq i, i+1$, the first sum becomes

$$\begin{aligned}&\sum_{i=1, i\neq j, j-1}^{N} \sum_{\mathbf{n}=0}^{\infty} (n_j n_i + n_j) P(R_i \mathbf{n}, t) = \\ &= \sum_{i=1, i\neq j, j-1}^{N} \sum_{\mathbf{n}=0}^{\infty} [n_j (n_i - 1) + n_j] P(\mathbf{n}, t) \\ &= \sum_{i=1, i\neq j, j-1}^{N} \sum_{\mathbf{n}=0}^{\infty} n_i n_j P(\mathbf{n}, t),\end{aligned}$$

by shifting indices as follows

$$n_i \to n_i - 1, \quad n_{i+1} \to n_{i+1} + 1.$$

Notice that if the sum starts from $n_i = 1$ or $n_i = -1$ for some i instead of $n_i = 0$, its value does not change since in the first case the extra term that will be missing from the transformed sum is zero, while in the latter case the probability $P(\mathbf{n}, t)$ is zero since negative populations are undefined and by default we require transition probabilities of the form $T(\mathbf{n} = [.., -1, ...]|\mathbf{n} = [..., 0, ...]) = 0$. In the case $j = i$, the term becomes

$$\sum_{\mathbf{n}=0}^{\infty}(n_j^2 + n_j)P(R_j\mathbf{n}, t) = \\ = \sum_{\mathbf{n}=0}^{\infty}(n_i n_j - n_j)P(\mathbf{n}, t),$$

again by shifting indices in the same fashion, and in the case $j = i+1$, it becomes

$$\sum_{\mathbf{n}=0}^{\infty}(n_j n_{j-1} + n_j)P(R_{j-1}\mathbf{n}, t) = \\ = \sum_{\mathbf{n}=0}^{\infty}(n_i n_j - n_{j-1})P(\mathbf{n}, t),$$

this time by shifting the indices

$$n_i \to n_i + 1, \;\; n_{i-1} \to n_{i-1} - 1.$$

Hence, the first sum reduces to

$$\sum_{\mathbf{n}}(n_{j+1} - n_j)P(\mathbf{n}, t) = M_{j+1} - M_j. \tag{A.50}$$

Similarly, the second sum becomes $M_{j-1} - M_j$ and the equations satisfied by the stochastic M_j for $j = 2, ..., N-1$ are given by the system

$$\frac{dM_i}{dt} = d^- M_{i+1} - (d^+ + d^-)M_i + d^+ M_{i-1}, \;\; i = 2, ..., N-1, \tag{A.51}$$

or in the case of the SRW model, by the system

$$\frac{dM_j}{dt} = d(M_{j+1} - 2M_j + M_{j-1}), \quad i = 2, ..., N-1. \tag{A.52}$$

A similar derivation for the cases $j = 1, N$ leads to the equations

$$\begin{aligned} \frac{dM_1}{dt} &= d^- M_2 - d^+ M_1, \\ \frac{dM_N}{dt} &= d^+ M_{N-1} - (d^+ + d^-) M_N, \end{aligned} \tag{A.53}$$

or, in the case of the SRW model, the equations

$$\begin{aligned} \frac{dM_1}{dt} &= d(M_2 - M_1), \\ \frac{dM_N}{dt} &= d(M_{N-1} - 2M_N). \end{aligned} \tag{A.54}$$

Bibliography

L. V. Ackerman and J. A. del Regato. *Cancer: Diagnosis, Treatment and Prognosis*. C. V. Mosby Co., 1954.

B. Alberts, A. Johnson, J. Lewis, M. Raff, K. Roberts, and P. Walter. *Molecular Biology of the Cell*. Garland Science, 2008.

W. Alt. Biased random walk models for chemotaxis and related diffusion approximations. *Journal of Mathematical Biology*, 9:147–177, 1980.

A. R. A. Anderson and M. A. J. Chaplain. Continuous and discrete mathematical models of tumor-induced angiogenesis. *Bulletin of Mathematical Biology*, 60(5): 857–899, 1998.

G. E. Ayala, H. Dai, M. Ittmann, R. Li, M. Powell, A. Frolov, T. M. Wheeler, T. C. Thompson, and D. Rowley. Growth and survival mechanisms associated with perineural invasion in prostate cancer. *Cancer Research*, 64:6082–6090, 2004.

G. E. Ayala, H. Dai, S. A. Tahir, R. Li, T. Timme, M. Ittmann, A. Frolov, T. M. Wheeler, D. Rowley, and T. C. Thompson. Stromal antiapoptotic paracrine loop in perineural invasion of prostatic carcinoma. *Cancer Research*, 66(10):5159–5164, 2006.

A. J. Ballantyne, A. B. McCarten, and M. L. Ibanez. The extension of cancer of

the head and neck through peripheral nerves. *American Journal of Surgery*, 106: 651–667, 1963.

J. L. Bennington. Cellular kinetics of invasive squamous carcinoma of the human cervix. *Cancer Research*, 29(5):1082–1088, 1969.

H. C. Berg. *Random Walks in Biology*. Princeton University Press, 1983.

H. C. Berg and E. M. Purcell. Physics of chemoreception. *Biophysical Journal*, 20 (2):193–219, 1977.

R. G. Bourne. The spread of squamous carcinoma of the skin via the cranial nerves. *Australasian Radiology*, 24(2):107–114, 1980.

F. Bresciani, R. Paoluzi, M. Benassi, C. Nervi, C. Casale, and E. Ziparo. Cell kinetics and growth of squamous cell carcinomas in man. *Cancer Research*, 34(9):2405–2415, 1974.

G. W. Brodland. Computational modelling of cell sorting. *Applied Mechanics Reviews*, 57(1):47–76, 2004.

C. I. Brown and A. E. Perry. Incidence of perineural invasion in histologically aggressive types of basal cell carcinoma. *The American Journal of Dermatopathology*, 22 (2):123–125, 2000.

R. Brown. A brief account of microscopical observations made in the month of june, july and august, 1827, on the particles contained in the pollen of plants; and the general existence of active molecules in organic and inorganic bodies. *Philosophical Magazine*, 4:161–173, 1828.

S. Chandrasekhar. Stochastic problems in physics and astronomy. *Reviews of Modern Physics*, 15(1):1–89, 1943.

M. A. J. Chaplain and A. M. Stuart. A model mechanism for the chemotactic response

of endothelial cells to tumour angiogenesis factor. *Mathematical Medicine and Biology*, 10(3):149–168, 1993.

E. A. Codling, Plank M. J., and S. Benhamou. Random walk models in biology. *Journal of the Royal Society Interface*, 5(8):813–834, 2008.

S. Condamin, O. Benichou, and M. Moreau. First-passage times for random walks in bounded domains. *Physical Review Letters*, 95(26):260601–1–260601–4, 2005.

S. Condamin, O. Benichou, V. Tejedor, R. Voituriez, and J. Klafter. First-passage times in complex scale-invariant media. *Nature*, 450:77–80, 2007.

J. Cruveilher. *Maladies des Nerfs. In: Anatomie Pathologique du Corps Humain.* Paris: JB Bailliere, 2 edition, 1835.

H. Dai, R. Li, T. M. Wheeler, A. D. de Vivar, A. Frolov, T. M. Wheeler, S. A. Tahir, I. Agoulnik, T. C. Thompson, D. Rowley, and G. E. Ayala. PIM-2 upregulation: Biological implications associated with disease progression and perineural invasion in prostate cancer. *The Prostate*, 65:276–286, 2005.

R. Dalal and D. Djakiew. Molecular characterization of neurotrophin expression and the corresponding tropomyosin receptor kinases (trks) in epithelial and stromal cells of the human prostate. *Molecular and Cellular Endocrinology*, 134:15–22, 1997.

P. D. Dale, P. K. Maini, and J. A. Sherratt. Mathematical modeling of corneal epithelial wound healing. *Mathematical Biosciences*, 124(2):127–147, 1994a.

P. D. Dale, J. A. Sherratt, and P. K. Maini. The speed of corneal epithelial wound healing. *Applied Mathematics Letters*, 7(2):11–14, 1994b.

E. Di Marco, M. Mathor, S. Bondanza, N. Cutuli, P. C. Marchisio, R. Cancedda, and M. De Luca. Nerve growth factor binds to normal human keratinocytes through

high and low affinity receptors and stimulates their growth by a novel autocrine loop. *The Journal of Biological Chemistry*, 268(30):22838–22846, 1993.

M. Dunn, M. B. Morgan, and T. W. Beer. Perineural invasion: Identification, significance and a standardized definition. *Dermatologic Surgery*, 35(2):214–221, 2009.

L. Edelstein-Keshet. *Mathematical Models in Biology*. Society for Industrial and Applied Mathematics, 2005.

A. Einstein. Über die von der molekularkinetischen theorie der wärme geforderte bewegung von in ruhenden flüssigkeiten suspendierten teilchen. *Ann. Physik*, 17: 549–560, 1905.

A. Einstein. Zur theorie der brownschen bewegung. *Annalen der Physik*, 324(2): 371–381, 1906.

J. Endrizzi and T. Seay. The relationship between early biochemical failure and perineural invasion in pathological T2 prostate cancer. *British Journal of Urology International*, 85:696–698, 2000.

R. Erban and S. J. Chapman. Reactive boundary conditions for stochastic simulations of reaction–diffusion processes. *Physical Biology*, 4(1):16, 2007.

R. Erban and S. J. Chapman. Stochastic modelling of reaction–diffusion processes: algorithms for bimolecular reactions. *Physical Biology*, 6(4):046001, 2009.

R. Erban, S. J. Chapman, and P. K. Maini. A practical guide to stochastic simulations of reaction-diffusion processes. *ArXiv e-prints*, 2007.

J. J. Fagan, B. Collins, L. Barnes, F. D'Amico, E. N. Myers, and J. T. Johnson. Perineural invasion in squamous cell carcinoma of the head and neck. *Archives of Otolaryngology - Head & Neck Surgery*, 124:637–640, 1998.

A. M. Feasel, T. J. Brown, M. A. Bogle, J. A. Tschen, and B. R. Nelson. Perineural invasion of cutaneous malignancies. *Dermatologic Surgery*, 27(6):531–542, 2001.

R.A. Fisher. The wave of advance of an advantageous gene. *Annals of Eugenics*, 7: 353–369, 1937.

P. Friedl and K. Wolf. Tumour cell invasion and migration: Diversity and escape mechanisms. *Nature Reviews*, 3:362–374, 2003.

E. Frindel, E. Malaise, and M. Tubiana. Cell proliferation kinetics in five human solid tumors. *Cancer*, 22(3):611–620, 1968.

A. Garcia-Serra, R. W. Hinerman, W. M. Mendelhall, R. J. Amdur, C. G. Morris, L. Sohn Williams, and A. A. Mancuso. Carcinoma of the skin with perineural invasion. *Head & Neck*, 25:1027–1033, 2003.

C. W. Gardiner. *Handbook of Stochastic Methods for Physics, Chemistry, and the Natural Sciences*. Springer Verlag, 1985.

R. A. Gatenby and E. T. Gawlinski. Reaction-diffusion model of cancer invasion. *Cancer Research*, 56:5745–5753, 1996.

D. J. Gawkrodger. *Dermatology: An Illustrated Colour Text*. Churchill Livingstone, Elsevier Ltd., 2003.

D. E. Geist, M. Garcia-Moliner, M. M. Fitzek, H. Cho, and G. S. Rogers. Perineural invasion of cutaneous squamous cell carcinoma and basal cell carcinoma: Raising awareness and optimizing management. *Dermatologic Surgery*, 34(12):1642–1651, 2008.

D. T. Gillespie. A general method for numerically simulating the stochastic time evolution of coupled chemical reactions. *Journal of Computational Physics*, 22(4): 403 – 434, 1976.

D. T. Gillespie. Exact stochastic simulation of coupled chemical reactions. *The Journal of Physical Chemistry*, 81(25):2340–2361, 1977.

D. T. Gillespie. A rigorous derivation of the chemical master equation. *Physica A: Statistical Mechanics and its Applications*, 188(1–3):404 – 425, 1992.

D. T. Gillespie. The chemical Langevin equation. *The Journal of Chemical Physics*, 113(1):297–306, 2000.

D. T. Gillespie. Stochastic simulation of chemical kinetics. *Annual Review of Physical Chemistry*, 58(1):35–55, 2007.

D. T. Gillespie. A diffusional bimolecular propensity function. *The Journal of Chemical Physics*, 131(16):164109, 2009.

S. Gilmore, B. De Ambrosis, and K. Sakellariou. Personal communication, 2009.

M. Gitterman. Mean first passage time for anomalous diffusion. *Physical Review E*, 62:6065–6070, 2000.

J. A. Glazier and F. Graner. Simulation of the differential adhesion driven rearrangement of biological cells. *Physics Reviews E*, 47(3):2128–2154, 1993.

S. Goldstein. On diffusion by discontinuous movements and on the telegraph equation. *Journal of Mechanics and Applied Mathematics*, 6:129–156, 1951.

D. E. Gormley and P. Hirsch. Agressive basal cell carcinoma of the scalp. *Archives of Dermatology*, 114:782–783, 1978.

G. Grimmet and D. Stirzaker. *Probability and Random Processes*. Oxford University Press, 2001.

D. Hanahan and R. A. Weinberg. The hallmarks of cancer. *Cell*, 100:57–70, 2000.

M. O. Hassan and J. Maksem. The prostatic perineural space and its relation to tumour spread. *American Journal of Surgical Pathology*, 4:143–148, 1980.

T. Hillen and H. G. Othmer. The diffusion limit of transport equations derived from velocity-jump processes. *SIAM Journal on Applied Mathematics*, 61(3):751–775, 2000.

http://globocan.iarc.fr/. The GLOBOCAN project 2008. CANCERMondial, International Agency for Research on Cancer, 2008.

http://info.cancerresearchuk.org/cancerstats/. Cancer incidence and survival by major ethnic group, England, 2002 - 2006. Cancer Research UK, National Cancer Intelligence Network, 2006.

http://www.cancer.gov/cancertopics/types/skin. Skin cancer. US National Cancer Institute, 2009.

J. A. Hutcheson, E. Vural, S. Korourian, and E. Hanna. Neural cell adhesion molecule expression in adenoid cystic carcinoma of the head and neck. *Laryngoscope*, 110: 946–948, 2000.

T. Ideker, T. Galitski, and L. Hood. A new approach to decoding life: Systems biology. *Annual Review of Genomics and Human Genetics*, 2(1):343–372, 2001.

G. H. Jacobs, J. J. Rippey, and M. Altini. Prediction of aggressive behaviour in basal cell carcinoma. *Cancer*, 49:533–537, 1982.

A. Johnson, J. Wiens, B. Milne, and T. Crist. Animal movements and population dynamics in heterogeneous landscapes. *Landscape Ecology*, 7:63–75, 1992.

M. Kac. Random walk and the theory of brownian motion. *American Mathematical Monthly*, 54:369–391, 1947.

E. F. Keller and L. A. Segel. Model for chemotaxis. *Journal of Theoretical Biology*, 30(2):225–234, 1971.

E. Kerkela and U. Saarialho-Kere. Matrix metalloproteinases in tumor progression: Focus on basal and squamous cell skin cancer. *Experimental Dermatology*, 12: 109–125, 2003.

A.N. Kolmogorov, I.G. Petrovskii, and N. Piskunov. Étude de l'équation de la diffusion avec croissance de la quantité de matière et son application à un problème bioloqique. *Bulletin of Moscow University*, 1:1–25, 1937.

T. G. Kurtz. The relationship between stochastic and deterministic models for chemical reactions. *Journal of Chemical Physics*, 57(7):2976–2978, 1972.

A. D. Lander. A calculus of purpose. *PLoS Biology*, 2(6):e164, 2004.

K. Landman and M. McGuiness. Mean action time for diffusive processes. *Journal of Applied Mathematics and Decision Sciences*, 4(2):125–141, 2000.

N. Lawrence and W. I. Cottel. Squamous cell carcinoma of skin with perineural invasion. *Journal of the American Academy of Dermatology*, 31:30–33, 1994.

Y. Lazebnik. Can a biologist fix a radio? – or, what I learned while studying apoptosis. *Biochemistry (Moscow)*, 69:1403–1406, 2004.

I. Leibovitch, S. C. Huilgol, D. Selva, D. Hill, S. Richards, and R. Paver. Cutaneous squamous cell carcinoma treated with mohs micrographic surgery in Australia ii. perineural invasion. *Journal of the American Academy of Dermatology*, 53(3):261–266, 2005.

H. Levine, D. A. Kessler, and W. J. Rappel. Directional sensing in eukaryotic chemotaxis: A balanced inactivation model. *Proceedings of the National Academy of Sciences*, 103(26):9761–9766, 2006.

R. Li, T. Wheeler, H. Dai, and G. Ayala. Neural cell adhesion molecule expression is upregulated in nerves with prostate cancer invasion. *Human Pathology*, 34(5): 457–461, 2003.

L. Liotta, K. Tryggvason, S. Garbisa, I. Hart, C. M. Foltz, and S. Shafie. Metastatic potential correlates with enzymatic degradation of basement membrane collagen. *Nature*, 284:67–68, 1980.

A. J. Lotka. Contribution to the theory of periodic reaction. *Journal of Physical Chemistry*, 14(3):271–274, 1910.

G. J. Mark. Basal cell carcinoma with intraneural invasion. *Cancer*, 40:2181–2187, 1977.

J. Masoliver, K. Lindenberg, and G. H. Weiss. A continuous-time generalization of the persistent random walk. *Physica A: Statistical Mechanics and its Applications*, 157(2):891–898, 1989.

R. M. May. Simple mathematical models with very complicated dynamics. *Nature*, 261:459–467, 1976.

L. McCawley and L. M. Matrisian. Matrix metalloproteinases: Multifunctional contributors to tumour progression. *Molecular Medicine Today*, 6:149–156, 2000.

M. W. McCord, W. M. Mendelhall, J. T. Parsons, R. J. Amdur, S. P. Stringer, N. J. Cassisi, and R. R. Million. Skin cancer of the neck and head with clinical perineural invasion. *International Journal of Radiation Oncology, Biology, Physics*, 47(1):89–93, 2000.

H. P. McKean. Application of brownian motion to the equation of kolmogorov-petrovskii-piskunov. *Communications on Pure and Applied Mathematics*, 28(3): 323–331, 1975.

H. McKenzie, M. Lewis, and E. Merrill. First passage time analysis of animal movement and insights into the functional response. *Bulletin of Mathematical Biology*, 71:107–129, 2009.

A. McNabb. Asymptotic behaviour of solutions of diffusion equations. *Journal of Mathematical Analysis and Applications*, 51:219–222, 1975a.

A. McNabb. Asymptotic behavior of solutions of a stefan problem. *Journal of Mathematical Analysis and Applications*, 51:633–642, 1975b.

A. McNabb. Mean action times, time lags and mean first passage times for some diffusion problems. *Mathematical and Computational Modelling*, 18:123–129, 1993.

A. McNabb and G. C. Wake. Heat conduction and finite measures for transition times between steady states. *IMA Journal of Applied Mathematics*, 47:193–206, 1991.

W. M. Mendelhall, R. J. Amdur, C. G. Morris, L. Sohn Williams, A. A. Mancuso, S. P. Stringer, and N. P. Mendelhall. Carcinoma of the skin of the head and neck with perineural invasion. *Head & Neck*, 24:78–83, 2002.

N. Metropolis and S. Ulam. The Monte Carlo method. *Journal of the American Statistical Association*, 44:335–341, 1949.

B. A. Moffat, K. A. Landman, R. J. W. Truscott, M. H. J. Sweeney, and J. M. Pope. Age-related changes in the kinetics of water transport in normal human lenses. *Experimental Eye Research*, 69(6):663–669, 1999.

A. Mogilner, R. Wollman, and W. F. Marshall. Quantitative modeling in cell biology: What is it good for? *Developmental Cell*, 11(3):279 – 287, 2006.

F. E. Mohs and T. G. Lathrop. Modes of spread of cancer of the skin. *AMA Archives of Dermatology and Syphilology*, 66:427–439, 1952.

D. Mollison. Spatial contact models for ecological and epidemic spread. *Journal of the Royal Statistical Society. Series B (Methodological)*, 39(3):283–326, 1977.

D. Mollison. The importance of demographic stochasticity in population dynamics. In R. Hiorns and D.Cooke, editors, *The Mathematical Theory of the Dynamics of Biological Populations II*, pages 99–107. Academic Press, London, UK, 1981.

D. Mollison and H. Daniels. The "deterministic simple epidemic" unmasked. *Mathematical Biosciences*, 117(1–2):147–153, 1993.

D. Mollison, R. M. Anderson, M. S. Bartlett, and R. Southwood. Modelling biological invasions: Chance, explanation, prediction. *Philosophical Transactions of the Royal Society of London B, Biological Sciences*, 314(1167):675–693, 1986.

E. W. Montroll. Random walks in multidimensional spaces, especially on periodic lattices. *Journal of the Society for Industrial and Applied Mathematics*, 4(4):241–260, 1956.

E. W. Montroll. Random walks on lattices. III. calculation of first-passage times with application to exciton trapping on photosynthetic units. *Journal of Mathematical Physics*, 10:753–765, 1969.

E. W. Montroll and G. H. Weiss. Random walks on lattices. II. *Journal of Mathematical Physics*, 6:167–181, 1965.

J. Moreira and A. Deutsch. Cellular automaton models of tumour development: A critical review. *Advances in Complex Systems*, 5(2):247–267, 2002.

J. D. Murray. *Mathematical Biology I: An Introduction*. Springer, 2002.

T. J. Newman. Life and death in biophysics. *Physical Biology*, 8(1):010201, 2011.

D. Noble. The future: putting humpty-dumpty together again. *Biochemical Society Transactions*, 31:156–158, 2003.

D. Noble. *The Music of Life: Biology Beyond Genes*. Oxford University Press, 2006.

J. D. Noh and H. Rieger. Random walks on complex networks. *Physical Review Letters*, 92:118701, 2004.

A. Okubo. Dynamical aspects of animal grouping: Swarms, schools, flocks, and herds. *Advances in Biophysics*, 22:1–94, 1986.

A. Okubo and S. A. Levin. *Diffusion and Ecological Problems: Modern Perspectives*. Springer Verlag, 2001.

H. G. Othmer. Models of dispersal in biological systems. *Journal of Mathematical Biology*, 26(3):263–298, 1988.

H. G. Othmer and T. Hillen. The diffusion limit of transport equations ii: Chemotaxis equations. *SIAM Journal on Applied Mathematics*, 62(4):1222–1250, 2002.

H. G. Othmer and A. Stevens. Aggregation, blowup, and collapse: The abc's of taxis in reinforced random walks. *SIAM Journal on Applied Mathematics*, 57(4): 1044–1081, 1997.

C. A. Parent and P. N. Devreotes. A cell's sense of direction. *Science*, 284(5415): 765–770, 1999.

P. Pathmanathan, J. Cooper, A. Fletcher, G. Mirams, P. Murray, J. Osborne, J. Pitt-Francis, A. Walter, and S. J. Chapman. A computational study of discrete mechanical tissue models. *Physical Biology*, 6(3):1–14, 2009.

C. Patlak. Random walk with persistence and external bias. *Bulletin of Mathematical Biology*, 15:311–338, 1953.

K. Pearson. The problem of the random walk. *Nature*, 72:294, 1905.

Joe Pitt-Francis, Pras Pathmanathan, Miguel O. Bernabeu, Rafel Bordas, Jonathan Cooper, Alexander G. Fletcher, Gary R. Mirams, Philip Murray, James M. Os-

borne, Alex Walter, S. Jon Chapman, Alan Garny, Ingeborg M.M. van Leeuwen, Philip K. Maini, Blanca Rodríguez, Sarah L. Waters, Jonathan P. Whiteley, Helen M. Byrne, and David J. Gavaghan. Chaste: A test-driven approach to software development for biological modelling. *Computer Physics Communications*, 180(12): 2452–2471, 2009.

M. Plank and B. Sleeman. Lattice and non-lattice models of tumour angiogenesis. *Bulletin of Mathematical Biology*, 66:1785–1819, 2004.

D. Ratner, L. Lowe, T. M. Johnson, and D. J. Fader. Perineural spread of basal cell carcinomas treated with mohs micrographic surgery. *Cancer*, 88:1605–1613, 2000.

L. Rayleigh. The problem of the random walk. *Nature*, 72:318, 1905.

S. Redner. *A Guide to First-Passage Processes*. Cambridge University Press, 2001.

E. Renshaw and R. Henderson. The correlated random walk. *Journal of Applied Probability*, 18(2):403–414, 1981.

P. H. Seefeld and J. A. Bargen. The spread of carcinoma of the rectum: Invasion of lymphatics, veins and nerves. *Annals of Surgery*, 118:76–90, 1943.

H. Seki, J. I. Tanaka, Y. Sato, Y. Kato, A. Umezawa, and K. Koyama. Neural cell adhesion molecule (NCAM) and perineural invasion in bile duct cancer. *Journal of Surgical Oncology*, 53:78–83, 1993.

J. A. Sherratt and J. D. Murray. Models of epidermal wound healing. *Proceedings of the Royal Society of London. Series B: Biological Sciences*, 241(1300):29–36, 1990.

J. A. Sherratt and J. D. Murray. Mathematical analysis of a basic model for epidermal wound healing. *Journal of Mathematical Biology*, 29:389–404, 1991.

S. Shirakawa, J. K. Luce, I. Tannock, and E. Frei III. Cell proliferation in human melanoma. *Journal of Clinical Investigation*, 49:1188–1199, 1970.

M. Simpson, B. Hughes, and K. Landman. Diffusing populations: Ghosts or folks. *Australasian Journal of Engineering Education*, 15(2):59–68, 2009.

J. G. Skellam. The formulation and interpretation of mathematical models of diffusionary processes in population biology. In M. S. Bartlett and R. W. Hiorns, editors, *The mathematical theory of the dynamics of biological populations*. Academic Press, 1973.

M. Smoluchowski. Zur kinetischen theorie der brownschen molekularbewegung und der suspensionen. *Ann. Physik*, 21:756–780, 1906.

M. Smoluchowski. Drei vortage über diffusion, brownsche bewegung, und koagulation von kolloidteilchen. *Physik Zeits*, 17:557,585, 1916.

G. G. Steel. The cell cycle in tumour: An examination of data gained by the technique of labeled mitoses. *Cell Proliferation*, 5(1):87–100, 1972.

C. L. Stokes and D. A. Lauffenburger. Analysis of the roles of microvessel endothelial cell random motility and chemotaxis in angiogenesis. *Journal of Theoretical Biology*, 152(3):377–403, 1991.

M. J. Straus and R. E. Moran. Cell cycle parameters in human solid tumors. *Cancer*, 40(4):1453–1461, 1977.

I. F. Tannock. Population kinetics of carcinoma cells, capillary endothelial cells, and fibroblasts in a transplanted mouse mammary tumor. *Cancer Research*, 30(10): 2470–2476, 1970.

H. B. Taylor and H. J. Norris. Epithelial invasion of nerves in benign diseases of the breast. *Cancer*, 20:2245–2249, 1967.

V. Tejedor, O. Bénichou, and R. Voituriez. Global mean first-passage times of random walks on complex networks. *Physical Review E*, 80:065104, 2009.

J. J. Terz, H. P. Curutchet, and W. Lawrence. Analysis of the cell kinetics of human solid tumors. *Cancer*, 28(5):1100–1110, 1971.

S. Tohya, A. Mochizuki, S. Imayama, and Y. Iwasa. On rugged shape of skin tumor (basal cell carcinoma). *Journal of Theoretical Biology*, 194(1):65 – 78, 1998.

C. J. Tomlin and J. D. Axelrod. Biology by numbers: mathematical modelling in developmental biology. *Nature Reviews Genetics*, 8(5):331–340, 2007.

I. M. M. van Leeuwen, G. R. Mirams, A. Walter, A. Fletcher, P. Murray, J. Osborne, S. Varma, S. J. Young, J. Cooper, B. Doyle, J. Pitt-Francis, L. Momtahan, P. Pathmanathan, J. P. Whiteley, S. J. Chapman, D. J. Gavaghan, O. E. Jensen, J. R. King, P. K. Maini, S. L. Waters, and H. M. Byrne. An integrative computational model for intestinal tissue renewal. *Cell Proliferation*, 2009.

P. F. Verhulst. Notice sur la loi que la population poursuit dans son accroissement. *Correspondance mathématique et physique*, 10:113–121, 1838.

V. Volterra. Variazioni e fluttuazioni del numero d'individui in specie animali conviventi. *Mem. Acad. Lincei Roma*, 2:31–113, 1926.

H. W. Walling, S. W. Fosko, P. A. Geraminejad, and C. J. Whitaker, D. C. andArpey. Aggressive basal cell carcinoma: Presentation, pathogenesis and management. *Cancer and Metastasis Reviews*, 23:389–402, 2004.

G. D. Weinstein, J. L. McCullough, and P. Ross. Cell proliferation in normal epidermis. *Journal of Investigative Dermatology*, 82(6):623–628, 1984.

G. H. Weiss. First passage time problems for one-dimensional random walks. *Journal of Statistical Physics*, 24:587–594, 1981.

G. H. Weiss. First passage times for correlated random walks and some generalizations. *Journal of Statistical Physics*, 37:325–330, 1984.

G. H. Weiss. Some applications of persistent random walks and the telegrapher's equation. *Physica A: Statistical Mechanics and its Applications*, 311(3–4):381–410, 2002.

WHO. The 10 leading causes of death by broad income group. http://www.who.int/mediacentre/factsheets/fs310/en/index.html, 2008.

K. Wolf and P. Friedl. Functional imaging of pericellular proteolysis in cancer cell invasion. *Biochimie*, 87:315–320, 2005.

C. Yates. *Comparing stochastic discrete and deterministic continuum models of cell migration*. PhD thesis, Oxford University, 2011.

R. C. Young and V. T. DeVita. Cell cycle characteristics of human solid tumors in vivo. *Cell Proliferation*, 3(3):285–290, 1970.

Z. Zhu, H. Friess, F. F. diMola, A. Zimmermann, H. U. Graber, M. Korc, and M. W. Buchler. Nerve growth factor expression correlates with perineural invasion and pain in human pancreatic cancer. *Journal of Clinical Oncology*, 17(8):2419–2428, 1999.